Article

Developmental Cell

Hedgehog Pathway Activation Requires Coreceptor-Catalyzed, Lipid-Dependent Relay of the Sonic Hedgehog Ligand

Graphical Abstract

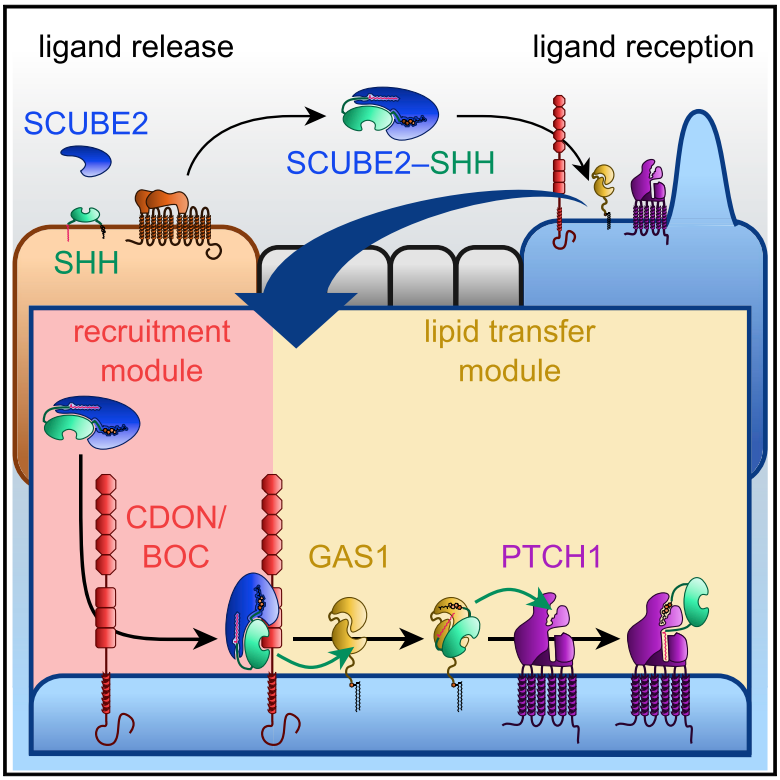

Authors

Bradley M. Wierbowski, Kostadin Petrov, Laura Aravena, Garrick Gu, Yangqing Xu, Adrian Salic

Correspondence

asalic@hms.harvard.edu

In Brief

Wierbowski et al. elucidate the pathway that shuttles the SHH morphogen from producing to responding cells. SCUBE releases lipidated SHH but blocks it from directly signaling through PTCH1. Signaling by SCUBE-SHH requires the coreceptors CDON/BOC and GAS1, which recruit SCUBE-SHH to responding cells and transfer SHH to PTCH1.

Highlights

- SCUBE binds lipidated SHH, forming a highly active and soluble morphogen complex
- SHH must be unloaded from SCUBE to allow SHH to signal through the PTCH1 receptor
- Coreceptors CDON/BOC and GAS1 cooperate to move SHH from SCUBE to PTCH1
- CDON/BOC recruit SCUBE-SHH to cells, then GAS1 catalyzes SHH transfer to PTCH1

Wierbowski et al., 2020, Developmental Cell *55*, 1–18
November 23, 2020
https://doi.org/10.1016/j.devcel.2020.09.017

CellPress

Please cite this article in press as: Wierbowski et al., Hedgehog Pathway Activation Requires Coreceptor-Catalyzed, Lipid-Dependent Relay of the Sonic Hedgehog Ligand, Developmental Cell (2020), https://doi.org/10.1016/j.devcel.2020.09.017

Developmental Cell

CellPress

Article

Hedgehog Pathway Activation Requires Coreceptor-Catalyzed, Lipid-Dependent Relay of the Sonic Hedgehog Ligand

Bradley M. Wierbowski,[1] Kostadin Petrov,[1] Laura Aravena,[1] Garrick Gu,[2] Yangqing Xu,[1] and Adrian Salic[1,3,*]
[1]Department of Cell Biology, Harvard Medical School, Boston, MA 02115, USA
[2]Williams College, Williamstown, MA 01267, USA
[3]Lead Contact
*Correspondence: asalic@hms.harvard.edu
https://doi.org/10.1016/j.devcel.2020.09.017

SUMMARY

Hedgehog signaling governs critical processes in embryogenesis, adult stem cell maintenance, and tumorigenesis. The activating ligand, Sonic hedgehog (SHH), is highly hydrophobic because of dual palmitate and cholesterol modification, and thus, its release from cells requires the secreted SCUBE proteins. We demonstrate that the soluble SCUBE-SHH complex, although highly potent in cellular assays, cannot directly signal through the SHH receptor, Patched1 (PTCH1). Rather, signaling by SCUBE-SHH requires a molecular relay mediated by the coreceptors CDON/BOC and GAS1, which relieves SHH inhibition by SCUBE. CDON/BOC bind both SCUBE and SHH, recruiting the complex to the cell surface. SHH is then handed off, in a dual lipid-dependent manner, to GAS1, and from GAS1 to PTCH1, initiating signaling. These results define an essential step in Hedgehog signaling, whereby coreceptors activate SHH by chaperoning it from a latent extracellular complex to its cell-surface receptor, and point to a broader paradigm of coreceptor function.

INTRODUCTION

During embryogenesis, critical secreted molecules called morphogens provide positional information that determines cellular fate. Morphogens are produced by groups of cells called signaling centers, from which they spread and generate extracellular concentration gradients. In faraway target cells, morphogens bind to specific receptors, triggering responses in proportion to their concentration, ultimately prompting distinct cellular fates. Morphogens belonging to the Hedgehog (Hh) family begin operating in early animal development and are used repeatedly in different contexts. For example, the vertebrate Hh ortholog Sonic hedgehog (SHH) (Echelard et al., 1993; Ma et al., 1993; Riddle et al., 1993), secreted by the notochord and prechordal mesoderm, spreads to the overlying neural tube, patterning it along the dorsoventral axis (Ingham and McMahon, 2001). The same SHH morphogen, produced by the zone of polarizing activity (ZPA), patterns the limb bud along the antero-posterior axis, specifying digit identity.

Many steps involved in morphogen signaling are tightly regulated. In general, morphogens are membrane-associated, a property that allows control over extracellular spreading. In the case of SHH, the unique modification with palmitate, at the N terminus (Pepinsky et al., 1998), and cholesterol, at the C terminus (Porter et al., 1996b; Beachy et al., 1997), ensures that SHH is strongly tethered to membranes (Peters et al., 2004). As a result, SHH requires two solubilizing factors for release from producing cells: the membrane protein Dispatched1 (DISP1) (Burke et al., 1999; Caspary et al., 2002; Kawakami et al., 2002; Ma et al., 2002) and a member of the SCUBE family of secreted proteins (Grimmond et al., 2001), such as SCUBE2 (Kawakami et al., 2005; Woods and Talbot, 2005; Hollway et al., 2006). During release from cells, SHH interacts in a lipid-dependent manner first with DISP1 and then with SCUBE2 (Tukachinsky et al., 2012). It is unclear, however, how the SHH morphogen remains soluble outside cells, to allow its spreading. One possibility is that SCUBE2 is involved in chaperoning SHH after release, maintaining its solubility by shielding the lipid appendages from the aqueous environment (Tukachinsky et al., 2012). Another hypothesis is that SCUBE proteins function only transiently during SHH release, promoting formation of a soluble SHH species (Jakobs et al., 2014).

Following release from producing cells, SHH traverses extracellular space, on its way to responding cells. The nature of the extracellular SHH species and the mechanism by which it moves between cells remain unclear (Petrov et al., 2017). Exosomes (Gradilla et al., 2014; Matusek et al., 2014), lipoprotein particles (Panáková et al., 2005), and specialized signaling filopodia known as cytonemes (Ramírez-Weber and Kornberg, 1999; Callejo et al., 2011; Bischoff et al., 2013; Chen et al., 2017; Hall et al., 2020) have all been proposed as possible carriers for extracellular SHH. However, whether or not such a carrier is involved, dually lipidated SHH must pass through an aqueous environment before reaching the surface of the target cell, a process

Please cite this article in press as: Wierbowski et al., Hedgehog Pathway Activation Requires Coreceptor-Catalyzed, Lipid-Dependent Relay of the Sonic Hedgehog Ligand, Developmental Cell (2020), https://doi.org/10.1016/j.devcel.2020.09.017

likely requiring a solubilizing factor. Ultimately, on target cells, SHH binds its receptor, the tumor suppressor membrane protein Patched1 (PTCH1) (Chen and Struhl, 1996; Marigo et al., 1996; Stone et al., 1996), whose function is to block downstream signaling by inhibiting the GPCR-like oncoprotein, Smoothened (SMO) (Alcedo et al., 1996; van den Heuvel and Ingham, 1996). SHH binding inhibits PTCH1, leading to SMO activation, which triggers the cytoplasmic steps of the Hh pathway (Ingham et al., 1991; Ingham and Hidalgo, 1993; Fuse et al., 1999). Interestingly, the interaction of SHH with PTCH1 is mediated in large part by the very lipid moieties that confer SHH insolubility and which must be shielded during extracellular transit (Qi et al., 2018a, 2018b; Qian et al., 2018; Rudolf et al., 2019). One of these interactions in particular, between the palmitoylated N terminus of SHH and PTCH1 (Qi et al., 2018b), is essential for PTCH1 inhibition and thus for triggering Hh signaling (Williams et al., 1999; Tukachinsky et al., 2016). It is currently unknown how SHH encounters PTCH1, and how the dual lipid-dependent SHH-PTCH1 complex is assembled on the cell surface.

Although PTCH1 inhibition is critical, *in vivo* studies indicate that the signaling process is more complicated. Hh pathway activation also requires the SHH coreceptors, a group of cell-surface proteins consisting of the closely related single-spanning transmembrane proteins CDON and BOC (hereby referred to, collectively, as CDON/BOC) (Okada et al., 2006; Tenzen et al., 2006; Yao et al., 2006; Zhang et al., 2006), and the unrelated GPI-anchored protein GAS1 (Lee et al., 2001; Allen et al., 2007; Martinelli and Fan, 2007). The three coreceptors bind SHH and, in their absence, Hh signaling is abolished (Allen et al., 2011). Previous studies proposed that coreceptors form constitutive complexes with PTCH1, to enhance affinity for SHH (Izzi et al., 2011). However, PTCH1 can engage SHH independently of coreceptors, as shown in recent cryoelectron microscopy (cryo-EM) structures of the SHH-PTCH1 complex (Gong et al., 2018; Qi et al., 2018a, 2018b; Qian et al., 2018; Rudolf et al., 2019). Furthermore, SHH binds to PTCH1 and to coreceptors through largely overlapping surfaces (Beachy et al., 2010), suggesting that these interactions involving SHH are perhaps mutually exclusive. Thus, how coreceptors promote SHH signaling remains an open question.

Here, we investigate the nature of the SHH morphogen and its delivery to target cells. We find that dually lipidated SHH forms a stable, highly active SCUBE-SHH complex, pointing to a continued role of SCUBE after SHH release from cells. Surprisingly, SCUBE inhibits the essential lipid-dependent interaction between SHH and PTCH1. As a result, SCUBE-bound SHH cannot directly signal via PTCH1 and requires a dedicated activation pathway, in which the coreceptors CDON/BOC and GAS1 play a critical role, by cooperating to dissociate SHH from SCUBE. SCUBE-SHH is first recruited to the cell surface as a ternary complex with CDON/BOC, after which GAS1 binds SHH in a lipid-dependent manner and removes it from SCUBE. SHH is then transferred from GAS1 to PTCH1, initiating signaling. Thus SCUBE, CDON/BOC, and GAS1 comprise a novel extracellular chaperone system that channels SHH to its receptor, via successive handoffs of the SHH lipid appendages. This distributed SHH reception mechanism, which permits sensitive and tunable signal detection, defines a key new step in Hh signal transduction and, more generally, a paradigm for coreceptor function upstream of a primary receptor.

RESULTS

SCUBE2 Forms a Stable Complex with SHH during Its Release from Producing Cells

Previous studies of SHH release used SCUBE2-conditioned media, rather than purified protein, as a source of SCUBE2 (Creanga et al., 2012; Tukachinsky et al., 2012), so it is unclear if secreted factors besides SCUBE proteins are required. We thus purified full-length SCUBE2 (Figures 1A and S1A–S1D) and tested its activity. SCUBE2 released SHH from cells in a dose-dependent manner (Figure 1B). Purified SCUBE2 forms oligomers (Figures S1E–S1G), but monomeric and oligomeric species released SHH similarly (Figure S1H), indicating they both represent functional forms of SCUBE2. Similar results were obtained for SCUBE1 and SCUBE3, the other two members of the SCUBE family (Figures S1I and S1J). These results indicate that SCUBE proteins, together with endogenous DISP1 (Petrov et al., 2020), are sufficient for SHH release.

SCUBE2 and SHH might interact transiently during SHH release, or they might associate stably (Figure 1C). We thus asked whether SCUBE2 and SHH form a complex after release. When SCUBE2 and SHH were co-expressed, and SCUBE2 was affinity purified from conditioned media, SHH co-eluted with SCUBE2 (Figures 1D and 1E). Reciprocally, full-length SCUBE2 co-purified with SHH immunoprecipitated with the anti-SHH monoclonal antibody 5E1 (Ericson et al., 1996) (Figure S2A). As an alternative means of purifying SCUBE2-SHH complexes, we tagged SHH with a human protein C (HPC) epitope, inserted at either of two internal sites (Figure S2B) that do not perturb SHH processing and release (Ma et al., 2002; Petrov et al., 2020). SHH(HPC) formed a complex with SCUBE2, as indicated by affinity purification to homogeneity through sequential steps (Figure S2C). We note that, even following tandem purification, SCUBE2 was present in slight excess over SHH, likely due to its tendency to oligomerize. Finally, SHH co-migrated with SCUBE2 by native gel electrophoresis, indicating complex formation (Figure 1F). The SCUBE2-SHH complex was resistant to high ionic strength but was readily disrupted by non-ionic detergents (Figure 1F). Since SHH in the complex was dually lipidated (Figure S2D), this behavior suggests that SCUBE2 interacts with the SHH lipid moieties, sequestering them from the aqueous environment and thus solubilizing SHH.

Finally, we asked if purified SCUBE2-SHH is active in signaling. The complex activated the Hh pathway (see Table S1 for EC_{50} measurements), as measured by SMO recruitment to primary cilia (Figures 1G and 1H), by transcriptional reporter assays (Figures S2E and S2F), and by qRT-PCR for the target gene *Gli1* (Figure 1I). SCUBE2-SHH was as potent as purified SHH-N, the palmitoylated N-terminal fragment of SHH known to retain all signaling activity. Like SCUBE2 alone, SCUBE2-SHH formed oligomers (Figures S2G and S2H), and both monomeric and oligomeric species were equally active in Hh signaling (Figure S2I). Similar results were obtained with purified SCUBE2-SHH(HPC) complexes (Figures S2J and S2K). Together, these results demonstrate that the SHH morphogen is secreted as a stable and highly active complex with a SCUBE protein.

Please cite this article in press as: Wierbowski et al., Hedgehog Pathway Activation Requires Coreceptor-Catalyzed, Lipid-Dependent Relay of the Sonic Hedgehog Ligand, Developmental Cell (2020), https://doi.org/10.1016/j.devcel.2020.09.017

CellPress

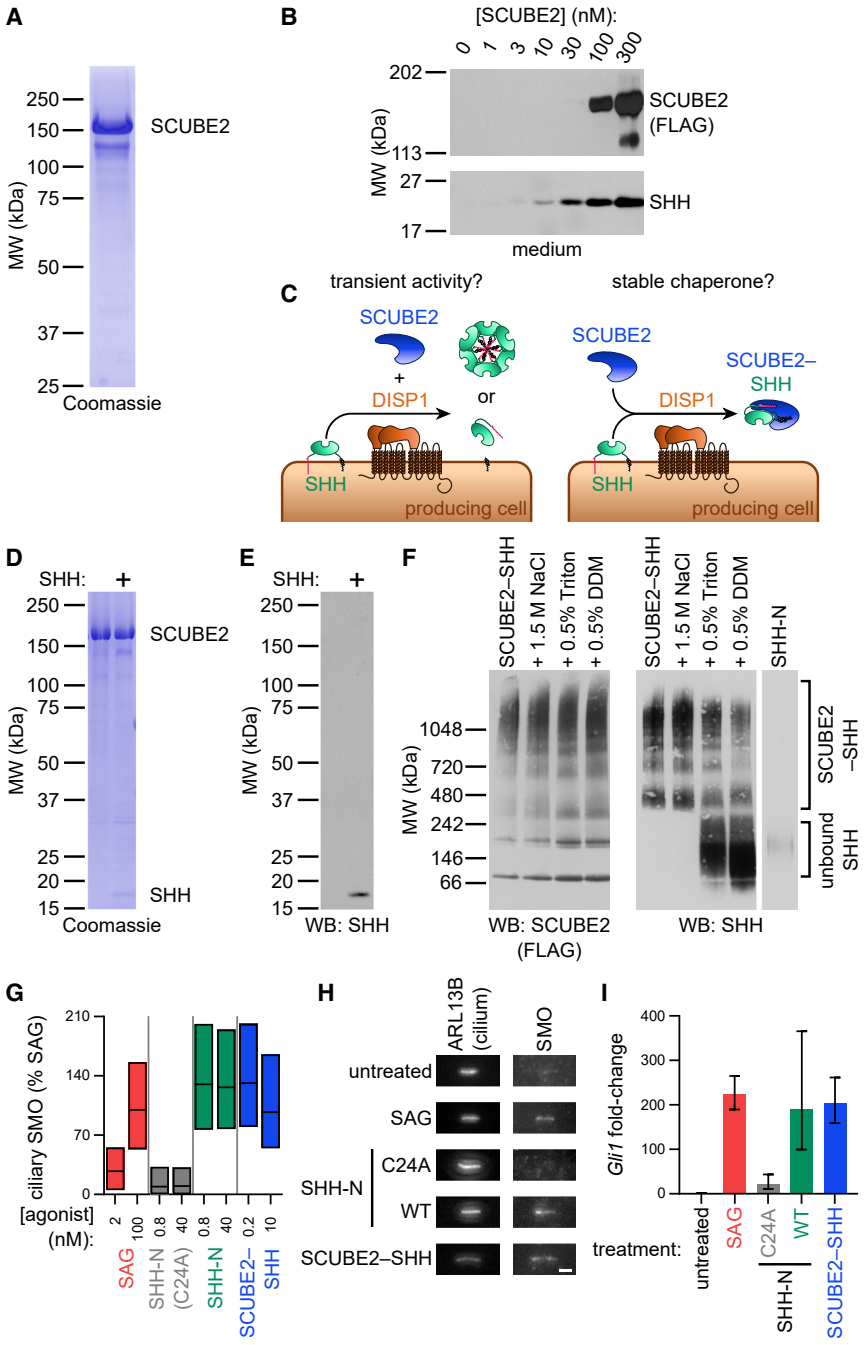

Figure 1. SHH Is Released as a Stable Complex with SCUBE Proteins

(A) Tagged SCUBE2 was affinity purified from conditioned media and was analyzed by SDS-PAGE and Coomassie staining.

(B) Purified SCUBE2 was added to SHH-producing HEK293T cells and released SHH was quantified by immunoblotting. SCUBE2 releases SHH in a dose-dependent manner. See Figure S1J for SHH release by SCUBE1 and SCUBE3.

(C) Models for SCUBE2 involvement in SHH release. Left: SCUBE2 stimulates SHH release, by promoting multimerization or removal of lipid termini. Right: SCUBE2 remains bound to SHH, as chaperone.

(D) As in (A), but with SHH co-expression. SHH copurifies with SCUBE2.

(E) As in (D), but with SHH detection by immunoblotting.

(F) Purified SCUBE2-SHH was incubated with 1.5 M NaCl, 0.5% Triton X-100, or 0.5% DDM, and then analyzed by Blue Native PAGE. Brackets indicate molecular weight ranges for SCUBE2-SHH and SHH. The complex is disrupted by detergents, but not by high ionic strength.

(G) Wild-type MEFs were incubated with two doses of purified SCUBE2-SHH, palmitoylated SHH-N, unlipidated SHH-N(C24A), or SAG, and intensity of endogenous SMO in cilia was measured by immunofluorescence microscopy. Hh signaling is triggered by SCUBE2-SHH, SHH-N, and SAG, but not by SHH-N(C24A). Data are normalized between median ciliary SMO intensity for untreated cells and cells treated with the higher SAG dose (100%). Box plots represent median and first and third quartiles of SMO intensity at cilia. At least 900 cilia were measured per condition.

(H) Representative images of cilia for the experiment in (G). Scale bar, 2 μm.

(I) As in (G), but Hh signaling was measured by qRT-PCR for *Gli1*. Bars represent average fold-change for three replicates, and error bars represent SEM.

See also Figures S1 and S2 for additional characterization of purified SCUBE2 and SCUBE2-SHH complexes.

SCUBE2 Blocks the Palmitate-Dependent SHH-PTCH1 Interaction Required for Hh Signaling

We next asked if and how SCUBE2 affects the SHH-PTCH1 interaction, which triggers Hh signaling. To this end, we compared binding of SCUBE2-SHH and palmitoylated-only SHH (SHH-N) to PTCH1, using a cell-based binding assay (see Figures S3A–S3K for assay validation; see Table S2 for all affinity measurements). Surprisingly, SCUBE2-bound SHH showed significantly reduced affinity for PTCH1 compared with SHH-N (Figures 2A and S3L), indicating that SCUBE2 interferes with the SHH-PTCH1 interaction.

SHH is known to engage PTCH1 via two interactions (Figure 2B): (1) a protein-protein interaction involving the pseudo-active site in the globular part of SHH (Fuse et al., 1999; Pepinsky et al., 2000; Tukachinsky et al., 2016; Gong et al., 2018) and (2) a lipid-protein interaction involving the palmitoylated N-terminal SHH peptide (hereby referred to as effector peptide) (Tukachinsky et al., 2016; Qi et al., 2018b). Each interaction contributes significantly to SHH-PTCH1 binding, as shown by the ~30-fold loss in affinity (Figure 2C) exhibited by two SHH-N variants (Figure S3M) that selectively perturb the two interactions: SHH-N^{PAS*}, which has mutations in the pseudo-active site and SHH-N$^{\Delta EP}$, which lacks the palmitoylated effector peptide.

To pinpoint which of the two SHH-PTCH1 interactions is affected by SCUBE2, we compared binding of SCUBE2-SHH

Please cite this article in press as: Wierbowski et al., Hedgehog Pathway Activation Requires Coreceptor-Catalyzed, Lipid-Dependent Relay of the Sonic Hedgehog Ligand, Developmental Cell (2020), https://doi.org/10.1016/j.devcel.2020.09.017

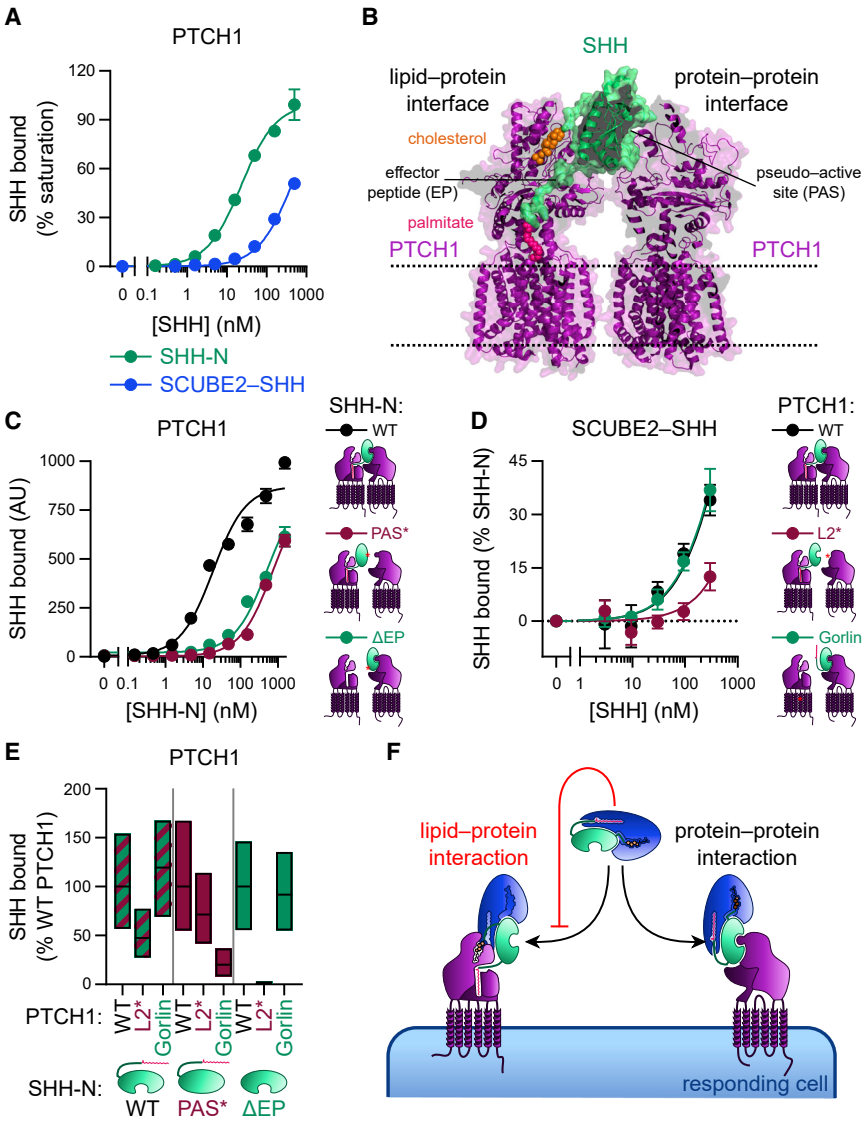

Figure 2. SCUBE2 Blocks the Palmitate-Dependent Interaction between SHH and PTCH1

(A) Purified SCUBE2-SHH or SHH-N was added to HEK293T cells expressing EGFP-tagged PTCH1, and bound ligand was quantified by anti-SHH (5E1) immunofluorescence. SCUBE2 reduces SHH affinity for PTCH1. Data are normalized between background signal (untreated cells) and maximum SHH-N binding (defined as 100%), and are fit with a three-parameter curve. Points represent average binding for four replicates, and error bars represent SEM. At least 200 cells were measured per replicate.

(B) Schematic of SHH–PTCH1 interactions (PDB: 6RVD). SHH engages PTCH1 through a protein-protein interaction, involving the SHH pseudo-active site (PAS) and the second extracellular loop (L2) of PTCH1, as well as through lipid-protein interactions, involving the palmitoylated N-terminal peptide (EP) of SHH and the cholesterol-modified C terminus of SHH. Mutants specifically defective in the protein-protein (SHH-N^{PAS*}, $PTCH1^{L2*}$) or palmitate-protein (SHH-$N^{\Delta EP}$, $PTCH1^{Gorlin}$) interaction between SHH and PTCH1 are tested below.

(C) As in (A), but with binding of fluorescently labeled SHH-N variants. SHH-N^{PAS*} and SHH-$N^{\Delta EP}$ have reduced affinity for PTCH1. At least 100 cells were measured per replicate.

(D) As in (A), but with binding of SCUBE2-SHH to wild-type or mutant PTCH1. Binding of SCUBE2-complexed SHH depends on an intact SHH-PTCH1 protein-protein interface. At least 500 cells were measured per replicate.

(E) As in (C), but comparing binding of wild-type or mutant SHH-N (150 nM), to wild-type or mutant PTCH1. Disruption of both SHH-PTCH1 interfaces results in synergistic binding defects. For each SHH-N variant, data are normalized between background signal (untreated cells) and binding to wild-type PTCH1 (100%). Box plots show the median and the first and third quartiles of bound ligand intensity. At least 300 cells were measured per condition. See Figures S3N–S3P for complete dose-response curves.

(F) Model of SCUBE2-SHH interaction with PTCH1. SCUBE2, which sequesters SHH lipid moieties, blocks the EP-dependent interaction of SHH with PTCH1, reducing affinity of SHH for PTCH1.

See Figure S3 for additional characterization of the cell-based ligand-receptor binding assay.

with wild-type PTCH1 and with two PTCH1 variants: $PTCH1^{L2*}$, which harbors mutations in the second large extracellular loop and is defective in binding the SHH pseudo-active site (Gong et al., 2018), and $PTCH1^{Gorlin}$, a point mutant defective in binding the palmitoylated SHH effector peptide (Tukachinsky et al., 2016). SCUBE2-SHH had equal affinity for wild-type PTCH1 and $PTCH1^{Gorlin}$ but failed to bind $PTCH1^{L2*}$ (Figure 2D). This was similar to the behavior of SHH-$N^{\Delta EP}$ (Figures 2E and S3N–S3P). As expected, SHH-N^{PAS*} had less affinity for $PTCH1^{Gorlin}$ than for wild-type PTCH1 or $PTCH1^{L2*}$ (Figures 2E and S3N–S3P). These results demonstrate that SCUBE2 selectively blocks the palmitate-dependent SHH-PTCH1 interaction (Figure 2F), suggesting that perhaps SCUBE2 interacts with the SHH palmitoyl moiety (see below). Consistent with this idea, inhibition of SHH palmitoylation greatly reduced the rate of SHH release by SCUBE2 (Figures S3Q and S3R).

SHH Coreceptors Are Essential for Signaling by SCUBE2-SHH

If SCUBE2 blocks the SHH effector peptide-PTCH1 interaction, which is necessary for Hh pathway activation (Tukachinsky et al., 2016), how can SCUBE2-SHH activate signaling so potently? To resolve this paradox, we wondered if the SHH coreceptors, CDON, BOC, and GAS1, might be involved in relieving the inhibition exerted by SCUBE2 on SHH (Figure 3A). We tested this hypothesis by assaying the response of cells lacking CDON, BOC, and GAS1 (coreceptor-null cells) (Mathew et al., 2014) to levels of SCUBE2-SHH that are

Please cite this article in press as: Wierbowski et al., Hedgehog Pathway Activation Requires Coreceptor-Catalyzed, Lipid-Dependent Relay of the Sonic Hedgehog Ligand, Developmental Cell (2020), https://doi.org/10.1016/j.devcel.2020.09.017

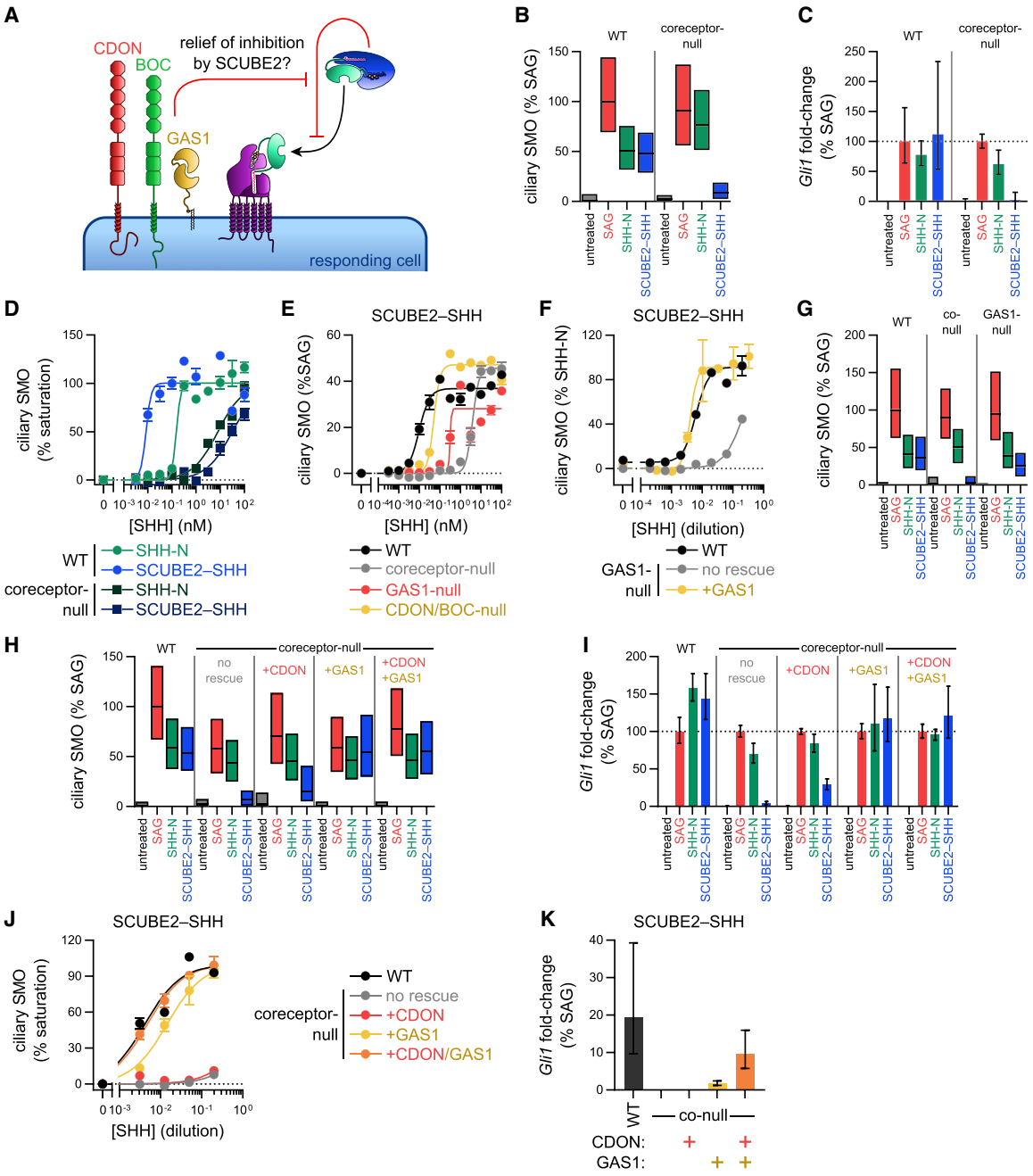

Figure 3. Coreceptors CDON/BOC and GAS1 Are Necessary for Signaling by SCUBE2-SHH

(A) Possible function of the three SHH coreceptors, CDON, BOC, and GAS1. CDON and BOC are homologous single-pass transmembrane proteins of the immunoglobulin superfamily. GAS1 is a GPI-anchored protein with homology to GDNF receptors. SHH coreceptors might relieve inhibition of SHH by SCUBE2, allowing SHH lipids to engage PTCH1.

(B) Wild-type or coreceptor-null MEFs (Mathew et al., 2014) were treated with saturating doses of SCUBE2-SHH conditioned medium, SHH-N conditioned medium, or SAG, and Hh pathway activation was measured by endogenous SMO recruitment to cilia. Coreceptor-null MEFs do not respond to SCUBE2-SHH, but respond to SHH-N and SAG. Data are normalized between ciliary SMO for untreated cells and cells treated with saturating SAG (100%). Box plots represent median and the first and third quartiles of SMO intensity. At least 500 cilia were measured per condition.

(C) As in (B), but Hh signaling was measured by qRT-PCR for *Gli1*. For each line, data are normalized between response for untreated cells and cells treated with saturating SAG (100%). Bars represent average fold-change for three replicates, with error bars indicating SEM.

(D) Dose-response of purified SCUBE2-SHH or SHH-N on wild-type and coreceptor-null MEFs. For each line, data are normalized between ciliary SMO for untreated cells and the theoretical maximum (100%), as fit with a four-parameter curve. Points represent average ciliary SMO for three replicates, and error bars represent SEM. At least 100 cilia were measured per replicate.

(E) As in (D), but with wild-type, GAS1-null, CDON/BOC-null, or coreceptor-null MEFs. GAS1-null MEFs exhibit a severe defect in responsiveness to SCUBE2-SHH, while CDON/BOC-null cells exhibit a modest defect.

(legend continued on next page)

Please cite this article in press as: Wierbowski et al., Hedgehog Pathway Activation Requires Coreceptor-Catalyzed, Lipid-Dependent Relay of the Sonic Hedgehog Ligand, Developmental Cell (2020), https://doi.org/10.1016/j.devcel.2020.09.017

saturating for wild-type cells. Dramatically, coreceptor-null cells did not respond to SCUBE2-SHH (Figures 3B and 3C); importantly, a strong response was observed to SHH-N, which can be delivered to cells without SCUBE2, and the synthetic SMO agonist, SAG (Chen et al., 2002), indicating that PTCH1, SMO, and the downstream Hh pathway were fully functional in these cells. As expected, SCUBE2-SHH, SHH-N, and SAG strongly activated signaling in wild-type cells (Figures 3B and 3C). Titration of purified SCUBE2-SHH revealed an EC_{50} ~3,000-fold higher for coreceptor-null cells compared with wild-type cells (~30 nM versus ~10 pM; Figure 3D). In contrast, purified SHH-N had only a ~50-fold difference in EC_{50} between coreceptor-null and wild-type cells (Figure 3D). We note that the high concentration of SCUBE2-SHH complex required to activate coreceptor-null cells is similar to the concentration required for PTCH1 binding (Figure 2A). In conclusion, at least one of the SHH coreceptors is critical for Hh pathway activation by SCUBE2-SHH.

CDON/BOC and GAS1 Promote SCUBE2-SHH Signaling with Different Efficacy

To test the requirement for individual coreceptors in SCUBE2-SHH signaling, we generated CDON/BOC-null and GAS1-null cells (Table S3). CDON/BOC-null cells had a modest defect in responding to SCUBE2-SHH (Figure 3E). In contrast, GAS1-null cells showed a strong defect (Figure 3E), which was rescued by stable GAS1 expression (Figure 3F). Importantly, GAS1-null cells responded normally to SHH-N and SAG (Figure 3G). Thus, GAS1 is critical for Hh pathway activation by SCUBE2-SHH, while CDON/BOC are required for maximal stimulation.

To test coreceptor sufficiency, we performed rescue experiments in coreceptor-null cells. Since CDON and BOC are highly related and behave similarly in various assays (see below), we used CDON for this coreceptor category. Overexpressed CDON partially rescued, while GAS1 fully rescued, the response of coreceptor-null cells to saturating levels of SCUBE2-SHH (Figures 3H and 3I). Co-expressing CDON in cells rescued with GAS1 did not further enhance the response, indicating that under these conditions (saturating SCUBE2-SHH and overexpressed GAS1), CDON is not limiting. Importantly, all cells responded similarly to SHH-N and SAG, further underscoring the specific role of coreceptors in SCUBE2-SHH signaling (Figures 3H and 3I). Thus, CDON and GAS1 are sufficient for responding to SCUBE2-SHH, but CDON supports only partial Hh pathway activation, while GAS1 allows a full response.

CDON/BOC and GAS1 Act Synergistically to Promote Signaling

The defective response of coreceptor-null cells to SCUBE2-SHH (~1,000-fold reduction) is more severe than the combined defects of CDON/BOC-null and GAS1-null cells (~5-fold and ~30-fold reduction, respectively), suggesting that CDON/BOC and GAS1 might synergize (Figure 3E). Indeed, at doses of SCUBE2-SHH that activate wild-type cells but not coreceptor-null cells rescued with GAS1, we observed that co-expression of CDON promoted signaling (Figures 3J and 3K). Thus, although CDON/BOC and GAS1 can function independently to promote SCUBE2-SHH signaling, it is likely they cooperate under normal conditions.

CDON/BOC Promote Signaling by Forming a Ternary Complex with SCUBE2-SHH

The strict coreceptor requirement for SCUBE2-SHH signaling suggested that SCUBE2 might interact with at least one of the coreceptors. Indeed, SCUBE2 bound robustly to CDON and BOC but did not bind GAS1 (Figure 4A), whereas SHH-N bound all three coreceptors (Figure 4B); furthermore, SCUBE1 and SCUBE3 also bound CDON (Figure S4A). Binding of fluorescent SCUBE2 to CDON was efficiently competed by excess unlabeled SCUBE2, but not by SHH-N (Figure 4C), indicating that SCUBE2 and SHH-N bind to distinct sites on CDON/BOC. Interestingly, affinity of SCUBE2 for CDON (Figure 4D) and BOC (Figure 4E) is very similar and considerably higher than the affinity of SHH-N for CDON (Figure 4F) and BOC (Figure 4G). Indeed, SHH in complex with SCUBE2 bound CDON/BOC with similar affinity as SCUBE2 alone, suggesting that it is SCUBE2 that drives recruitment of the SCUBE2-SHH complex by CDON/BOC to the cell surface.

We next mapped the SCUBE2-CDON/BOC interaction. For SCUBE2, we found a truncation mutant, $SCUBE2^{\Delta Spacer}$, which does not bind CDON (Figures S4B–S4D) but can still promote SHH release from cells (Figure S4E). For CDON/BOC, we found that SCUBE2 binds the first and second FN(III)-like repeats (FN1,2) (Figures 4H, S4F, and S4G), adjacent to the previously described SHH-binding site in the third FN(III)-like repeat (FN3) (Tenzen et al., 2006; Yao et al., 2006) (Figures 4I and S4H). SCUBE2-CDON binding was competed by purified CDON-FN1,2 but not by CDON-FN3 (Figures S4I and S4K), while the converse was true for SHH-N-CDON binding (Figures S4J and S4L). Notably, the regions of CDON (Figure 4H) and BOC (Figure S4G) required for SCUBE2 binding are precisely those required, together with FN3, to promote Hh signaling *in vivo* (Song et al., 2015). Finally, SCUBE2 in the SCUBE2-SHH complex bound to cells expressing CDON-FN3, although SCUBE2 alone did not

(F) As in (D), but treating wild-type MEFs, GAS1-null MEFs, or GAS1-null MEFs rescued with overexpressed GAS1. GAS1-null MEFs exhibit a ~30-fold reduction in SCUBE2-SHH EC_{50}, which is fully rescued upon GAS1 expression. Data are normalized between ciliary SMO for untreated cells and cells treated with saturating levels of SHH-N (100%).

(G) As in (B), but including GAS1-null MEFs. GAS1-null MEFs have a defect in responding to SCUBE2-SHH, but respond normally to SHH-N and SAG. At least 200 cilia were measured per condition.

(H) As in (B), but with coreceptor-null MEFs rescued with CDON, GAS1, or both. GAS1 fully rescues responsiveness to SCUBE2-SHH, while CDON rescues the response only partially.

(I) As in (H), but Hh signaling was measured by qRT-PCR for *Gli1*. Data are represented as in (C).

(J) As in (H), but with serial dilutions of SCUBE2-SHH-conditioned medium. Data are represented as in (D). CDON and GAS1 synergize at lower SCUBE2-SHH dose (1:640 dilution).

(K) As in (J), but cells were treated with SCUBE2-SHH conditioned medium at 1:640 dilution, and Hh signaling was measured by qRT-PCR for *Gli1*. Data are represented as in (C).

Please cite this article in press as: Wierbowski et al., Hedgehog Pathway Activation Requires Coreceptor-Catalyzed, Lipid-Dependent Relay of the Sonic Hedgehog Ligand, Developmental Cell (2020), https://doi.org/10.1016/j.devcel.2020.09.017

CellPress

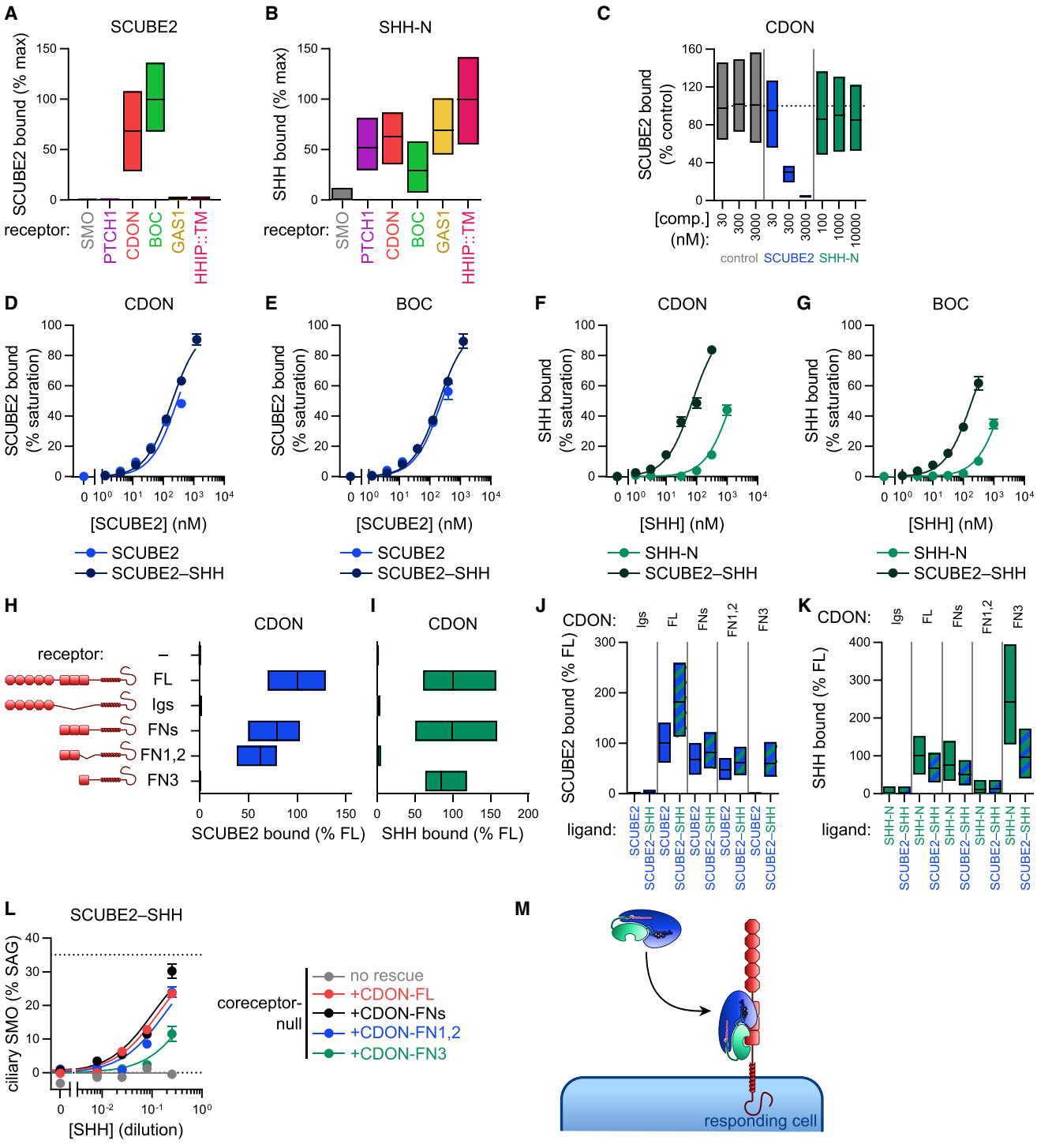

Figure 4. CDON/BOC Promote Hh Signaling by Binding SCUBE2-SHH

(A) Fluorescently labeled SCUBE2 (300 nM) was incubated with cells expressing EGFP-tagged SHH-binding proteins, and bound ligand was quantified by fluorescence microscopy. SCUBE2 binds to CDON/BOC, but not to other SHH interactors. Data are normalized between binding to EGFP-tagged SMO (negative control) and the highest bound signal (100%). Box plots represent median and the first and third quartiles of binding. At least 400 cells were measured per condition.

(B) As in (A), but using fluorescently labeled SHH-N (3 μM).

(C) Fluorescently labeled SCUBE2 (30 nM) was incubated with CDON-expressing cells, in the presence of increasing doses of unlabeled SCUBE2, SHH-N, or FLAG-HaloTag7 protein (FLAG-HT7, negative control). SCUBE2 and SHH-N do not compete for binding to CDON. Data are represented as in (A) but normalized between background signal (untreated cells) and binding in the presence of negative control competitor (100%).

(legend continued on next page)

Please cite this article in press as: Wierbowski et al., Hedgehog Pathway Activation Requires Coreceptor-Catalyzed, Lipid-Dependent Relay of the Sonic Hedgehog Ligand, Developmental Cell (2020), https://doi.org/10.1016/j.devcel.2020.09.017

(Figures 4J and 4K), indicating that SHH bridges CDON-FN3 and SHH. Conversely, SHH in the SCUBE2-SHH complex bound CDON-FN1,2 (Figures S4M and S4N), indicating that SCUBE2 bridges CDON-FN1,2 and SHH. These data indicate that the two components of SCUBE2-SHH bind to distinct sites in CDON/BOC, forming a ternary complex.

Finally, we examined the role of the interaction between CDON/BOC and SCUBE2-SHH in signaling. As shown in Figure 4L, CDON-FN1,2 enhanced SCUBE2-SHH signaling in coreceptor-null cells more strongly than did CDON-FN3, consistent with the higher affinity of SCUBE2 for CDON. Similarly, SHH complexed with SCUBE2$^{\Delta Spacer}$, which cannot bind CDON/BOC, had decreased signaling activity compared with wild-type SCUBE2-SHH (Figure S4O). These results show that the SCUBE2-CDON/BOC interaction (Figure 4M) is important for SHH reception.

SHH Is Directly Transferred from SCUBE2 to GAS1

Unlike CDON/BOC, GAS1 does not bind SCUBE2 and therefore must promote SCUBE2-SHH signaling by a different mechanism. We noticed that, when cells expressing GAS1 were incubated with SCUBE2-SHH, SHH bound to cells, but SCUBE2 did not (Figures 5A and 5B). In contrast, cells expressing two other SHH-binding proteins, a membrane-anchored, single-chain version of the anti-SHH antibody 5E1 (scFv5E1::TM, Figures S3B–S3D), or CDON-FN3, bound the entire SCUBE2-SHH complex (Figures 5A, 5B, 4J, and 4K). These results suggested that SHH is transferred from SCUBE2 to GAS1.

We hypothesized that GAS1 itself might suffice to unload SHH from SCUBE2, which we tested *in vitro* using purified components. The SCUBE2-SHH complex was incubated with the ectodomain of GAS1 (GAS1-Ecto, Figures S5A and S5B), and the reaction mix was analyzed by native gel electrophoresis. Strikingly, we observed a time-dependent transfer of SHH from SCUBE2-SHH to a discrete, low-molecular-weight species co-migrating with GAS1-Ecto (Figure 5C). Importantly, no SCUBE2 migrated with the newly formed SHH species. The rate of SHH transfer was greatly reduced at low temperature and accelerated at higher temperature (Figure S5C). To confirm that the low-molecular-weight species consists of SHH bound to GAS1-Ecto, we incubated SCUBE2-SHH with GAS1-Ecto conjugated to dextran (Figure S5D); SHH was now transferred to a species matching the molecular weight of dextran-GAS1-Ecto, indicating formation of a GAS1-Ecto-SHH complex (Figure S5E). Importantly, the ectodomain of GFRα1 (GFRα1-Ecto) (Figures S5F and S5G), a structural homolog of GAS1 (Cabrera et al., 2006) not involved in Hh signaling, did not accept SHH from SCUBE2-SHH (Figure S5H), demonstrating specificity of SHH transfer. In contrast to SHH transfer to GAS1, when SCUBE2-SHH was incubated with purified CDON ectodomain (CDON-Ecto) (Figures S5I and S5J), both SCUBE2 and SHH were shifted upward on the native gel, indicative of CDON-Ecto-SCUBE2-SHH complex formation (Figure 5D). Together, the results above show that GAS1 unloads SHH directly from SCUBE2, a unique property among SHH coreceptors.

GAS1 Is a Dual Palmitate- and Cholesterol-Binding Protein

The complete transfer of SHH from SCUBE2 to GAS1 suggests that GAS1 might bind both SHH lipid moieties. We next sought to determine whether GAS1 binds palmitate and cholesterol. Several results indicate that GAS1 binds palmitate. First, GAS1 bound SHH-N in a strict palmitate-dependent manner (Figures 5E and S6A); in contrast, CDON, BOC, and PTCH1 bound SHH-N irrespective of palmitoylation state (Figure S6B). Palmitate-dependence of SHH-N-GAS1 binding was not due to the GPI anchor of GAS1, as the same results were obtained when GAS1 was anchored via a transmembrane helix (Figure S6C). Second, GAS1 bound SHH effector peptide in a palmitate-dependent manner (Figure S6D), indicating that the globular part of SHH is dispensable for binding to GAS1. Third, purified GAS1 bound radioactive palmitate *in vitro* (see below). Consistent with GAS1 binding palmitate, GAS1-Ecto antagonized Hh pathway activation by SHH-N and SCUBE2-SHH (Figure 5F), as well as by palmitoylated effector peptide (Figure S6E); as

(D) Binding of fluorescently labeled SCUBE2, alone or in complex with SHH, to cells expressing EGFP-tagged CDON. SCUBE2 binds to CDON with mid-nanomolar affinity. Data are normalized between background signal (untreated cells) and maximum binding (100%) and are fit with a three-parameter curve. Points represent average binding for four replicates, and error bars represent SEM. At least 300 cells were measured per replicate. See Figure S4A for binding of SCUBE1 and SCUBE3.

(E) As in (D), but for BOC. SCUBE2 affinity for CDON and BOC is very similar.

(F) As in (D), but using anti-SHH (C9C5) immunofluorescence to compare SHH-N to SCUBE2-SHH. SHH in complex with SCUBE2 has an affinity for CDON similar to that of SCUBE2 alone, considerably higher than that of SHH-N alone.

(G) As in (F), but for BOC.

(H) As in (A), but with binding of fluorescently labeled SCUBE2 (30 nM) to CDON truncation mutants. Data are normalized between binding to SMO (negative control) and to full-length CDON (100%). SCUBE2 binds to the first and second FN(III)-like domains (FN1,2) of CDON. See Figure S4G for the corresponding BOC experiment.

(I) As in (H), but using fluorescently labeled SHH-N (300 nM). SHH-N binds to the third FN(III)-like domain (FN3) of CDON, as reported (Tenzen et al., 2006; Yao et al., 2006). See Figure S4H for the corresponding BOC experiment.

(J) As in (H), but using fluorescently labeled SCUBE2 (1.5 μM), alone or in complex with SHH (300 nM). SCUBE2 is recruited to CDON-FN3 via SHH. At least 600 cells were measured per condition. See Figures S4M and S4N for evidence of recruitment of SHH to CDON by SCUBE2.

(K) As in (J), but using anti-SHH (C9C5) immunofluorescence to compare SHH-N with SCUBE2-SHH.

(L) Dose-response of SCUBE2-SHH conditioned medium on coreceptor-null MEFs or coreceptor-null MEFs rescued with CDON truncation mutants. Hh pathway activation was measured by endogenous SMO recruitment to cilia. The SCUBE2-interacting CDON-FN1,2 domain enhances signaling more strongly than the SHH-interacting CDON-FN3 domain. For each line, data are normalized between ciliary SMO for untreated cells and cells treated with saturating SAG (100%). Upper dotted line represents maximum signaling by SCUBE2-SHH on wild-type cells. Data are fit with a three-parameter curve. Points represent average ciliary SMO for three replicates, and error bars represent SEM. At least 100 cilia were measured per replicate. See also Figure S4O, showing reduced activity of SHH complexed with a SCUBE2 mutant defective in CDON binding.

(M) Proposed model of CDON/BOC function. CDON/BOC bind both SCUBE2 (via FN1,2) and SHH (via FN3) to recruit the complex to the surface of responding cells.

See Figure S4 for additional characterization of the SCUBE2-CDON/BOC interaction.

Please cite this article in press as: Wierbowski et al., Hedgehog Pathway Activation Requires Coreceptor-Catalyzed, Lipid-Dependent Relay of the Sonic Hedgehog Ligand, Developmental Cell (2020), https://doi.org/10.1016/j.devcel.2020.09.017

CellPress

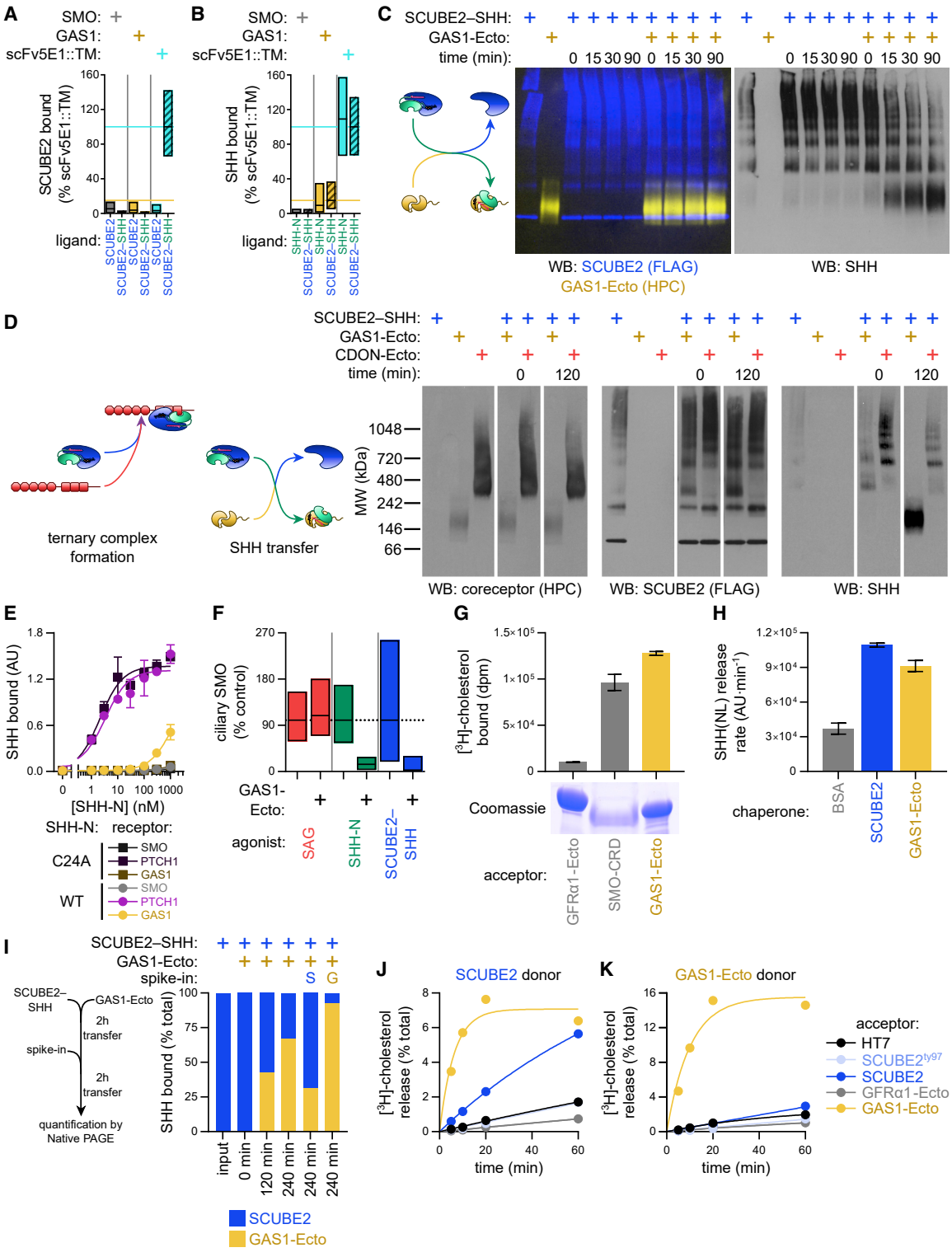

Figure 5. GAS1 Is a Palmitate- and Cholesterol-Binding Protein that Unloads SHH from SCUBE2

(A) Fluorescently labeled SCUBE2 (600 nM), alone or in complex with SHH(HPC7) (300 nM), was incubated with cells expressing EGFP-tagged GAS1, scFv5E1::TM (positive control), or SMO (negative control), and bound SCUBE2 was measured by fluorescence microscopy. Even when complexed with SHH(HPC), SCUBE2 is not recruited to GAS1, in contrast to scFv5E1::TM. Data are normalized between binding of SCUBE2-SHH(HPC) to the negative and positive controls. At least 600 cells were measured per condition.

(legend continued on next page)

Please cite this article in press as: Wierbowski et al., Hedgehog Pathway Activation Requires Coreceptor-Catalyzed, Lipid-Dependent Relay of the Sonic Hedgehog Ligand, Developmental Cell (2020), https://doi.org/10.1016/j.devcel.2020.09.017

expected, GAS1-Ecto had no effect on Hh pathway activation by SAG (Figure 5F). Importantly, Hh signaling inhibition was observed at doses of GAS1-Ecto (Figure S6F) similar to those required for GAS1 binding to SHH-N (Figures 5E and S3H).

To determine whether GAS1 also binds cholesterol, GAS1-Ecto was incubated with radiolabeled cholesterol, was immunopurified, and co-purifying radioactivity was measured. As shown in Figure 5G, GAS1-Ecto, but not the related GFRα1-Ecto, bound cholesterol to a similar extent as an equimolar amount of the extracellular cysteine-rich domain (CRD) of SMO, a well-characterized cholesterol-binding protein (Nachtergaele et al., 2013; Nedelcu et al., 2013; Byrne et al., 2016; Huang et al., 2016). This result indicates that GAS1 binds cholesterol.

Since GAS1 binds both SHH lipid moieties, GAS1-Ecto should be capable of solubilizing doubly lipidated SHH, similar to SCUBE2. Indeed, GAS1-Ecto co-expression caused release of wild-type SHH (Figure S6G) from producing cells. Furthermore, purified GAS1-Ecto added to cells expressing NanoLuc luciferase-tagged SHH (SHH(NL)) (Petrov et al., 2020) led to the rapid release of SHH(NL), at a rate comparable to that caused by purified SCUBE2 (Figure 5H). Finally, we found that GAS1-Ecto formed a stable complex with SHH (dually lipidated), with SHH-N (palmitoylated-only), or with SHH(C24A) (cholesterylated-only) (Taylor et al., 2001), but not with SHH-N(C24A) (unlipidated) (Figure S6H). Thus, GAS1 independently binds both SHH lipid moieties, and at least one lipid is necessary and sufficient to form a stable GAS1-SHH complex.

SHH Transfer from SCUBE2 to GAS1 Is Mass Action-Driven and Favors GAS1-SHH Complex Formation

We next asked whether transfer of SHH from SCUBE2 to GAS1 is reversible. Excess SCUBE2-SHH was incubated with GAS1-Ecto until SHH transfer reached saturation (Figures 5I and S6I). Then SCUBE2 or GAS1-Ecto was added in 5-fold molar excess relative to initial GAS1-Ecto, and the reaction was allowed to proceed further. Additional GAS1-Ecto drove the SHH transfer reaction forward, while additional SCUBE2 caused back transfer of SHH from GAS1-Ecto to SCUBE2 (Figures 5I and S6I). These results demonstrate that GAS1 and SCUBE2 participate in a mass-action-driven SHH transfer reaction. We also observed robust transfer of SHH from SCUBE2-SHH to SCUBE2 (Figure S6J), and from GAS1-Ecto-SHH to GAS1-Ecto, indicating that SHH complexation by SCUBE2 and GAS1 is dynamic, with SHH being constantly exchanged between identical lipid-binding protein molecules.

We next asked what the role of individual lipid moieties in SHH transfer is. Complexes of GAS1-Ecto with SHH modified with one or both lipids were incubated with empty SCUBE2, and we assayed SHH back transfer (Figure S6K). In all cases, SHH was transferred to SCUBE2, indicating that each SHH lipid moiety can be independently transferred.

In several SHH transfer reactions (Figures 5C, 5I, S5C, and S5H), we observed that more SHH bound to GAS1-Ecto than to SCUBE2, even though SCUBE2 and GAS1 were present at comparable concentrations in excess of SHH (Table S4). We thus wondered whether this bias arises from differential affinity of SCUBE2 and GAS1 for SHH lipids. To address this question, we measured the rate of cholesterol transfer from SCUBE2 (Figure 5J) or GAS1-Ecto (Figure 5K) bound to beads, to SCUBE2 or GAS1-Ecto in solution. SCUBE2 beads transferred cholesterol to both SCUBE2 and GAS1-Ecto, but the latter released cholesterol much more rapidly (Figure 5J). Strikingly, GAS1-Ecto beads did not transfer cholesterol to SCUBE2 but readily transferred to GAS1-Ecto (Figure 5K). Similar results were observed with

(B) As in (A), but using anti-HPC immunofluorescence to compare binding of SCUBE2-SHH(HPC7) and SHH-N(HPC7). SHH(HPC) accumulates, without SCUBE2, on GAS1-expressing cells incubated with SCUBE2-SHH(HPC).
(C) Purified SCUBE2-SHH (400 nM) was incubated at room temperature, with or without purified GAS1 ectodomain (GAS1-Ecto) (2 μM), prior to separation by Blue Native PAGE and immunoblotting. SHH is transferred from SCUBE2 to GAS1-Ecto.
(D) As in (C), but SCUBE2-SHH was incubated with GAS-Ecto (10 μM) or CDON ectodomain (CDON-Ecto) (10 μM). GAS1-Ecto unloads SHH from SCUBE2, whereas CDON-Ecto forms a ternary complex.
(E) Purified palmitoylated SHH-N (circles) or unpalmitoylated SHH-N(C24A) (squares) was added to cells expressing EGFP-tagged GAS1, PTCH1 (positive control), or SMO (negative control), and bound ligand was measured by fluorescence microscopy. GAS1 binds SHH-N in a palmitate-dependent manner. Data are normalized between binding to negative and positive controls and are fit with a three-parameter curve. Points represent average binding for four replicates, and error bars represent SEM. At least 200 cells were measured per replicate.
(F) MEFs were treated with the indicated Hh pathway activators, in the presence of purified GAS1-Ecto (2 μM) or control competitor (FLAG-HT7) (2 μM). Recruitment of endogenous SMO to cilia was measured by immunofluorescence. GAS1-Ecto antagonizes signaling by SCUBE2-SHH and SHH-N. For each agonist, data are normalized between ciliary SMO for untreated cells and cells treated in the presence of control competitor (100%). Box plots represent median and the first and third quartiles of SMO intensity. At least 200 cilia were measured per condition.
(G) Equimolar amounts of purified HPC-tagged GAS1-Ecto, SMO-CRD (positive control), or GFRα1-Ecto (negative control) were incubated with [^{3}H]-cholesterol, and affinity captured on anti-HPC beads. Bound protein was eluted with HPC peptide (gel, bottom), and associated radioactivity was measured (graph, top). GAS1-Ecto binds cholesterol, similar to SMO-CRD. Bars represent average radioactivity for three replicates, and error bars represent SEM.
(H) Purified GAS1-Ecto, SCUBE2, or BSA (negative control) was added (1 μM) to HEK293T cells stably expressing NanoLuc luciferase-tagged SHH [SHH(NL)], and SHH(NL) release was measured as a function of time. Purified GAS1-Ecto releases dually lipidated SHH with a similar rate to SCUBE2. Bars represent average release rate across six time points, and error bars represent standard error of the linear fit to the release time course.
(I) SCUBE2-SHH (400 nM) was incubated at room temperature with GAS1-Ecto (2 μM). After 2 h, when considerable SHH had transferred from SCUBE2 to GAS1, excess (10 μM) SCUBE2, GAS1-Ecto, or buffer was added, and the reaction allowed to continue for 2 h (schematic, left). Samples were analyzed in as in (C), and the percentage of SHH associated with SCUBE2 (blue) and GAS1-Ecto (yellow) was quantified for each lane (graph, right). SHH transfer between SCUBE2 and GAS1-Ecto is driven by mass action. See Figure S6I for the corresponding blot.
(J) SCUBE2 was loaded with [^{3}H]-cholesterol and was captured on beads. The beads were incubated with purified GAS1-Ecto, SCUBE2, or negative controls (2 μM), and released radioactivity was measured as a function of time across four time points of a single measurement. Data are fit with a one-phase association curve. Both SCUBE2 and GAS1-Ecto accept cholesterol from SCUBE2.
(K) As in (J), but with [^{3}H]-cholesterol-loaded GAS1-Ecto on beads. Only GAS1-Ecto, but not SCUBE2, accepts cholesterol from GAS1-Ecto.
See Figures S5 and S6 for further characterization of SHH transfer from SCUBE2 to GAS1-Ecto and of GAS1 lipid binding.

Please cite this article in press as: Wierbowski et al., Hedgehog Pathway Activation Requires Coreceptor-Catalyzed, Lipid-Dependent Relay of the Sonic Hedgehog Ligand, Developmental Cell (2020), https://doi.org/10.1016/j.devcel.2020.09.017

CellPress

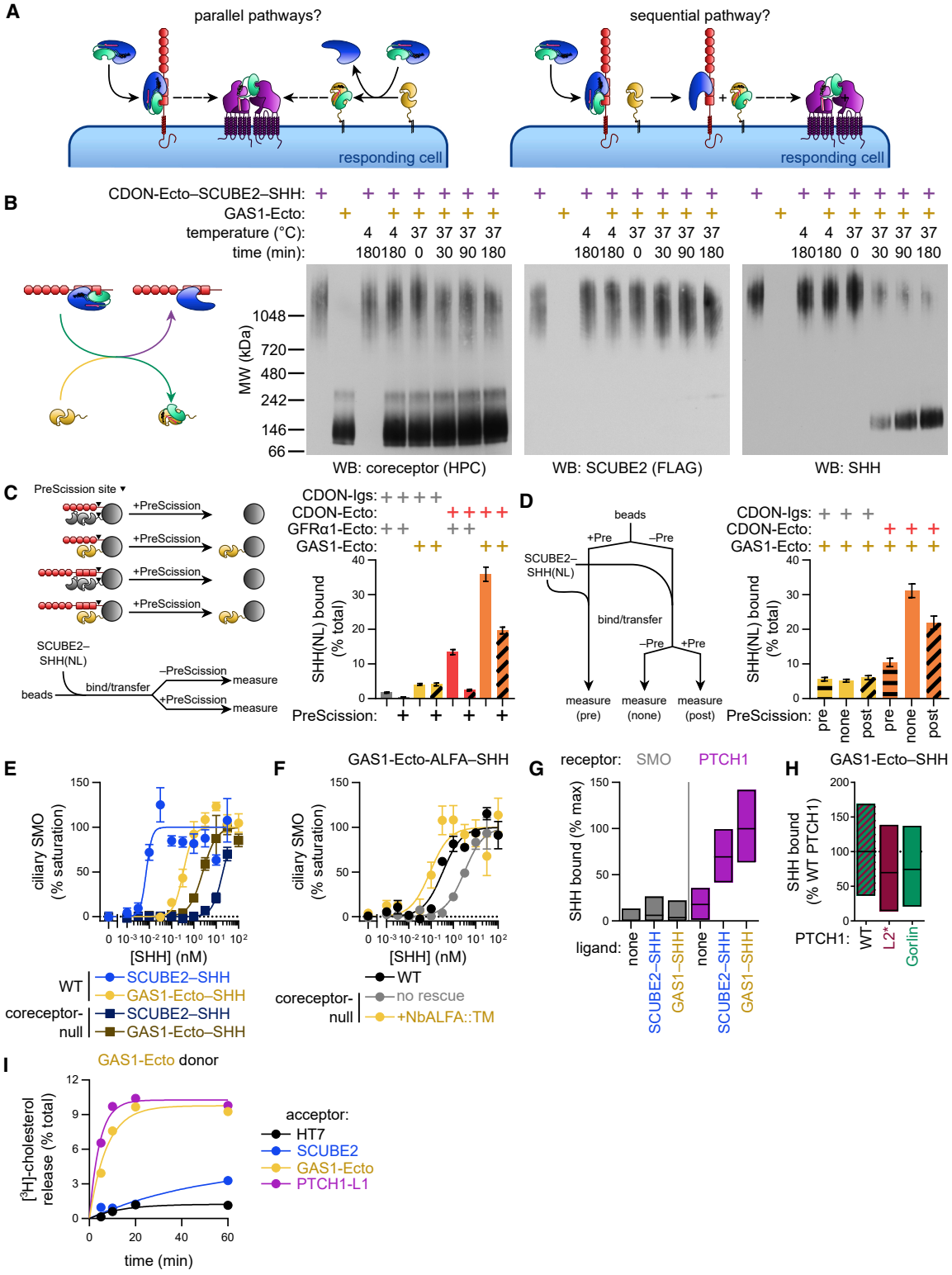

Figure 6. CDON/BOC and GAS1 Cooperate to Unload SHH from SCUBE2 and Transfer SHH to PTCH1

(A) Two possible pathway architectures for SHH coreceptors. Left: CDON/BOC and GAS1 act in parallel to promote SHH reception upstream of PTCH1. Right: CDON/BOC and GAS1 act together, in series.

(B) Purified CDON-SCUBE2-SHH ternary complex (400 nM) was incubated with purified GAS1-Ecto (2 μM), and the reaction was analyzed by Blue Native PAGE and immunoblotting. GAS1-Ecto unloads SHH from CDON-SCUBE2-SHH. See Figure S7E for purification of the CDON-SCUBE2-SHH complex.

(legend continued on next page)

Please cite this article in press as: Wierbowski et al., Hedgehog Pathway Activation Requires Coreceptor-Catalyzed, Lipid-Dependent Relay of the Sonic Hedgehog Ligand, Developmental Cell (2020), https://doi.org/10.1016/j.devcel.2020.09.017

radiolabeled palmitate, although the transfer saturated too rapidly to obtain kinetic data (Figures S6L and S6M). Together, these results show that while SHH lipid transfer between SCUBE2 and GAS1 is reversible, the forward reaction from SCUBE2 to GAS1 is favored at the level of lipid binding itself.

CDON/BOC Facilitates SHH Transfer to GAS1 by Concentrating SCUBE2-SHH

While either CDON/BOC or GAS1 suffices to promote at least some level of signaling by SCUBE2-SHH, a maximum response requires both coreceptor classes (Figure 3). We envision two possibilities (Figure 6A): (1) CDON/BOC and GAS1 function independently, promoting signaling through two parallel pathways that integrate at the level of PTCH1, and (2) CDON/BOC and GAS1 can act together, in a sequential pathway that leads to PTCH1.

Since CDON and GAS1 compete for binding SHH-N (McLellan et al., 2008) (Figures S7A–S7D), we first asked whether GAS1 can accept SHH from SCUBE2-SHH bound to CDON. When the purified ternary CDON-Ecto-SCUBE2-SHH complex (Figure S7E) was incubated with GAS1-Ecto, a GAS1-Ecto-SHH complex was formed in a time-dependent manner (Figure 6B). Thus, SHH can be transferred from CDON-SCUBE2-SHH to GAS1, even though SHH is bound to both SCUBE2 and CDON. This result is consistent with CDON and GAS1 functioning cooperatively in SCUBE2-SHH reception.

The SHH transfer reactions above were performed in solution, at relatively high concentrations (high nanomolar to low micromolar; Table S4) of purified components. To determine if CDON facilitates transfer of SHH from SCUBE2 to GAS1, we developed a bead-based recruitment/transfer assay (Figures 6C and S7F) that recreates a situation closer to that found on the cell surface, where a dilute solution of SCUBE2-SHH interfaces with locally concentrated coreceptors. When beads bearing CDON-Ecto or GAS1-Ecto were incubated with purified SCUBE2-SHH, a much greater amount of SHH accumulated on CDON-Ecto beads compared with GAS1-Ecto beads (Figure 6C). However, beads bearing both CDON-Ecto and GAS1-Ecto accumulated a greater than additive amount of SHH, suggesting that CDON and GAS1 cooperated to enhance SHH accumulation (Figure 6C). To distinguish between SHH bound to CDON-Ecto and to GAS1-Ecto, CDON-Ecto was selectively eluted from beads using an engineered PreScission protease site (Figure 6C). As expected, SHH bound to CDON-Ecto beads was eluted upon protease treatment, but not SHH bound to GAS1-Ecto beads (Figure 6C). Protease treatment reduced SHH bound to CDON-Ecto/GAS1-Ecto beads by a similar amount as for the beads bearing only CDON-Ecto; however, significantly more SHH was left on protease-treated CDON-Ecto/GAS1-Ecto beads than on beads bearing only GAS1-Ecto (Figure 6C). When CDON-Ecto was removed from CDON-Ecto/GAS1-Ecto beads prior to incubation with SCUBE2-SHH, much less SHH was bound than the amount left when CDON-Ecto was removed after incubation (Figures 6D and S7G–S7I), confirming that CDON-Ecto must be present together with GAS1-Ecto to enhance SHH accumulation. Together, these results show that CDON facilitates SHH transfer to GAS1, by locally concentrating the SCUBE2-SHH complex.

SHH Is Transferred from GAS1 to PTCH1

Since GAS1 is sufficient to promote signaling by SCUBE2-SHH, we reasoned that GAS1 should readily transfer SHH to PTCH1. To address this, we first investigated the signaling activity of purified GAS1-Ecto-SHH. GAS1-Ecto-SHH was significantly less potent than SCUBE2-SHH on wild-type cells (Figure 6E), consistent with loss of SCUBE2-dependent recruitment via CDON/BOC. However, on coreceptor-null cells, the opposite was observed: GAS1-Ecto-SHH was more potent than SCUBE2-SHH (Figure 6E). This activity profile resembles closely that of SHH-N, in which the palmitate moiety is accessible to PTCH1 (Figure 3D), suggesting that, in contrast to SCUBE2, GAS1 binds SHH in a manner that allows formation of the palmitate-dependent SHH-PTCH1 interaction. Notably, the signaling potency of GAS1-Ecto-SHH on coreceptor-null cells was enhanced by its

(C) Purified SCUBE2-SHH(NL) (20 nM) was incubated with beads bearing combinations of CDON-Ecto, GAS1-Ecto, and their respective negative controls (see schematic). After 1 h, beads were treated with PreScission protease, to remove all proteins except GAS1-Ecto, and bead-bound luminescence was measured. CDON-dependent recruitment of SCUBE2-SHH(NL) to beads drives SHH(NL) transfer from SCUBE2 to GAS1. Bars represent average for three replicates, and error bars represent SD. See also immunoblot in Figure S7F.

(D) As in (C), but beads were treated with PreScission protease before or after incubation with SCUBE2-SHH(NL). CDON-Ecto is required to promote transfer of SHH(NL) from SCUBE2 to GAS1-Ecto. See also Figures S7G–S7I.

(E) Dose-response of purified GAS1-Ecto-SHH and SCUBE2-SHH on wild-type and coreceptor-null MEFs. GAS1-Ecto-SHH is less potent than SCUBE2-SHH on wild-type cells, but more potent than SCUBE2-SHH on coreceptor-null cells. Data are normalized between ciliary SMO for untreated cells and the theoretical maximum (100%), as fit with a four-parameter curve. Points represent average ciliary SMO for three replicates, and error bars represent SEM. At least 100 cilia were measured per replicate.

(F) As in (E) but comparing purified ALFA-tagged GAS1-Ecto-SHH complex on wild-type and coreceptor-null MEFs, stably expressing or not membrane-anchored ALFA nanobody (NbALFA::TM). Direct recruitment of GAS1-Ecto-SHH to the surface of coreceptor-null cells enhances signaling.

(G) GAS1-Ecto-SHH or SCUBE2-SHH (500 nM) was incubated with cells expressing EGFP-tagged PTCH1 or SMO (negative control), and bound SHH was measured by anti-SHH (C9C5) immunofluorescence. More SHH is transferred to PTCH1 from GAS1 than from SCUBE2. Data are normalized between binding of SCUBE2-SHH to the negative and positive controls. At least 300 cells were measured per condition.

(H) As in (G), but with GAS1-Ecto-SHH (500 nM) incubated with cells expressing PTCH1 mutants defective in the protein-protein ($PTCH1^{L2^*}$) or palmitate-protein ($PTCH1^{Gorlin}$) interface with SHH. SHH is transferred normally from GAS1 to the PTCH1 mutants. Data are normalized between background signal (untreated cells) and binding to wild-type PTCH1 (100%). At least 1,000 cells were measured per condition.

(I) GAS1-Ecto was loaded with [^{3}H]-cholesterol and was captured on beads. The beads were incubated with purified GAS1-Ecto, SCUBE2, a soluble version of the first large extracellular loop of PTCH1 (PTCH1-L1), or HT7 negative control (2 μM), and released radioactivity was measured as a function of time across four time points of a single measurement. Data are fit with a one-phase association curve. Cholesterol is rapidly transferred from GAS1-Ecto to PTCH1-L1 and GAS1-Ecto, but not to SCUBE2.

See Figure S7 for additional characterization of purified proteins, bead-based recruitment/transfer assay, and heterologous cell-surface recruitment assay.

Please cite this article in press as: Wierbowski et al., Hedgehog Pathway Activation Requires Coreceptor-Catalyzed, Lipid-Dependent Relay of the Sonic Hedgehog Ligand, Developmental Cell (2020), https://doi.org/10.1016/j.devcel.2020.09.017

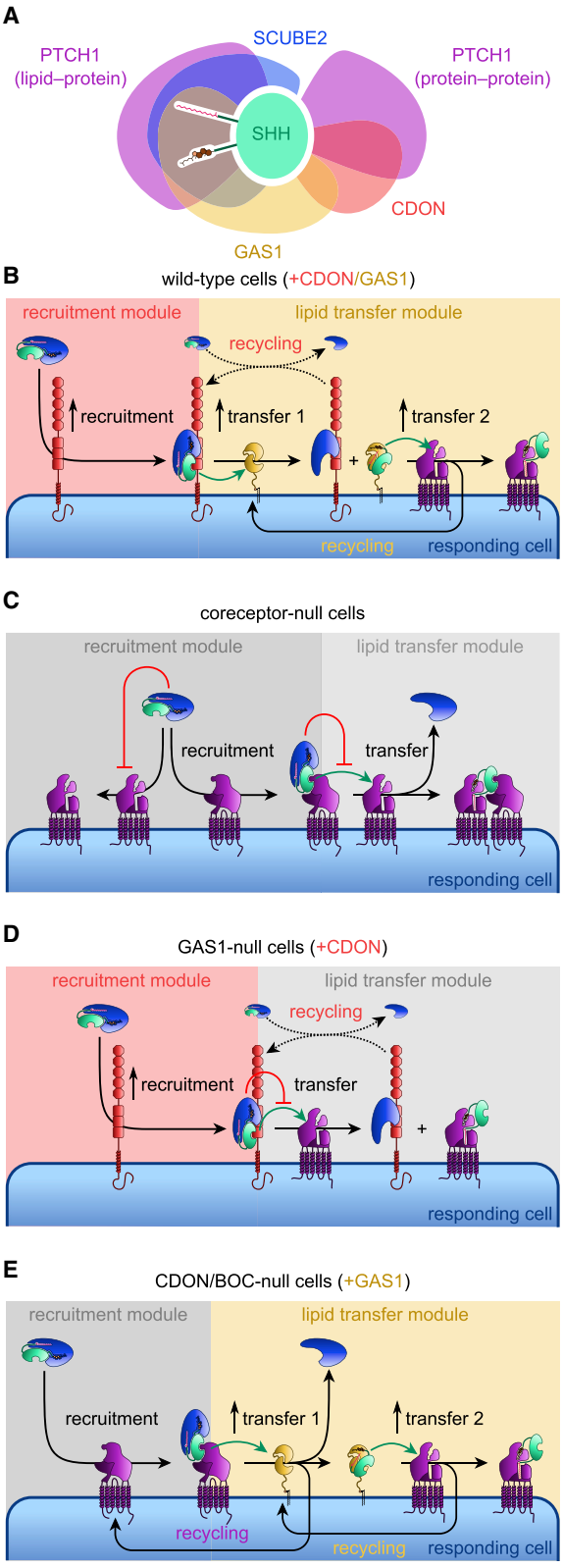

Figure 7. The Coreceptor-Catalyzed Pathway for Lipid-Dependent SHH-PTCH1 Complex Assembly

(A) Schematic of SHH interactions involved in SHH delivery. Interfaces between SHH and PTCH1 (Qi et al., 2018a; Qian et al., 2018; Rudolf et al., 2019) and CDON (McLellan et al., 2008) are based on published structures, while interfaces between SHH and SCUBE2 and GAS1 are drawn based on the present study. SHH engages in successive, mutually exclusive interactions during its movement from SCUBE2 to PTCH1.

(B) SHH reception in wild-type cells, which contain both CDON/BOC and GAS1. CDON/BOC recruits SCUBE2-SHH to the cell surface, facilitating SHH transfer to GAS1, followed by transfer to PTCH1.

(C) SHH reception in coreceptor-null cells. PTCH1 recruits SCUBE2-SHH only poorly to the cell surface, and accepts SHH from SCUBE2 at a low basal rate.

(D) SHH reception in cells with CDON/BOC only. CDON/BOC recruit SCUBE2-SHH more readily than PTCH1 but do not enhance SHH transfer from SCUBE2 to PTCH1.

(E) SHH reception in cells with GAS1 only. GAS1 does not recruit SCUBE2-SHH to the cell surface but catalyzes SHH transfer from SCUBE2 to PTCH1.

direct recruitment to the cell surface via a heterologous membrane receptor (Figure 6F; see Figures S7J–S7L for validation of the ALFA recruitment system), suggesting that, as with transfer of SHH from CDON to GAS1, transfer of SHH from GAS1 to PTCH1 is facilitated by local co-concentration.

Next, we compared binding of SCUBE2-SHH and GAS1-Ecto-SHH to PTCH1. At high SCUBE2-SHH concentration, SHH, but not SCUBE2, accumulated on PTCH1-expressing cells (Figures S7M and S7N), similar to what we observed when SCUBE2-SHH was incubated with GAS1-expressing cells (Figures 5A and 5B). Thus, SHH is transferred from SCUBE2 to PTCH1 at some rate, once SCUBE2-SHH is recruited to PTCH1 via the pseudo-active site in SHH. Importantly, GAS1-Ecto-SHH transferred a greater amount of SHH to PTCH1-expressing cells compared with SCUBE2-SHH (Figure 6G). Additionally, GAS1-Ecto-SHH transferred SHH just as readily to PTCH1$^{L2^*}$, defective in SHH-PTCH1 protein-protein interaction, and PTCH1^{Gorlin}, defective in SHH palmitate-PTCH1 interaction, as to wild-type PTCH1 (Figure 6H), suggesting that SHH in the GAS1-Ecto-SHH complex can engage PTCH1 via either the protein-dependent or lipid-dependent interfaces, in contrast to SHH bound to SCUBE2.

Finally, we asked whether SHH transfer from GAS1 to PTCH1 might be driven by differential affinity for SHH lipids, similar to transfer from SCUBE2 to GAS1. We focused on the SHH cholesterol moiety, which binds to a surface-exposed pocket within the first large extracellular loop of PTCH1 (PTCH1-L1) (Qian et al., 2018; Rudolf et al., 2019) (Figure 2B), because, conveniently, PTCH1-L1 can be purified in isolation (Figures S7O and S7P). Cholesterol was rapidly transferred from GAS1-Ecto to PTCH1-L1, but not to SCUBE2 (Figure 6I); as before, cholesterol was also rapidly exchanged between GAS1 molecules. These results suggest that transfer of SHH from GAS1 to PTCH1 is driven, at least in part, by affinity for the SHH cholesterol moiety.

DISCUSSION

Our results suggest the following scenario for SHH movement from producing cells to responding cells. SHH is released as a soluble and highly potent SCUBE2-SHH complex, assembled by DISP1, which transfers the SHH lipid moieties from the membrane to SCUBE2 (Tukachinsky et al., 2012). Surprisingly, we find that SCUBE2-SHH cannot directly signal through PTCH1, because SCUBE2 blocks the palmitate-mediated interaction between SHH and PTCH1 (Figure 7A), required to trigger Hh

Please cite this article in press as: Wierbowski et al., Hedgehog Pathway Activation Requires Coreceptor-Catalyzed, Lipid-Dependent Relay of the Sonic Hedgehog Ligand, Developmental Cell (2020), https://doi.org/10.1016/j.devcel.2020.09.017

pathway activation (Tukachinsky et al., 2016). We demonstrate that the coreceptors CDON/BOC and GAS1 are critical for signaling by SCUBE2-SHH, cooperating to unload SHH and to promote formation of a signaling-competent SHH-PTCH1 complex. In a first step, CDON/BOC bind SCUBE2-SHH with high affinity by interacting with both components, thus recruiting the complex to the cell surface. Second, the SHH lipid moieties are handed off from SCUBE2 to GAS1, causing complete dissociation of SHH from CDON/BOC-SCUBE2. Third, another dual lipid handoff occurs between GAS1 and PTCH1, resulting in SHH finally bound to PTCH1. Our findings thus reveal a novel coreceptor-catalyzed pathway for SHH reception (Figure 7B), providing a mechanistic basis for the essential role of the coreceptors in Hh signaling *in vivo* (Allen et al., 2011).

The biochemical nature of endogenous Hh ligands has been the subject of considerable study and debate (Petrov et al., 2017). The pioneering work of Zeng et al. (2001) described a potent, high-molecular-weight (~100 kDa) SHH species produced by cultured cells and limb bud explants, close in size to a monomeric 1:1 SCUBE2-SHH complex (120 kDa). We thus propose that SCUBE2-SHH is a minimal, defined species that recapitulates the properties of the endogenous Hh ligand, including its strict dependence on DISP1 for release from producing cells, and on CDON/BOC and GAS1 for reception by responding cells (Allen et al., 2011). We find that the SCUBE2-SHH complex is held together largely by hydrophobic interactions between SCUBE2 and the SHH lipid moieties. This result stands in contrast with a previous model, which proposed that SCUBE2 promotes SHH release by enhancing sheddase-mediated removal of lipidated SHH termini (Jakobs et al., 2014).

Based on our results, SHH reception by responding cells can be divided into a recruitment step and a lipid transfer step. In cells lacking coreceptors (Figure 7C), PTCH1 must perform both recruitment and lipid transfer functions, though it is optimal for neither. Because SCUBE2 blocks the palmitate-dependent interaction between SHH and PTCH1, PTCH1 engages SCUBE2-SHH only through the pseudo-active site of SHH, thus reducing affinity. After binding, direct transfer of SHH lipids from SCUBE2 to PTCH1 can occur, but with low efficiency, as suggested by Hh pathway activation in coreceptor-null cells by very high levels of SCUBE2-SHH. In contrast, PTCH1 engages SHH-N through both interaction modes, explaining the higher potency we observe for SHH-N relative to SCUBE2-SHH in coreceptor-null cells.

CDON/BOC and GAS1 serve as dedicated recruitment and lipid transfer modules, respectively. CDON/BOC enhance SCUBE2-SHH recruitment to the membrane, by virtue of higher affinity for the complex compared with PTCH1. However, CDON/BOC alone promote signaling only modestly, because SHH lipid transfer to PTCH1 remains limiting (Figure 7D). GAS1 provides a more efficient mechanism for enhancing SCUBE2-SHH potency, by catalyzing SHH transfer from SCUBE2 to PTCH1. The ability of GAS1 to continuously accept SHH from SCUBE2 and pass it to PTCH1 means it can integrate considerable SHH signal even without CDON/BOC (Figure 7E). However, concentrating SCUBE2-SHH at the membrane via CDON/BOC drives SHH transfer to GAS1 more rapidly than when SCUBE2-SHH engages GAS1 from dilute solution. Thus, CDON/BOC and GAS1 enhance SCUBE2-SHH signaling synergistically (Figure 7B).

What happens to the CDON/BOC-SCUBE2 complex after SHH is transferred to GAS1? We speculate that CDON/BOC is recycled, by exchanging "spent" SCUBE2 for "fresh" SCUBE2-SHH (Figure 7B). Our results suggest two possible scenarios. Since SHH can be transferred between SCUBE2 molecules, SCUBE2-SHH in solution could transfer SHH to CDON/BOC-SCUBE2. Alternatively, SCUBE2-SHH could displace unliganded SCUBE2 on CDON/BOC, driven by higher affinity of CDON/BOC for SCUBE2-SHH; this is supported by our observation that CDON preferentially binds SCUBE2-SHH even in presence of excess SCUBE2 (Figure S7E). We note that, while we did not detect a difference between the affinities of SCUBE2 and SCUBE2-SHH for CDON, our measurements likely underestimate SCUBE2-SHH affinity, as SCUBE2-SHH preparations contain significant amounts of unliganded SCUBE2.

The relative contributions of GAS1 and CDON/BOC to SCUBE2-SHH reception match the phenotypes observed *in vivo*, in mouse embryos (Allen et al., 2011). The key role of GAS1 is consistent with the generally more severe consequence of GAS1 loss compared with CDON or BOC loss, in both the neural tube and limb bud. The more peripheral role of CDON/BOC in SCUBE2-SHH reception is consistent with the variable requirement for CDON/BOC *in vivo*. In the limb bud, CDON/BOC are entirely dispensable; only in the context of GAS1 loss, BOC compensates weakly (Allen et al., 2011). In the neural tube, however, loss of CDON/BOC resembles loss of GAS1 (Allen et al., 2011). This result suggests that the importance of CDON/BOC may vary with tissue topology. In the polarized epithelium of the neural tube, where SHH contacts cells via the basolateral surface, perhaps capture of SCUBE2-SHH by CDON/BOC and subsequent transfer of SHH to GAS1 is important for moving SHH to the apical surface, where the primary cilium, the site of PTCH1, is located.

The SHH release and reception mechanisms described here are compatible with the proposed role of cytonemes (Callejo et al., 2011; Bischoff et al., 2013; Chen et al., 2017; Hall et al., 2020) and exosomes (Gradilla et al., 2014; Matusek et al., 2014) as SHH carriers. In both cases, SHH faces the biochemical problem of having to traverse the aqueous space between donor membrane and responding cell membrane. Thus, the same successive lipid-dependent transfers are needed to move SHH from DISP1 to SCUBE2, then to the coreceptors, and finally to PTCH1, irrespective of the distance between the two membranes. Importantly, even though purified SCUBE2-SHH is soluble, this does not imply that endogenous SHH is freely diffusible, since the space available for diffusion between membranes might be highly restricted. It remains to be determined where the various SHH transfers occur, and what is the lifetime of each intermediate species.

Dual lipidation is a conserved feature of Hh ligands, both in vertebrates and in *Drosophila*. Like SHH, the *Drosophila* Hh ligand requires Dispatched for release, as well as the CDON/BOC orthologs, Ihog/Boi, for reception. Interestingly, however, SCUBE and GAS1 are absent from *Drosophila*. How then is the *Drosophila* Hh ligand chaperoned from producing cells to the Ptc receptor? One possibility is that the secreted protein Shifted (Shf) plays a SCUBE-like role. In support of this view, Shf is necessary for Hh ligand release from cells and for long-distance signaling in *Drosophila* (Glise et al., 2005; Gorfinkiel et al., 2005).

Additionally, Shf binds Hh (Glise et al., 2005; Gorfinkiel et al., 2005), is likely a lipid-binding protein (Liepinsh et al., 2006; Malinauskas et al., 2011), and interacts with Ihog/Boi (Avanesov and Blair, 2013; Bilioni et al., 2013). Perhaps, in contrast to SCUBE2, Shf transfers the Hh lipids directly to Ptc. Alternatively, another factor, such as the GPI-anchored Dlp (Yao et al., 2006; Williams et al., 2010; Yan et al., 2010; Kim et al., 2011), which was recently shown to bind the Wg lipid moiety (McGough et al., 2020), might perform a GAS1-like function in *Drosophila* Hh reception.

It appears that SHH lipids are always engaged with physiological binding partners, ensuring that SHH will not aggregate. An interesting aspect is that interactions of SHH lipids with proteins are dynamic, allowing SHH to be transferred between mutually exclusive binding partners (Figure 7A). In particular, SCUBE2 molecules readily exchange SHH among themselves. We speculate that this ability, together with SCUBE2 propensity for oligomerization, might provide a novel mechanism for intercellular SHH transport, distinct from simple diffusion. For example, SCUBE2 is expressed in the dorsal neural tube (Grimmond et al., 2001; Kawakami et al., 2005; Woods and Talbot, 2005), opposite the site of SHH production in the notochord and floor plate (Echelard et al., 1993; Riddle et al., 1993). A concentration gradient of SCUBE2 within the neural tube, maintained by interaction with cell-surface factors, such as glycosaminoglycans or CDON/BOC, could serve as a ''bucket-brigade''-like conduit for SHH, guiding its travel in a defined direction. Several aspects of these SHH lipid-dependent processes remain to be elucidated. In particular, it will be useful to obtain a molecular understanding of how SHH lipids are recognized and handed off along the entire pathway of ligand synthesis, release from cells, and reception.

The distributed SHH coreceptor system stands in contrast with traditional coreceptors, which facilitate signaling by binding ligand in cooperation with a primary receptor. CDON/BOC and GAS1 define a different ligand reception paradigm: a duo of ''pre-receptors'' that transit SHH through sequential interactions upstream of the PTCH1 receptor. We speculate that, during evolution, this system provided opportunities for modulating SHH signaling via feedback inhibition (Chen and Struhl, 1996), either by downregulating coreceptors (Tenzen et al., 2006; Allen et al., 2007) or by upregulating PTCH1 (Marigo and Tabin, 1996) and other SHH antagonists (Chuang and McMahon, 1999). Molecular separation of ligand recruitment and lipid transfer functions perhaps permitted ad hoc neofunctionalization of the SHH coreceptors. For example, both CDON (Cardozo et al., 2014) and BOC (Bergeron et al., 2011; Echevarría-Andino and Allen, 2020) also have Hh pathway antagonistic functions in certain tissue contexts, as would be expected if they recruit SCUBE-SHH nonproductively, to cells lacking PTCH1, or less productively, to cells lacking GAS1. We speculate that similar ''pre-receptors'' may operate in ligand reception in other signaling pathways, permitting similarly complex regulatory interactions.

SUPPORTING CITATIONS

The following reference appears in the Supplemental Information: Song et al., 2015.

STAR★METHODS

Detailed methods are provided in the online version of this paper and include the following:

- KEY RESOURCES TABLE
- RESOURCE AVAILABILITY
  - Lead Contact
  - Materials Availability
  - Data and Code Availability
- EXPERIMENTAL MODEL AND SUBJECT DETAILS
  - Cell Culture
  - Generation of Stable Cell Lines
  - Generation of CRISPR/Cas9 Knockout (KO) Lines
- METHOD DETAILS
  - Antibodies
  - DNA Constructs
  - Hh Pathway Reporter Assays
  - Quantitative RT-PCR (qRT-PCR)
  - Protein Expression and Purification
  - Immunoblotting
  - Identification and Mutation of SCUBE2 Furin Cleavage Site
  - SHH Release Assays
  - Characterization of SHH Lipidation
  - Site-Specific Labeling of HT7 Fusion Proteins
  - Cell-Based Ligand-Receptor Binding Assays
  - Immunoprecipitation of SCUBE2 and CDON-FN(III)1,2
  - Blue Native PAGE SHH Transfer Assays
  - Radioactive Lipid Binding and Transfer Assays
  - Bead-Based NanoLuc SHH Transfer Assays
  - NbALFA::TM Recruitment Assays
  - Gel and Blot Image Processing
- QUANTIFICATION AND STATISTICAL ANALYSIS

SUPPLEMENTAL INFORMATION

Supplemental Information can be found online at https://doi.org/10.1016/j.devcel.2020.09.017.

ACKNOWLEDGMENTS

We thank M. Broadus and P. Huang for assistance with protein purification, Y.C. Liu for assistance with gene editing and qRT-PCR, H. Tukachinsky for general assistance and helpful discussions, and M. Bao for suggestions on the manuscript. We thank B. Allen for the generous gift of coreceptor-null MEFs. B.M.W. was supported by NIH training grant T32GM007226 and by NIH predoctoral fellowship F31GM120833. This work was supported by NIH grants R01GM122920 and R01GM135262 to A.S.

AUTHOR CONTRIBUTIONS

B.M.W. and A.S. designed reagents and experiments. B.M.W. generated reagents, purified proteins, and performed activity assays, qRT-PCR, ligand-receptor binding experiments, and *in vitro* transfer experiments. K.P. designed and purified PTCH1-L1, developed streptavidin-based peptide ligands, and performed SHH(NL) release experiments. A.S. generated reagents and performed experiments. L.A. generated reagents and purified recombinant CDON-FN proteins. G.G. generated cell-surface CDON/BOC truncation mutant constructs. Y.X. wrote image analysis software. B.M.W. and Y.X. performed image analysis. B.M.W. and A.S. analyzed data. B.M.W. and A.S. wrote the manuscript.

DECLARATION OF INTERESTS

The authors declare no competing interests.

Received: April 21, 2020
Revised: August 4, 2020
Accepted: September 14, 2020
Published: October 9, 2020

REFERENCES

Alcedo, J., Ayzenzon, M., Von Ohlen, T., Noll, M., and Hooper, J.E. (1996). The Drosophila smoothened gene encodes a seven-pass membrane protein, a putative receptor for the hedgehog signal. Cell *86*, 221–232.

Allen, B.L., Song, J.Y., Izzi, L., Althaus, I.W., Kang, J.S., Charron, F., Krauss, R.S., and McMahon, A.P. (2011). Overlapping roles and collective requirement for the coreceptors GAS1, CDO, and BOC in SHH pathway function. Dev. Cell *20*, 775–787.

Allen, B.L., Tenzen, T., and McMahon, A.P. (2007). The Hedgehog-binding proteins Gas1 and Cdo cooperate to positively regulate Shh signaling during mouse development. Genes Dev. *21*, 1244–1257.

Avanesov, A., and Blair, S.S. (2013). The Drosophila WIF1 homolog shifted maintains glypican-independent Hedgehog signaling and interacts with the Hedgehog co-receptors Ihog and Boi. Development *140*, 107–116.

Beachy, P.A., Cooper, M.K., Young, K.E., Von Kessler, D.P., Park, W.J., Hall, T.M., Leahy, D.J., and Porter, J.A. (1997). Multiple roles of cholesterol in hedgehog protein biogenesis and signaling. Cold Spring Harb. Symp. Quant. Biol. *62*, 191–204.

Beachy, P.A., Hymowitz, S.G., Lazarus, R.A., Leahy, D.J., and Siebold, C. (2010). Interactions between Hedgehog proteins and their binding partners come into view. Genes Dev. *24*, 2001–2012.

Bergeron, S.A., Tyurina, O.V., Miller, E., Bagas, A., and Karlstrom, R.O. (2011). Brother of cdo (Umleitung) is cell-autonomously required for Hedgehog-mediated ventral CNS patterning in the zebrafish. Development *138*, 75–85.

Bilioni, A., Sánchez-Hernández, D., Callejo, A., Gradilla, A.C., Ibáñez, C., Mollica, E., Carmen Rodríguez-Navas, M., Simon, E., and Guerrero, I. (2013). Balancing Hedgehog, a retention and release equilibrium given by Dally, Ihog, Boi and shifted/DmWif. Dev. Biol. *376*, 198–212.

Bischoff, M., Gradilla, A.C., Seijo, I., Andrés, G., Rodríguez-Navas, C., González-Méndez, L., and Guerrero, I. (2013). Cytonemes are required for the establishment of a normal Hedgehog morphogen gradient in Drosophila epithelia. Nat. Cell Biol. *15*, 1269–1281.

Blose, S.H., Meltzer, D.I., and Feramisco, J.R. (1984). 10-nm filaments are induced to collapse in living cells microinjected with monoclonal and polyclonal antibodies against tubulin. J. Cell Biol. *98*, 847–858.

Burke, R., Nellen, D., Bellotto, M., Hafen, E., Senti, K.A., Dickson, B.J., and Basler, K. (1999). Dispatched, a novel sterol-sensing domain protein dedicated to the release of cholesterol-modified hedgehog from signaling cells. Cell *99*, 803–815.

Byrne, E.F.X., Sircar, R., Miller, P.S., Hedger, G., Luchetti, G., Nachtergaele, S., Tully, M.D., Mydock-Mcgrane, L., Covey, D.F., Rambo, R.P., et al. (2016). Structural basis of smoothened regulation by its extracellular domains. Nature *535*, 517–522.

Cabrera, J.R., Sanchez-Pulido, L., Rojas, A.M., Valencia, A., Mañes, S., Naranjo, J.R., and Mellström, B. (2006). Gas1 is related to the glial cell-derived neurotrophic factor family receptors α and regulates Ret signaling. J. Biol. Chem. *281*, 14330–14339.

Callejo, A., Bilioni, A., Mollica, E., Gorfinkiel, N., Andrés, G., Ibáñez, C., Torroja, C., Doglio, L., Sierra, J., and Guerrero, I. (2011). Dispatched mediates Hedgehog basolateral release to form the long-range morphogenetic gradient in the Drosophila wing disk epithelium. Proc. Natl. Acad. Sci. USA *108*, 12591–12598.

Cardozo, M.J., Sánchez-Arrones, L., Sandonis, A., Sánchez-Camacho, C., Gestri, G., Wilson, S.W., Guerrero, I., and Bovolenta, P. (2014). Cdon acts as a Hedgehog decoy receptor during proximal-distal patterning of the optic vesicle. Nat. Commun. *5*, 4272.

Caspary, T., García-García, M.J., Huangfu, D., Eggenschwiler, J.T., Wyler, M.R., Rakeman, A.S., Alcorn, H.L., and Anderson, K.V. (2002). Mouse Dispatched homolog1 is required for long-range, but not juxtacrine, Hh signaling. Curr. Biol. *12*, 1628–1632.

Chen, J.K., Taipale, J., Young, K.E., Maiti, T., and Beachy, P.A. (2002). Small molecule modulation of smoothened activity. Proc. Natl. Acad. Sci. USA *99*, 14071–14076.

Chen, W., Huang, H., Hatori, R., and Kornberg, T.B. (2017). Essential basal cytonemes take up Hedgehog in the Drosophila wing imaginal disc. Development *144*, 3134–3144.

Chen, Y., and Struhl, G. (1996). Dual roles for patched in sequestering and transducing Hedgehog. Cell *87*, 553–563.

Chuang, P.T., and McMahon, A.P. (1999). Vertebrate Hedgehog signalling modulated by induction of a Hedgehog-binding protein. Nature *397*, 617–621.

Cong, L., Ran, F.A., Cox, D., Lin, S., Barretto, R., Habib, N., Hsu, P.D., Wu, X., Jiang, W., Marraffini, L.A., and Zhang, F. (2013). Multiplex genome engineering using CRISPR/Cas systems. Science *339*, 819–823.

Creanga, A., Glenn, T.D., Mann, R.K., Saunders, A.M., Talbot, W.S., and Beachy, P.A. (2012). Scube/You activity mediates release of dually lipid-modified Hedgehog signal in soluble form. Genes Dev. *26*, 1312–1325.

Echelard, Y., Epstein, D.J., St-Jacques, B., Shen, L., Mohler, J., McMahon, J.A., and McMahon, A.P. (1993). Sonic hedgehog, a member of a family of putative signaling molecules, is implicated in the regulation of CNS polarity. Cell *75*, 1417–1430.

Echevarría-Andino, M.L., and Allen, B.L. (2020). The hedgehog co-receptor BOC differentially regulates SHH signaling during craniofacial development. bioRxiv https://www.biorxiv.org/content/10.1101/2020.02.04.934497v1.full#:~:text=Full%20Text-,Abstract,to%20mediate%20proper%20HH%20signaling.

Ericson, J., Morton, S., Kawakami, A., Roelink, H., and Jessell, T.M. (1996). Two critical periods of Sonic Hedgehog signaling required for the specification of motor neuron identity. Cell *87*, 661–673.

Fuse, N., Maiti, T., Wang, B., Porter, J.A., Hall, T.M., Leahy, D.J., and Beachy, P.A. (1999). Sonic hedgehog protein signals not as a hydrolytic enzyme but as an apparent ligand for patched. Proc. Natl. Acad. Sci. USA *96*, 10992–10999.

Glise, B., Miller, C.A., Crozatier, M., Halbisen, M.A., Wise, S., Olson, D.J., Vincent, A., and Blair, S.S. (2005). Shifted, the Drosophila ortholog of Wnt inhibitory factor-1, controls the distribution and movement of hedgehog. Dev. Cell *8*, 255–266.

Glockshuber, R., Malia, M., Pfitzinger, I., and Plückthun, A. (1990). A comparison of strategies to stabilize immunoglobulin Fv-fragments. Biochemistry *29*, 1362–1367.

Gong, X., Qian, H., Cao, P., Zhao, X., Zhou, Q., Lei, J., and Yan, N. (2018). Structural basis for the recognition of Sonic Hedgehog by human Patched1. Science *361*, eaas8935.

Gorfinkiel, N., Sierra, J., Callejo, A., Ibañez, C., and Guerrero, I. (2005). The Drosophila ortholog of the human Wnt inhibitor factor shifted controls the diffusion of lipid-modified hedgehog. Dev. Cell *8*, 241–253.

Götzke, H., Kilisch, M., Martínez-Carranza, M., Sograte-Idrissi, S., Rajavel, A., Schlichthaerle, T., Engels, N., Jungmann, R., Stenmark, P., Opazo, F., and Frey, S. (2019). The ALFA-tag is a highly versatile tool for nanobody-based bioscience applications. Nat. Commun. *10*, 4403.

Gradilla, A.C., González, E., Seijo, I., Andrés, G., Bischoff, M., González-Mendez, L., Sánchez, V., Callejo, A., Ibáñez, C., Guerra, M., et al. (2014). Exosomes as Hedgehog carriers in cytoneme-mediated transport and secretion. Nat. Commun. *5*, 5649.

Grimmond, S., Larder, R., Van Hateren, N., Siggers, P., Morse, S., Hacker, T., Arkell, R., and Greenfield, A. (2001). Expression of a novel mammalian epidermal growth factor-related gene during mouse neural development. Mech. Dev. *102*, 209–211.

Hall, E.T., Stewart, D.P., Dillard, M., Wagner, B., Sykes, A., Temirov, J., Cheney, R.E., Mori, M., Robinson, C.G., and Ogden, S.K. (2020). Myosin 10

and a Cytoneme-localized ligand complex promote morphogen transport. bioRxiv biorxiv.org/content/10.1101/2020.05.06.080820v1.full#:~:text=Summary,cell%20fate%20during%20tissue%20patterning.&text=Herein%20we%20show%20that%20the,cytonemes%20occurs%20by%20vesicular%20transport.

Hollway, G.E., Maule, J., Gautier, P., Evans, T.M., Keenan, D.G., Lohs, C., Fischer, D., Wicking, C., and Currie, P.D. (2006). Scube2 mediates Hedgehog signalling in the zebrafish embryo. Dev. Biol. *294*, 104–118.

Huang, P., Nedelcu, D., Watanabe, M., Jao, C., Kim, Y., Liu, J., and Salic, A. (2016). Cellular cholesterol directly activates smoothened in hedgehog signaling. Cell *166*, 1176–1187.e14.

Huston, J.S., Levinson, D., Mudgett-Hunter, M., Tai, M.S., Novotný, J., Margolies, M.N., Ridge, R.J., Bruccoleri, R.E., Haber, E., and Crea, R. (1988). Protein engineering of antibody binding sites: recovery of specific activity in an anti-digoxin single-chain Fv analogue produced in Escherichia coli. Proc. Natl. Acad. Sci. USA *85*, 5879–5883.

Ingham, P.W., and Hidalgo, A. (1993). Regulation of wingless transcription in the Drosophila embryo. Development *117*, 283–291.

Ingham, P.W., and McMahon, A.P. (2001). Hedgehog signaling in animal development: paradigms and principles. Genes Dev *15*, 3059–3087.

Ingham, P.W., Taylor, A.M., and Nakano, Y. (1991). Role of the Drosophila patched gene in positional signalling. Nature *353*, 184–187.

Izzi, L., Lévesque, M., Morin, S., Laniel, D., Wilkes, B.C., Mille, F., Krauss, R.S., McMahon, A.P., Allen, B.L., and Charron, F. (2011). Boc and Gas1 each form distinct Shh receptor complexes with Ptch1 and are required for Shh-mediated cell proliferation. Dev. Cell *20*, 788–801.

Jakobs, P., Exner, S., Schürmann, S., Pickhinke, U., Bandari, S., Ortmann, C., Kupich, S., Schulz, P., Hansen, U., Seidler, D.G., and Grobe, K. (2014). Scube2 enhances proteolytic Shh processing from the surface of Shh-producing cells. J. Cell Sci. *127*, 1726–1737.

Kawakami, A., Nojima, Y., Toyoda, A., Takahoko, M., Satoh, M., Tanaka, H., Wada, H., Masai, I., Terasaki, H., Sakaki, Y., et al. (2005). The zebrafish-secreted matrix protein you/scube2 is implicated in long-range regulation of hedgehog signaling. Curr. Biol. *15*, 480–488.

Kawakami, T., Kawcak, T., Li, Y.J., Zhang, W., Hu, Y., and Chuang, P.T. (2002). Mouse dispatched mutants fail to distribute hedgehog proteins and are defective in hedgehog signaling. Development *129*, 5753–5765.

Kim, M.S., Saunders, A.M., Hamaoka, B.Y., Beachy, P.A., and Leahy, D.J. (2011). Structure of the protein core of the glypican Dally-like and localization of a region important for hedgehog signaling. Proc. Natl. Acad. Sci. USA *108*, 13112–13117.

Labun, K., Montague, T.G., Gagnon, J.A., Thyme, S.B., and Valen, E. (2016). CHOPCHOP v2: a web tool for the next generation of CRISPR genome engineering. Nucleic Acids Res. *44*, W272–W276.

Lee, C.S., Buttitta, L., and Fan, C.M. (2001). Evidence that the WNT-inducible growth arrest-specific gene 1 encodes an antagonist of sonic hedgehog signaling in the somite. Proc. Natl. Acad. Sci. USA *98*, 11347–11352.

Liepinsh, E., Bányai, L., Patthy, L., and Otting, G. (2006). NMR structure of the WIF domain of the human Wnt-inhibitory factor-1. J. Mol. Biol. *357*, 942–950.

Liu, Y.C., Couzens, A.L., Deshwar, A.R., B McBroom-Cerajewski, L.D., Zhang, X., Puviindran, V., Scott, I.C., Gingras, A.C., Hui, C.C., and Angers, S. (2014). The PPFIA1-PP2A protein complex promotes trafficking of Kif7 to the ciliary tip and Hedgehog signaling. Sci. Signal. *7*, ra117.

Los, G.V., Encell, L.P., Mcdougall, M.G., Hartzell, D.D., Karassina, N., Zimprich, C., Wood, M.G., Learish, R., Ohana, R.F., Urh, M., et al. (2008). HaloTag: a novel protein labeling technology for cell imaging and protein analysis. ACS Chem. Biol. *3*, 373–382.

Ma, C., Zhou, Y., Beachy, P.A., and Moses, K. (1993). The segment polarity gene hedgehog is required for progression of the morphogenetic furrow in the developing Drosophila eye. Cell *75*, 927–938.

Ma, Y., Erkner, A., Gong, R., Yao, S., Taipale, J., Basler, K., and Beachy, P.A. (2002). Hedgehog-mediated patterning of the mammalian embryo requires transporter-like function of dispatched. Cell *111*, 63–75.

Malinauskas, T., Aricescu, A.R., Lu, W., Siebold, C., and Jones, E.Y. (2011). Modular mechanism of Wnt signaling inhibition by Wnt inhibitory factor 1. Nat. Struct. Mol. Biol. *18*, 886–893.

Marigo, V., Davey, R.A., Zuo, Y., Cunningham, J.M., and Tabin, C.J. (1996). Biochemical evidence that patched is the Hedgehog receptor. Nature *384*, 176–179.

Marigo, V., and Tabin, C.J. (1996). Regulation of patched by sonic hedgehog in the developing neural tube. Proc. Natl. Acad. Sci. USA *93*, 9346–9351.

Martinelli, D.C., and Fan, C.M. (2007). Gas1 extends the range of Hedgehog action by facilitating its signaling. Genes Dev. *21*, 1231–1243.

Mathew, E., Zhang, Y., Holtz, A.M., Kane, K.T., Song, J.Y., Allen, B.L., and Pasca di Magliano, M.P. (2014). Dosage-dependent regulation of pancreatic cancer growth and angiogenesis by Hedgehog signaling. Cell Rep. *9*, 484–494.

Matusek, T., Wendler, F., Polès, S., Pizette, S., D'Angelo, G., Fürthauer, M., and Thérond, P.P. (2014). The ESCRT machinery regulates the secretion and long-range activity of Hedgehog. Nature *516*, 99–103.

Maun, H.R., Wen, X., Lingel, A., De Sauvage, F.J., Lazarus, R.A., Scales, S.J., and Hymowitz, S.G. (2010). Hedgehog pathway antagonist 5E1 binds hedgehog at the pseudo-active site. J. Biol. Chem. *285*, 26570–26580.

McGough, I.J., Vecchia, L., Bishop, B., Malinauskas, T., Beckett, K., Joshi, D., O'Reilly, N., Siebold, C., Jones, E.Y., and Vincent, J.P. (2020). Glypicans shield the Wnt lipid moiety to enable signalling at a distance. Nature *585*, 85–90.

McLellan, J.S., Zheng, X., Hauk, G., Ghirlando, R., Beachy, P.A., and Leahy, D.J. (2008). The mode of Hedgehog binding to Ihog homologues is not conserved across different phyla. Nature *455*, 979–983.

Montague, T.G., Cruz, J.M., Gagnon, J.A., Church, G.M., and Valen, E. (2014). CHOPCHOP: a CRISPR/Cas9 and TALEN web tool for genome editing. Nucleic Acids Res. *42*, W401–W407.

Mostoslavsky, G., Fabian, A.J., Rooney, S., Alt, F.W., and Mulligan, R.C. (2006). Complete correction of murine Artemis immunodeficiency by lentiviral vector-mediated gene transfer. Proc. Natl. Acad. Sci. USA *103*, 16406–16411.

Nachtergaele, S., Whalen, D.M., Mydock, L.K., Zhao, Z., Malinauskas, T., Krishnan, K., Ingham, P.W., Covey, D.F., Siebold, C., and Rohatgi, R. (2013). Structure and function of the smoothened extracellular domain in vertebrate Hedgehog signaling. eLife *2*, e01340.

Nedelcu, D., Liu, J., Xu, Y., Jao, C., and Salic, A. (2013). Oxysterol binding to the extracellular domain of smoothened in Hedgehog signaling. Nat. Chem. Biol. *9*, 557–564.

Ohana, R.F., Encell, L.P., Zhao, K., Simpson, D., Slater, M.R., Urh, M., and Wood, K.V. (2009). HaloTag7: a genetically engineered tag that enhances bacterial expression of soluble proteins and improves protein purification. Protein Expr. Purif. *68*, 110–120.

Okada, A., Charron, F., Morin, S., Shin, D.S., Wong, K., Fabre, P.J., Tessier-Lavigne, M., and Mcconnell, S.K. (2006). Boc is a receptor for sonic hedgehog in the guidance of commissural axons. Nature *444*, 369–373.

Panáková, D., Sprong, H., Marois, E., Thiele, C., and Eaton, S. (2005). Lipoprotein particles are required for Hedgehog and Wingless signalling. Nature *435*, 58–65.

Pepinsky, R.B., Rayhorn, P., Day, E.S., Dergay, A., Williams, K.P., Galdes, A., Taylor, F.R., Boriack-Sjodin, P.A., and Garber, E.A. (2000). Mapping Sonic hedgehog-receptor interactions by steric interference. J. Biol. Chem. *275*, 10995–11001.

Pepinsky, R.B., Zeng, C., Wen, D., Rayhorn, P., Baker, D.P., Williams, K.P., Bixler, S.A., Ambrose, C.M., Garber, E.A., Miatkowski, K., et al. (1998). Identification of a palmitic acid-modified form of human Sonic hedgehog. J. Biol. Chem. *273*, 14037–14045.

Peters, C., Wolf, A., Wagner, M., Kuhlmann, J., and Waldmann, H. (2004). The cholesterol membrane anchor of the Hedgehog protein confers stable membrane association to lipid-modified proteins. Proc. Natl. Acad. Sci. USA *101*, 8531–8536.

Petrov, K., Wierbowski, B.M., Liu, J., and Salic, A. (2020). Distinct cation gradients power cholesterol transport at different key points in the Hedgehog signaling pathway. Dev. Cell. https://doi.org/10.1016/j.devcel.2020.08.002.

Petrov, K., Wierbowski, B.M., and Salic, A. (2017). Sending and receiving hedgehog signals. Annu. Rev. Cell Dev. Biol. *33*, 145–168.

Petrova, E., Rios-Esteves, J., Ouerfelli, O., Glickman, J.F., and Resh, M.D. (2013). Inhibitors of Hedgehog acyltransferase block Sonic Hedgehog signaling. Nat. Chem. Biol. *9*, 247–249.

Porter, J.A., Young, K.E., and Beachy, P.A. (1996b). Cholesterol modification of hedgehog signaling proteins in animal development. Science *274*, 255–259.

Porter, J.A., Ekker, S.C., Park, W.J., von Kessler, D.P., Young, K.E., Chen, C.H., Ma, Y., Woods, A.S., Cotter, R.J., Koonin, E.V., and Beachy, P.A. (1996a). Hedgehog patterning activity: role of a lipophilic modification mediated by the carboxy-terminal autoprocessing domain. Cell *86*, 21–34.

Qi, X., Schmiege, P., Coutavas, E., and Li, X. (2018a). Two patched molecules engage distinct sites on Hedgehog yielding a signaling-competent complex. Science *362*, eaas8843.

Qi, X., Schmiege, P., Coutavas, E., Wang, J., and Li, X. (2018b). Structures of human patched and its complex with native palmitoylated sonic hedgehog. Nature *560*, 128–132.

Qian, H., Cao, P., Hu, M., Gao, S., Yan, N., and Gong, X. (2018). Inhibition of tetrameric Patched1 by Sonic Hedgehog through an asymmetric paradigm. Nat. Commun. *10*, 2320.

Ramírez-Weber, F.A., and Kornberg, T.B. (1999). Cytonemes: cellular processes that project to the principal signaling center in Drosophila imaginal discs. Cell *97*, 599–607.

Ran, F.A., Hsu, P.D., Wright, J., Agarwala, V., Scott, D.A., and Zhang, F. (2013). Genome engineering using the CRISPR-Cas9 system. Nat. Protoc. *8*, 2281–2308.

Reeves, P.J., Callewaert, N., Contreras, R., and Khorana, H.G. (2002). Structure and function in rhodopsin: high-level expression of rhodopsin with restricted and homogeneous N-glycosylation by a tetracycline-inducible N-acetylglucosaminyltransferase I-negative HEK293S stable mammalian cell line. Proc. Natl. Acad. Sci. USA *99*, 13419–13424.

Riddle, R.D., Johnson, R.L., Laufer, E., and Tabin, C. (1993). Sonic hedgehog mediates the polarizing activity of the ZPA. Cell *75*, 1401–1416.

Rudolf, A.F., Kinnebrew, M., Kowatsch, C., Ansell, T.B., El Omari, K.E., Bishop, B., Pardon, E., Schwab, R.A., Malinauskas, T., Qian, M., et al. (2019). The morphogen Sonic hedgehog inhibits its receptor patched by a pincer grasp mechanism. Nat. Chem. Biol. *15*, 975–982.

Schmittgen, T.D., and Livak, K.J. (2008). Analyzing real-time PCR data by the comparative C(T) method. Nat. Protoc. *3*, 1101–1108.

Song, J.Y., Holtz, A.M., Pinskey, J.M., and Allen, B.L. (2015). Distinct structural requirements for CDON and BOC in the promotion of Hedgehog signaling. Dev. Biol. *402*, 239–252.

Stone, D.M., Hynes, M., Armanini, M., Swanson, T.A., Gu, Q., Johnson, R.L., Scott, M.P., Pennica, D., Goddard, A., Phillips, H., et al. (1996). The tumour-suppressor gene patched encodes a candidate receptor for Sonic hedgehog. Nature *384*, 129–134.

Taipale, J., Chen, J.K., Cooper, M.K., Wang, B., Mann, R.K., Milenkovic, L., Scott, M.P., and Beachy, P.A. (2000). Effects of oncogenic mutations in smoothened and Patched can be reversed by cyclopamine. Nature *406*, 1005–1009.

Taylor, F.R., Wen, D., Garber, E.A., Carmillo, A.N., Baker, D.P., Arduini, R.M., Williams, K.P., Weinreb, P.H., Rayhorn, P., Hronowski, X., et al. (2001). Enhanced potency of human Sonic hedgehog by hydrophobic modification. Biochemistry *40*, 4359–4371.

Tenzen, T., Allen, B.L., Cole, F., Kang, J.S., Krauss, R.S., and McMahon, A.P. (2006). The cell surface membrane proteins Cdo and Boc are components and targets of the Hedgehog signaling pathway and feedback network in mice. Dev. Cell *10*, 647–656.

Tukachinsky, H., Kuzmickas, R.P., Jao, C.Y., Liu, J., and Salic, A. (2012). Dispatched and scube mediate the efficient secretion of the cholesterol-modified hedgehog ligand. Cell Rep *2*, 308–320.

Tukachinsky, H., Petrov, K., Watanabe, M., and Salic, A. (2016). Mechanism of inhibition of the tumor suppressor patched by Sonic Hedgehog. Proc. Natl. Acad. Sci. USA *113*, E5866–E5875.

van den Heuvel, M., and Ingham, P.W. (1996). smoothened encodes a receptor-like serpentine protein required for hedgehog signalling. Nature *382*, 547–551.

Waterhouse, A.M., Procter, J.B., Martin, D.M., Clamp, M., and Barton, G.J. (2009). Jalview version 2–a multiple sequence alignment editor and analysis workbench. Bioinformatics *25*, 1189–1191.

Williams, E.H., Pappano, W.N., Saunders, A.M., Kim, M.S., Leahy, D.J., and Beachy, P.A. (2010). Dally-like core protein and its mammalian homologues mediate stimulatory and inhibitory effects on Hedgehog signal response. Proc. Natl. Acad. Sci. USA *107*, 5869–5874.

Williams, K.P., Rayhorn, P., Chi-Rosso, G., Garber, E.A., Strauch, K.L., Horan, G.S., Reilly, J.O., Baker, D.P., Taylor, F.R., Koteliansky, V., and Pepinsky, R.B. (1999). Functional antagonists of sonic hedgehog reveal the importance of the N terminus for activity. J. Cell Sci. *112*, 4405–4414.

Woods, I.G., and Talbot, W.S. (2005). The you gene encodes an EGF-CUB protein essential for Hedgehog signaling in zebrafish. PLoS Biol. *3*, e66.

Yan, D., Wu, Y., Yang, Y., Belenkaya, T.Y., Tang, X., and Lin, X. (2010). The cell-surface proteins Dally-like and Ihog differentially regulate Hedgehog signaling strength and range during development. Development *137*, 2033–2044.

Yao, S., Lum, L., and Beachy, P. (2006). The Ihog cell-surface proteins bind hedgehog and mediate pathway activation. Cell *125*, 343–357.

Zeng, X., Goetz, J.A., Suber, L.M., Scott, W.J., Schreiner, C.M., and Robbins, D.J. (2001). A freely diffusible form of Sonic hedgehog mediates long-range signalling. Nature *411*, 716–720.

Zhang, W., Kang, J.S., Cole, F., Yi, M.J., and Krauss, R.S. (2006). Cdo functions at multiple points in the sonic hedgehog pathway, and cdo-deficient mice accurately model human holoprosencephaly. Dev. Cell *10*, 657–665.

Please cite this article in press as: Wierbowski et al., Hedgehog Pathway Activation Requires Coreceptor-Catalyzed, Lipid-Dependent Relay of the Sonic Hedgehog Ligand, Developmental Cell (2020), https://doi.org/10.1016/j.devcel.2020.09.017

STAR★METHODS

KEY RESOURCES TABLE

REAGENT or RESOURCE	SOURCE	IDENTIFIER
Antibodies		
chicken polyclonal anti-mARL13B	Petrov et al., 2020	N/A
goat polyclonal anti-mSMO	Nedelcu et al., 2013	N/A
mouse monoclonal anti-FLAG M1	A.C. Kruse; ATCC	Cat# HB-9259; RRID: CVCL_J730
mouse monoclonal anti-HPC	A.C. Kruse	N/A
mouse monoclonal anti-tubulin (clone DM1A)	Sigma; Blose et al., 1984	Cat# T6199; RRID: AB_477583
rabbit monoclonal anti-SHH (clone C9C5)	Cell Signaling Technology	Cat# 2207S; RRID: AB_2188191
mouse monoclonal anti-SHH (clone 5E1)	DSHB; Ericson et al., 1996	Cat# 5e1; RRID: AB_528466
rat anti-HA (clone 3F10)–HRP conjugate	Roche	Cat# 12013819001; RRID: AB_390917
sheep anti-mouse IgG–HRP conjugate	Jackson ImmunoResearch	Cat# 515-005-003; RRID: AB_2340287
donkey anti-rabbit IgG–HRP conjugate	GE Healthcare	Cat# NA934; RRID: AB_772206
donkey anti-chicken IgY–Alexa Fluor 647 conjugate	Jackson ImmunoResearch	Cat# 703-605-155; RRID: AB_2340379
donkey anti-goat IgG–Alexa Fluor 488 conjugate	Thermo	Cat# A-11055; RRID: AB_2534102
donkey anti-goat IgG–Alexa Fluor 594 conjugate	Jackson ImmunoResearch	Cat# 705-585-003; RRID: AB_2340432
donkey anti-rabbit IgG–Alexa Fluor 647 conjugate	Thermo	Cat# A-31573; RRID: AB_2536183
Bacterial and Virus Strains		
E. coli BL21 (DE3) pLysS	Sigma	Cat# 69451
Chemicals, Peptides, and Recombinant Proteins		
cycloheximide	Sigma	Cat# C7698
RU-SKI 43 hydrochloride (HHAT inhibitor)	Tocris Bioscience; Petrova et al., 2013	Cat# 4886
SAG (SMO agonist)	Axxora; Chen et al., 2002	Cat# BV-1939
TRIzol Reagent	Thermo	Cat# 15596018
RQ1 RNase-Free DNase	Promega	Cat# M6101
LunaScript RT SuperMix Kit	NEB	Cat# E3010L
PowerUp SYBR Green Master Mix	Thermo	Cat# A25742
cholesterol [24,25-3H]	American Radiolabeled Chemicals	Cat# ART 1987
palmitic acid [9,10-3H(N)]	American Radiolabeled Chemicals	Cat# ART 0129
Ultima Gold liquid scintillation cocktail	Perkin-Elmer	Cat# 6013329
Alexa Fluor 568 NHS ester	Thermo	Cat# A20003
Alexa Fluor 647 NHS ester	Thermo	Cat# A20006
HaloTag TMR Ligand	Promega	Cat# G8251
70-kDa amino dextran	Thermo	Cat# D1862
HaloTag Succinimidyl Ester (O4) Ligand	Promega	Cat# P6751
HaloTag Amine (O4) Ligand	Promega	Cat# P6741
FLAG elution peptide: NH_2-DYKDDDDK-OH	Genscript	N/A
HPC elution peptide: NH_2-EDQVDPRLIDGK-OH	Genscript	N/A

(*Continued on next page*)

Please cite this article in press as: Wierbowski et al., Hedgehog Pathway Activation Requires Coreceptor-Catalyzed, Lipid-Dependent Relay of the Sonic Hedgehog Ligand, Developmental Cell (2020), https://doi.org/10.1016/j.devcel.2020.09.017

Continued

REAGENT or RESOURCE	SOURCE	IDENTIFIER
palmitoylated SHH effector peptide (EP): palm-SGPGRGFGKRRHPKKLTPLAYK-OH	Biomatik; Tukachinsky et al., 2016	N/A
unpalmitoylated SHH EP: NH_2-SGPGRGFGKRR HPKKLTPLAYK-OH	Biomatik; Tukachinsky et al., 2016	N/A
biotinylated, palmitoylated SHH EP: palm-CGP GRGFGKRRHPKKLTPLAYKK-biotin	Biomatik; Tukachinsky et al., 2016	N/A
biotinylated, unpalmitoylated SHH EP: NH_2-CGPGRG FGKRRHPKKLTPLAYKK-biotin	Biomatik; Tukachinsky et al., 2016	N/A
streptavidin–Alexa Fluor 594 conjugate	Thermo	Cat# S11227
PreScission protease	GE Healthcare	Cat# 27084301
See Table S7 for a list of all purified proteins utilized in this study.	This paper	N/A
Critical Commercial Assays		
MiSeq Reagent Kit v2	Illumina	Cat# MS-102-2001
Affi-Gel 10 Gel	Bio-Rad	Cat# 1536099
CNBr-activated Sepharose	GE Healthcare	Cat# 17-0430-01
HaloLink Resin	Promega	Cat# G1914
Superdex 200, 10/300 GL	GE Healthcare	Cat# 17517501
HiLoad Superdex 200 16/60 pg	GE Healthcare	Cat# 28989335
HiLoad Superdex 200 26/60 pg	GE Healthcare	Cat# 28989336
illustra NAP-5 Columns	GE Healthcare	Cat# 17085301
Amicon Ultra-0.5 Centrifugal Filter Unit – 10kDa cutoff	Millipore	Cat# UFC5010
Amicon Ultra-4 Centrifugal Filter Unit – 10kDa cutoff	Millipore	Cat# UFC8010
Dual-Glo® Luciferase Assay	Promega	Cat# E2940
Nano-Glo® Luciferase Assay	Promega	Cat# N1120
Experimental Models: Cell Lines		
Human: HEK293T	ATCC	Cat# CRL-3216; RRID: CVCL_0063
Human: *MGAT1* $^{-/-}$ HEK293S	A.C. Kruse; ATCC; Reeves et al., 2002	Cat# CRL-3022; RRID: CVCL_A785
Mouse: Flp-In-3T3	Thermo	Cat# R76107
Mouse: Shh-LIGHT2	ATCC; Taipale et al., 2000	Cat# CRL-2795; RRID: CVCL_2721
Mouse: *Cdon* $^{-/-}$; *Boc* $^{-/-}$; *Gas1* $^{-/-}$ (coreceptor-null) MEF	B.L. Allen; Mathew et al., 2014	N/A
Mouse: *Gas1* $^{-/-}$ (GAS1-null) MEF	This paper	N/A
Mouse: *Cdon* $^{-/-}$; *Boc* $^{-/-}$ (CDON/BOC-null) MEF	This paper	N/A
See Table S6 for a complete list of cell lines utilized in this study.	This paper	N/A
Oligonucleotides		
m*Rpl27* qRT-PCR forward primer: 5'-GTCGAGATGG GCAAGTTCAT-3'	Nedelcu et al., 2013	N/A
m*Rpl27* qRT-PCR reverse primer: 5'-GCTTGGCGATCTTCTTCTTG-3'	Nedelcu et al., 2013	N/A
m*Gli1* qRT-PCR forward primer: 5'-TACCATGAGCC CTTCTTTAGGA-3'	Liu et al., 2014	N/A
m*Gli1* qRT-PCR reverse primer: 5'-GCATCATTGAA CCCCGAGTAG-3'	Liu et al., 2014	N/A
See Table S3 for a list of CRISPR gRNA oligonucleotides and sequencing primers.	This paper	N/A
Recombinant DNA		
human GAS1 gene block (hGAS1gb)	IDT; this paper	N/A

(*Continued on next page*)

Please cite this article in press as: Wierbowski et al., Hedgehog Pathway Activation Requires Coreceptor-Catalyzed, Lipid-Dependent Relay of the Sonic Hedgehog Ligand, Developmental Cell (2020), https://doi.org/10.1016/j.devcel.2020.09.017

Continued

REAGENT or RESOURCE	SOURCE	IDENTIFIER
single-chain variable fragment 5E1 (scFv5E1) gene block	IDT; Maun et al., 2010; this paper	N/A
anti-ALFA tag nanobody (NbALFA) gene block	IDT; Götzke et al., 2019; this paper	N/A
See Table S5 for a list of all plasmids utilized in this study.	This paper	N/A
Software and Algorithms		
CHOPCHOP	CHOPCHOP	http://chopchop.cbu.uib.no/; RRID: SCR_015723
MetaMorph Microscopy Automation and Image Analysis Software	Molecular Devices	http://www.moleculardevices.com/Products/Software/Meta-Imaging-Series/MetaMorph.html; RRID: SCR_002368
MATLAB	MathWorks	http://www.mathworks.com/products/matlab/; RRID: SCR_001622
FIJI	National Institutes of Health	http://fiji.sc; RRID: SCR_002285
JalView	Waterhouse et al., 2009	http://www.jalview.org/; RRID: SCR_006459
PyMOL	Schrodinger	http://www.pymol.org/; RRID:SCR_000305
Prism 8	GraphPad	http://www.graphpad.com/; RRID: SCR_002798
Photoshop CS5	Adobe	https://www.adobe.com/products/photoshop.html; RRID: SCR_014199
Inkscape	Inkscape	https://inkscape.org/en/; RRID: SCR_014479

RESOURCE AVAILABILITY

Lead Contact

Further information and requests for reagents should be directed to, and will be fulfilled by, the Lead Contact, Adrian Salic (asalic@hms.harvard.edu).

Materials Availability

The plasmids and cell lines generated in this study are available from the Lead Contact upon request.

Data and Code Availability

This study did not generate datasets. MATLAB scripts utilized for image analysis pipelines are available from the Lead Contact upon request.

EXPERIMENTAL MODEL AND SUBJECT DETAILS

Cell Culture

A complete list of cell lines utilized in this study is provided in Table S6. *Cdon* $^{-/-}$; *Boc* $^{-/-}$; *Gas1* $^{-/-}$ (coreceptor-null) MEFs (Mathew et al., 2014) were obtained from Ben Allen (University of Michigan). *MGAT1* $^{-/-}$ HEK293S cells (Reeves et al., 2002) were a gift from Andrew Kruse (Harvard Medical School). All cell lines were maintained under standard growth conditions (37°C, 5% CO_2), unless otherwise noted. HEK293T, HEK293S, and MEF lines were grown in DMEM (Corning) supplemented with 10% (v/v) fetal bovine serum (VWR) and penicillin/streptomycin (Corning). NIH 3T3 lines were grown in DMEM supplemented with 10% (v/v) bovine calf serum (GE Healthcare) and penicillin/streptomycin. HEK293T and HEK293S cells are female. NIH 3T3 cells are male. The sex of wild-type and coreceptor-null MEF cells used in this study has not been determined.

Generation of Stable Cell Lines

Stable cell lines were generated by lentiviral transduction. Briefly, genes of interest were subcloned into derivatives of the third-generation lentiviral vector pHAGE (Mostoslavsky et al., 2006), modified with different promoters (CMV or EF1α), or resistance markers (blasticidin, puromycin, or hygromycin). Lentiviral particles were produced by transient transfection of HEK293T cells. Lentiviral

particle–conditioned media were incubated with cells of interest for 48 h, in the presence of polybrene (1μg/mL, Sigma). Stably transduced cells were isolated by selection for 72 h with the appropriate antibiotic.

Generation of CRISPR/Cas9 Knockout (KO) Lines

Synthetic oligonucleotides (IDT) containing CRISPR gRNA sequences (Table S3) were annealed and cloned into pX330 (Cong et al., 2013) or pX459 (Ran et al., 2013). Parental cell lines were transiently transfected with gRNA-expressing plasmids, after which fluorescence-activated cell sorting (FACS) or puromycin selection was employed to enrich for transfected cells. Single clones were isolated by growth in 96-well plates, and were characterized by sequencing target locus amplicons (MiSeq, Illumina), to identify knockout (KO) clones (Initiative for Gene Editing and Neurodegeneration, HMS). Primers flanking target loci (Table S3) were designed using CHOPCHOP (Montague et al., 2014; Labun et al., 2016). DNA lesions present in the KO cell lines used in this study are shown in Table S3.

METHOD DETAILS

Antibodies

For immunoblotting, primary antibodies were used at a final concentration of 1-2μg/mL, in TBST [10mM Tris-HCl, pH 7.6; 150mM NaCl; 0.2% Triton X-100 (v/v)] with 5% non-fat dry milk (m/v). For blotting with mouse monoclonal anti-FLAG-M1 and anti-HPC antibodies, all buffers were supplemented with 2mM $CaCl_2$. HRP–conjugated secondary antibodies were used at 0.2μg/mL. The secondary antibodies were: sheep anti-mouse IgG–HRP conjugate (Jackson ImmunoResearch) and donkey anti-rabbit IgG–HRP conjugate (GE Healthcare).

For immunofluorescence, primary antibodies were used at a final concentration of 1μg/mL, in TBST with 2.5% (m/v) bovine serum albumin (BSA). Fluorescent secondary antibodies were used at 1μg/mL. The secondary antibodies were: donkey anti-chicken IgY–Alexa Fluor 647 conjugate (Jackson ImmunoResearch), donkey anti-goat IgG–Alexa Fluor 594 conjugate (Jackson ImmunoResearch), donkey anti-goat IgG–Alexa Fluor 488 conjugate (Thermo), and donkey anti-rabbit IgG–Alexa Fluor 647 conjugate (Thermo).

Mouse monoclonal anti-SHH antibody (clone 5E1) (Ericson et al., 1996) was obtained from the Developmental Studies Hybridoma Bank (University of Iowa). Mouse monoclonal anti-FLAG-M1 and mouse monoclonal anti-HPC antibodies were a generous gift from Andrew Kruse (Harvard Medical School). Purified mouse anti-SHH (5E1), anti-FLAG-M1 and anti-HPC monoclonal antibodies were fluorescently labeled using Alexa Fluor 568 NHS ester or Alexa Fluor 647 NHS ester (Thermo), according to the manufacturer's instructions. Fluorescent primary antibodies were used at a final concentration of 1μg/mL, in TBST with 2mM $CaCl_2$ and 2.5% BSA.

DNA Constructs

A list of the plasmids utilized in this study can be found in Table S5. Additional information on DNA constructs is provided below.

The coding sequence for mouse *Scube2* corresponds to NCBI reference sequence NM_020052.2 and encodes a *Scube2* variant with nine EGF-like repeats, a spacer region, two cysteine-rich repeats, and a CUB domain. Mutants were generated by PCR mutagenesis, were subcloned into pHAGE vectors, and were confirmed by DNA sequencing (DF/HCC DNA Resource Core).

To facilitate purification of SCUBE2-SHH complexes under mild conditions, SHH was internally tagged (Ma et al., 2002; Petrov et al., 2020). One copy of the HPC epitope (EDQVDPRLIDGK), flanked by two glycine residues on either side, was introduced between residues 91 and 92 (HPC5) or residues 130 and 131 (HPC7) of human SHH.

Both human and mouse *GAS1* coding sequences have several regions of ~90% GC content. To facilitate PCR amplification and mutagenesis, we gene synthesized a codon-optimized human *GAS1* gene block (IDT), from which all GAS1 constructs used in this study were derived.

For cell-based ligand-receptor binding assays, we designed a single-chain variable fragment (scFv) version (Huston et al., 1988; Glockshuber et al., 1990) of the 5E1 anti-SHH antibody (scFv5E1), based on the amino acid sequence of a chimeric murine:human 5E1 Fab (Maun et al., 2010) (PDB: 3MXW). The resultant construct was synthesized as a codon-optimized gene block (IDT), and contains the V_L and V_H chains of 5E1 connected by a $(GGGGS)_4$ linker.

The sequence encoding the anti-ALFA tag nanobody (NbALFA) (Götzke et al., 2019) was synthesized as a codon-optimized gene block (IDT), and was subcloned to generate a cell-surface-displayed NbALFA fusion (NbALFA::TM) in the pHAGE vector. The fusion consisted of the following elements: the influenza virus hemagglutinin signal peptide, one copy of the HPC epitope, NbALFA, $(GGGSGGGT)_3$ linker, and the transmembrane and intracellular domains of human CDON.

The region of murine *Ptch1* corresponding to residues G134 to T412 was subcloned into a pHAGE expression vector bearing the influenza virus hemagglutinin signal peptide, HPC epitope, and a PreScission protease site to generate a construct for production of a secreted version of the first extracellular loop of PTCH1 (PTCH1-L1).

Hh Pathway Reporter Assays

SMO Recruitment to Primary Cilia

Localization of endogenous SMO to cilia was assayed by immunofluorescence microscopy. Cells were plated on gelatin-coated coverslips in 24-well plates, at a density of $1x10^5$ cells/well. The next day, cells were switched to serum-free DMEM. On the following day, cells were treated with the indicated agonists or antagonists in serum-free DMEM. After the indicated amount of time, cells were fixed

Please cite this article in press as: Wierbowski et al., Hedgehog Pathway Activation Requires Coreceptor-Catalyzed, Lipid-Dependent Relay of the Sonic Hedgehog Ligand, Developmental Cell (2020), https://doi.org/10.1016/j.devcel.2020.09.017

with 3.7% formaldehyde (w/v) in PBS for 30 min at room temperature, after which endogenous SMO and ARL13B (ciliary marker) were detected by immunofluorescence staining, as described (Nedelcu et al., 2013). Coverslips were mounted on slides in PBS with 50% glycerol (v/v), and were stored at -20°C until imaging. Coverslips were imaged on a Nikon TE2000E microscope, using an OrcaER camera (Hamamatsu) and a 40x PlanApo 0.95NA air objective (Nikon). For each coverslip, z-stacks consisting of 5 focal planes, 1μm apart, were acquired for 30 fields of view, for both SMO and ARL13B channels, using MetaMorph software (Molecular Devices). Images were analyzed using custom analysis software written in FIJI (NIH) and MATLAB (Nedelcu et al., 2013). Briefly, maximum intensity projections were generated from the z-stacks. Cilia were segmented by local adaptive thresholding of the ARL13B images, and background-subtracted SMO intensity was calculated for each cilium object. Ciliary SMO intensity is typically represented as box plots that span from the first to the third intensity quartiles. For dose-response experiments, the median SMO intensity (average of three subsets per condition) was fit with a four-parameter curve in Prism.

Shh-LIGHT2 Luminescence Assay

Hh pathway activation in Shh-LIGHT2 cells was measured by dual luciferase assay, as described (Taipale et al., 2000). Cells were plated in 96-well plates, grown to confluence, and starved overnight in serum-free DMEM. Cells were then treated in triplicate with the indicated factors in serum-free DMEM for 36 h. Luminescence was measured from cell lysates using the Dual-Glo Luciferase Assay System (Promega) in a Victor3 Multilabel plate reader (Perkin-Elmer). Pathway activation is represented as mean firefly:*Renilla* luciferase ratio, with error bars representing standard deviation. For dose-response experiments, mean values were fit with a four-parameter curve in Prism (GraphPad).

Fluorescence Reporter Assay

To generate Hh fluorescence reporter cells (SHH-Fluor), a construct encoding nuclear-localized mCherry (NLS-mCherry) under the control of a Hh-responsive promoter (Taipale et al., 2000) was stably introduced into Flp-In-3T3 cells (Thermo) by Flp recombination, according to the manufacturer's instructions. The resulting cells were stably transduced with a lentivirus encoding CFP-tagged histone H2B (H2B::CFP) under the control of the CMV promoter, to mark nuclei, and single clones were isolated by limited dilution. Clones were characterized for their responsiveness to Hh pathway stimulation, to identify one with a high dynamic range of NLS-mCherry induction. To assay Hh pathway activation, cells were plated in duplicate in 96-well plates and were serum-starved overnight in DMEM with 0.5% BCS (v/v). Cells were then treated with various factors in DMEM with 0.5% BCS for 72 h. Cells were washed in PBS, fixed in 3.7% formaldehyde (m/v) in PBS for 30 min, and washed twice with PBS prior to imaging. Cells were imaged by fluorescence microscopy using a 10x PlanApo 0.45NA air objective (Nikon). For each well, CFP and mCherry images were acquired for four fields of view. Images were analyzed using custom image analysis software written in MATLAB (Mathworks). Briefly, nuclei were segmented using CFP images, and then the background-subtracted mCherry signal was measured for each nucleus object. Pathway activation represents median mCherry:area ratio. Average pathway activation for each of the two replicate wells was fit with a four-parameter curve in Prism.

Quantitative RT-PCR (qRT-PCR)

Hh pathway transcriptional output was measured by qRT-PCR as described (Nedelcu et al., 2013). MEFs were plated in triplicate in 6-well plates, and were starved overnight in DMEM, after which they were treated for 24 h with the indicated agents in DMEM. Total RNA was isolated using TRIzol (Thermo), followed by DNase I treatment (Promega), and purification by a second round of TRIzol. Reverse transcription was performed with LunaScript RT SuperMix (NEB). To quantify Hh pathway activation, the Hh target gene *Gli1* and the control gene, *Rpl27*, were measured by PCR, using PowerUp SYBR Green Master Mix (Thermo) and primers listed in the Key Resources Table. Expression of *Gli1* relative to *Rpl27* was calculated by the comparative C_T method (Schmittgen and Livak, 2008). Error bars represent standard error for three replicates.

Protein Expression and Purification

A list of the proteins utilized in this study, including information regarding tagging, purification, and figures in which they were used, can be found in Table S7. General purification procedures are described below.

Mammalian Expression and Purification of Secreted Proteins

Secreted fusion proteins were stably or transiently expressed in *MGAT1* $^{-/-}$ HEK293S cells, and were affinity purified from conditioned media. The proteins were tagged with a FLAG or HPC epitope, and some of the fusions included a HaloTag7 (HT7) module (Los et al., 2008; Ohana et al., 2009), for various downstream applications. Where indicated, tags were removed by cleavage with PreScission protease (GE Healthcare). Briefly, cells expressing fusion proteins of interest were grown to confluency, were switched into DMEM with 1% FBS (v/v), and conditioned media were harvested every 48 h for a total of three collections. Conditioned media were supplemented $CaCl_2$ to 2mM, centrifuged and filtered to remove debris, and then were loaded onto columns packed with anti-FLAG or anti-HPC affinity resin. After extensive washing with TBS with 2mM $CaCl_2$, bound protein was eluted with elution buffer (20mM HEPES, pH 7.5; 200mM NaCl; 5mM EDTA; 100μg/mL FLAG or HPC peptide). Eluted proteins were concentrated using 10-kDa cutoff centrifugal filter units (Millipore) and were further purified by gel filtration on a Superdex 200 10/300 GL column (GE Healthcare). Fractions corresponding to monomeric species were collected, pooled, concentrated above 1mg/mL, and flash frozen in liquid nitrogen for storage at -80°C. In the case of SCUBE2, most of the FLAG affinity–purified protein eluted from gel filtration as a broad peak between the void volume and the volume corresponding to a monomer. We observed no difference in SHH release activity between the high–molecular weight SCUBE2 fractions and the monomer; thus, unless otherwise noted, purified SCUBE2 and SCUBE2-SHH complexes were not subjected to size-exclusion chromatography.

Please cite this article in press as: Wierbowski et al., Hedgehog Pathway Activation Requires Coreceptor-Catalyzed, Lipid-Dependent Relay of the Sonic Hedgehog Ligand, Developmental Cell (2020), https://doi.org/10.1016/j.devcel.2020.09.017

Purification of SHH Complexes

For purification of chaperone-SHH complexes, EDTA was omitted from the elution buffer, as some SHH interactions are known to be Ca^{2+}-dependent (McLellan et al., 2008; Beachy et al., 2010). For tandem affinity purification of SCUBE2-SHH complexes containing untagged SHH, the FLAG eluate was supplemented with 2mM $CaCl_2$ and was loaded on a column packed with anti-SHH (5E1) resin (5mg 5E1 per mL of CNBr-activated Sepharose). After washing with TBS with 2mM $CaCl_2$, bound protein was eluted with 100mM Na-citrate, pH 3 and the eluate was immediately neutralized using 1M Na-HEPES, pH 8. For tandem affinity purification of SCUBE2-SHH complexes containing HPC-tagged SHH [SCUBE2-SHH(HPC)], the FLAG eluate was supplemented with 2mM $CaCl_2$ and loaded on anti-HPC resin, and HPC affinity purification was performed as described above. Tandem affinity purification of the CDON-Ecto-SCUBE2-SHH complex was performed as above, except that CDON-Ecto was HPC-tagged and SHH was untagged. Complexes were matched for SHH concentration by immunoblotting serial dilutions alongside a serial dilution of a recombinant unlipidated SHH-N(C24A) standard.

Bacterial Expression and Purification of Proteins

Proteins were expressed in *E. coli* (BL21 DE3 pLysS, Novagen) as 6xHis-tagged (pET, Millipore), MBP-tagged (pMAL, NEB), or GST-tagged (pGEX, GE Healthcare) variants, or as intein fusions (IMPACT-TWIN system, NEB). Expression and purification was performed according to manufacturers' instructions. Following affinity purification, the recombinant proteins were concentrated using 10-kDa cutoff centrifugal filter units and were then subjected to gel filtration on a HiLoad Superdex 16/60 pg or HiLoad Superdex 26/60 pg column (GE Healthcare). Fractions corresponding to monomeric species were pooled, concentrated above 1mg/mL, and flash frozen in liquid nitrogen for storage at -80°C.

Immunoblotting

Samples were separated by SDS-PAGE, using 5-15% polyacrylamide gradient gels or 4-20% Mini-PROTEAN TGX precast gels (Bio-Rad). Gels were soaked for 30 min at room temperature in transfer buffer [48mM Tris, pH 9.2; 39mM glycine; 1.3mM SDS; 20% (v/v) methanol] and subjected to semi-dry transfer (Trans-Blot SD, Bio-Rad) to nitrocellulose membranes (Millipore). Membranes were blocked at room temperature in TBST with 5% non-fat dry milk, incubated with primary antibodies overnight at 4°C, and washed with TBST. Membranes were then incubated with secondary antibodies for 1 h at room temperature and then washed with TBST and TBS prior to chemiluminescent detection. For Blue Native PAGE, samples were separated on 3-12% NativePAGE Bis-Tris gels (Thermo) according to the manufacturer's protocol. Gels were soaked for 30 min at room temperature in transfer buffer and were subjected to semi-dry transfer to PVDF membranes (Bio-Rad). Membranes were fixed for 25 min in 8% (v/v) acetic acid, air-dried, incubated in methanol to remove Coomassie dye, and then subjected to immunoblotting as described above.

Identification and Mutation of SCUBE2 Furin Cleavage Site

In our initial purifications of wild-type SCUBE2, >50% of the eluted protein was a cleavage product comprising an N-terminal SCUBE2 fragment of about 40kDa. To identify the cleavage site, the cleavage product and full-length SCUBE2 were separated by SDS-PAGE, and mass spectrometric analysis was performed on the excised bands (Taplin Mass Spectrometry Facility, HMS). Based on comparing tryptic peptide abundance in the two samples, we mapped the cleavage site in the region between amino acids 249-296 (between the fifth and sixth EGF-like repeats). Sequence analysis of this region identified a furin family protease consensus site (RXKR), which is conserved from zebrafish to humans. To improve the purification yield of full-length SCUBE2, a stabilized construct ($SCUBE2^{\Delta Furin}$) was generated by introducing three mutations (R274A, R276A, R277A) in the RVKRR sequence. $SCUBE2^{\Delta Furin}$ behaved indistinguishably from wild-type SCUBE2 in activity assays, and was used as template for SCUBE2 constructs used in this study.

SHH Release Assays

SHH release assays were performed essentially as described (Tukachinsky et al., 2012). For blotting-based assays, confluent HEK293T cultures were washed three times with serum-free DMEM, and were then incubated for 24 h in DMEM. Conditioned media and cell lysates were analyzed by immunoblotting for SCUBE2, SHH, and other relevant species. For NanoLuc-based assays using purified release factors, HEK293T cells stably expressing SHH(NL5) were used (Petrov et al., 2020). After washing with DMEM without serum, the cells were treated with cycloheximide (100μg/mL) (Sigma) for 30 min prior to the addition of purified proteins. Aliquots of conditioned medium were collected at the indicated times, centrifuged to remove cellular debris, and NanoLuc luciferase activity was measured using Nano-Glo Luciferase Assay Substrate (Promega), according to the manufacturer's instructions. In experiments testing the role of palmitoylation on SHH release, cells were first treated overnight with HHAT inhibitor RU-SKI 43 (Petrova et al., 2013) (Tocris Bioscience).

Characterization of SHH Lipidation

We used electrophoretic mobility on SDS-PAGE (Porter et al., 1996a) to determine lipidation status of SHH in the purified SCUBE2-SHH complex. Briefly, we compared the mobility of SCUBE2-bound SHH with that of SHH modified only with palmitate or else with that of SHH modified with both palmitate and cholesterol. Additionally, we used the change in electrophoretic mobility following base hydrolysis, to verify cholesterol modification (Porter et al., 1996b). Base hydrolysis was performed by adjusting the SHH-containing

Please cite this article in press as: Wierbowski et al., Hedgehog Pathway Activation Requires Coreceptor-Catalyzed, Lipid-Dependent Relay of the Sonic Hedgehog Ligand, Developmental Cell (2020), https://doi.org/10.1016/j.devcel.2020.09.017

samples to 90% methanol (v/v) and 50mM KOH, followed by incubation for 1 h at room temperature, to hydrolyze the ester linkage between the C terminus of SHH and the cholesteryl moiety. The reactions were neutralized with Tris-HCl, were dried by SpeedVac, and were subjected to SDS-PAGE and immunoblotting.

Site-Specific Labeling of HT7 Fusion Proteins

Purified HT7 fusion proteins were fluorescently labeled as described (Tukachinsky et al., 2016). Briefly, proteins were incubated for 1 h at room temperature with a five-fold molar excess of HaloTag tetramethylrhodamine (TMR) ligand (Promega). The labeled protein was separated from excess HaloTag ligand using a NAP-5 desalting column (GE Healthcare). For Blue Native PAGE gel shift experiments, 70kDa amino dextran (Thermo) was reacted with a two-fold molar excess of HaloTag succinimidyl ester (O4) ligand (Promega), according to the manufacturer's instructions. The resulting HaloTag dextran ligand was precipitated by addition of 3 volumes of ethanol. The precipitate was collected by centrifugation, washed with ethanol, dried, resuspended in water and further purified on a NAP-5 desalting column. HaloTag dextran ligand was reacted with purified HPC-HT7::GAS1-Ecto, for 1 h at room temperature. Dextran-conjugated GAS1-Ecto species were purified on a Superdex 200 10/300 GL size-exclusion column.

Cell-Based Ligand-Receptor Binding Assays

HEK293T cells were plated in poly-D-lysine–coated wells and were transfected with EGFP-tagged receptor constructs. After 48 h, cells were incubated in phenol red–free DMEM with the indicated ligands, for 1.5 h at 37°C, unless otherwise noted. For competition experiments, ligand and competitor were mixed for 30 min at room temperature prior to addition to cells. Following incubation, cells were washed once with phenol red–free DMEM and then fixed in 3.7% formaldehyde (m/v) in PBS. Fixed cells were washed twice with PBS and either imaged directly (for fluorescent ligands), or subjected to immunofluorescence staining and detection (for unlabeled ligands). Before staining, the fixed cells wells were treated for 3 min with methanol at -20°C, to expose epitopes. Immunofluorescence was then performed as described above. The cells were imaged using a 10x PlanApo 0.45NA air objective (Nikon). For each well, receptor and ligand images were acquired for four fields of view, using MetaMorph software (Molecular Devices). Images were analyzed using custom software written in MATLAB. Briefly, transfected cells were segmented based on the GFP signal, and the corresponding background-subtracted ligand fluorescence intensity was calculated for each cell object. Bound ligand is represented as distributions of ligand:area ratio for segmented cells, as box plots that span from the first to third intensity quartiles. For dose-response experiments, the median ligand:area ratio (average of four fields) was fit with a three-parameter curve in Prism.

For assaying the palmitate-dependent interaction between SHH and GAS1, we used a custom synthesized N-terminally palmitoylated effector peptide comprising residues 24-45 of human SHH, and including a C-terminal biotin modification (Tukachinsky et al., 2016) (Biomatik). The peptide was incubated with an equimolar amount of streptavidin–Alexa Fluor 594 (Thermo), for 1 h at room temperature, after which unoccupied biotin binding sites were blocked by addition of excess free biotin. The fluorescent conjugates thus obtained were immediately used in cell-based binding assays.

Immunoprecipitation of SCUBE2 and CDON-FN(III)1,2

Purified FLAG-HT7::SCUBE2 or FLAG-HT7 (negative control) was mixed with each of four purified, MBP-tagged CDON FN(III) domains (CDON-FN1,2, CDON-FN1, CDON-FN2, and CDON-FN3), in binding buffer (TBS with 2mM $CaCl_2$ and 0.2% DDM). After incubation at room temperature for 1 h, the samples were subjected to immunoprecipitation with anti-FLAG-M1 beads. Beads were washed three times with binding buffer. Bound proteins were eluted in SDS sample buffer and were analyzed by SDS-PAGE followed by Coomassie staining.

Blue Native PAGE SHH Transfer Assays

Purified SCUBE2-SHH (typically at 400nM, based on SHH concentration) was mixed with the indicated factors in SHH transfer buffer (20mM HEPES, pH 8; 200mM NaCl). Reactions were set up at staggered time intervals, and, following incubation at room temperature, the samples were placed on ice and were immediately separated by Blue Native PAGE. Immunoblotting was performed as described above. For initial time points, chilled proteins were mixed on ice immediately before gel loading.

To assay SHH transfer from SCUBE2 to GAS1-Ecto, SCUBE2-SHH (400 nM) was mixed with GAS1-Ecto or GFRα1-Ecto (negative control) (2μM). To assess temperature-dependence, the reaction mixes were incubated in parallel at 4°C or 37°C. To assess specificity, SCUBE2-SHH (400nM) was incubated with GAS1-Ecto or other proteins (10μM). To test reversibility, SCUBE2-SHH (400nM) was first incubated with GAS1-Ecto (2μM) for 1 h, to allow the transfer reaction to saturate. At this time, empty buffer, unliganded SCUBE2 (10μM), or GAS1-Ecto (10μM) was added, and reactions were incubated for an additional 2 h.

Radioactive Lipid Binding and Transfer Assays

To measure cholesterol binding to purified proteins, 10μM of HPC-tagged GAS1-Ecto, GFRα1-Ecto (negative control), or SMO-CRD (positive control) was incubated with [^{3}H]-cholesterol (30μCi/mL) in TBST with 2mM $CaCl_2$ at room temperature for 1 h. Proteins were captured on anti-HPC agarose beads, by tumbling at room temperature for 1 h, after which beads were washed four times with wash buffer (20mM HEPES, pH 7.5; 150mM NaCl). Bound proteins were eluted in HPC elution buffer, and radioactivity was measured in the eluate by liquid scintillation counting using Ultima Gold scintillation cocktail (Perkin-Elmer) and a Tri-Carb 2910 TR scintillation counter (Perkin-Elmer).

Please cite this article in press as: Wierbowski et al., Hedgehog Pathway Activation Requires Coreceptor-Catalyzed, Lipid-Dependent Relay of the Sonic Hedgehog Ligand, Developmental Cell (2020), https://doi.org/10.1016/j.devcel.2020.09.017

To generate protein–lipid beads for radioligand transfer assays, 12μM of HT7-SCUBE2 or HT7-GAS1-Ecto was incubated with either [^{3}H]-cholesterol (100μCi/mL) or [^{3}H]-palmitic acid (100μCi/mL) in TBST at room temperature for 1 h. HaloLink beads (Promega) were added, and proteins were covalently captured by tumbling at room temperature for 1 h. Beads were washed four times with wash buffer and were placed on ice until use. The beads thus prepared were mixed with purified proteins (2μM) on ice, and the transfer reactions were tumbled at room temperature. At the indicated times, aliquots of the supernatant were removed, and radioactivity was measured. HT7-tagged proteins used for radioligand transfer were reacted with excess HaloTag amine (O4) ligand (Promega) before addition to protein–lipid HaloLink beads, to prevent them from reacting with the beads.

Bead-Based NanoLuc SHH Transfer Assays

To generate coreceptor-bearing beads, HPC-tagged coreceptor ectodomains were bound to anti-HPC beads by tumbling at room temperature for 1 h in bead blocking solution (20mM HEPES, pH 8; 200mM NaCl; 2mM $CaCl_2$; 2mg/mL chicken egg albumin). Beads were washed twice with bead blocking solution.

For recruitment/transfer reactions, purified SCUBE2-SHH(NL7) was added to 15μL coreceptor beads (bearing 200pmol of each protein) and tumbled at room temperature for 1 h. After 1 h, reactions were mock-treated or treated for 30 min with recombinant PreScission protease (1nmol), to remove HPC-tagged proteins that contained PreScission cleavage sites. Beads were washed twice with bead blocking solution and bound proteins were eluted with HPC elution buffer. NanoLuc luminescence of the supernatant and bead eluate was quantified in triplicate as described above (SHH Release Assays), and was used to calculate the fraction of total SHH(NL7) bound to beads.

NbALFA::TM Recruitment Assays

To test recruitment of ALFA-tagged proteins, coreceptor-null MEFs, stably expressing HPC-tagged NbALFA::TM or not, were incubated with purified EGFP-ALFA (1μM) for 2 h at 37°C. Cells were washed with PBS, fixed, stained with anti-HPC–Alexa Fluor 647 conjugate, and imaged by fluorescence microscopy. To test rescue of SCUBE2-SHH signaling by surface recruitment of coreceptor ectodomains, wild-type MEFs, coreceptor-null MEFs, or coreceptor-null MEFs stably expressing HPC-tagged Nb-ALFA::TM were treated with the indicated ALFA-tagged purified proteins (1μM). For dose-response assays, the cells above were treated with the indicated doses of purified ALFA-tagged GAS1-Ecto-SHH complex.

Gel and Blot Image Processing

Images of blots and gels in which the lanes broadened during electrophoretic migration were corrected to a rectangular shape in Photoshop CS5, by horizontal skew of the bottom left and right corners. Similarly, in blot or gel images featuring cropped regions at high and low molecular weights (i.e. with noticeably different lane width), images from lower–molecular weight regions have been resized along the horizontal axis, to improve vertical alignment with higher–molecular weight regions. Original images are available upon request.

To better distinguish them from immunoblot images, Coomassie gel images acquired in grayscale were pseudocolored in FIJI with a custom LUT that interpolates between #1919c6 (0) and #fefefe (255). In some figures containing Blue Native PAGE immunoblots, two grayscale blots were overlaid and pseudocolored blue and yellow using the "*Image>Color>Merge Channels*…" function in FIJI.

QUANTIFICATION AND STATISTICAL ANALYSIS

Statistical parameters for experiments involving quantitative comparisons are reported in figure legends and in the Method Details. Shh-LIGHT2 luciferase experiments and qRT-PCR experiments were performed in triplicate, with bar height representing the mean response and error bars representing SD or SEM. All imaging-based assays report on median fluorescence intensity values for the number of cells or cilia indicated in the figure legends. Results are typically represented as box plots that span between the first and third quartiles of the datasets, with the population median indicated by a horizontal line. For imaging experiments that measure dose-dependent responses, population median values are used to fit a three-parameter (ligand–receptor binding) or four-parameter (ciliary SMO) response curve in Prism (GraphPad). Where indicated in figure legends, measures of ligand binding or Hh pathway activation have been normalized to a positive control, as described. All qualitative experiments (e.g. SHH release experiments, SHH transfer experiments, immunoprecipitation) were performed at least twice on separate days and, where possible, with independent preparations of the reagents involved.

Developmental Cell, Volume *55*

Supplemental Information

Hedgehog Pathway Activation Requires Coreceptor-Catalyzed, Lipid-Dependent Relay of the Sonic Hedgehog Ligand

Bradley M. Wierbowski, Kostadin Petrov, Laura Aravena, Garrick Gu, Yangqing Xu, and Adrian Salic

Figure S1.

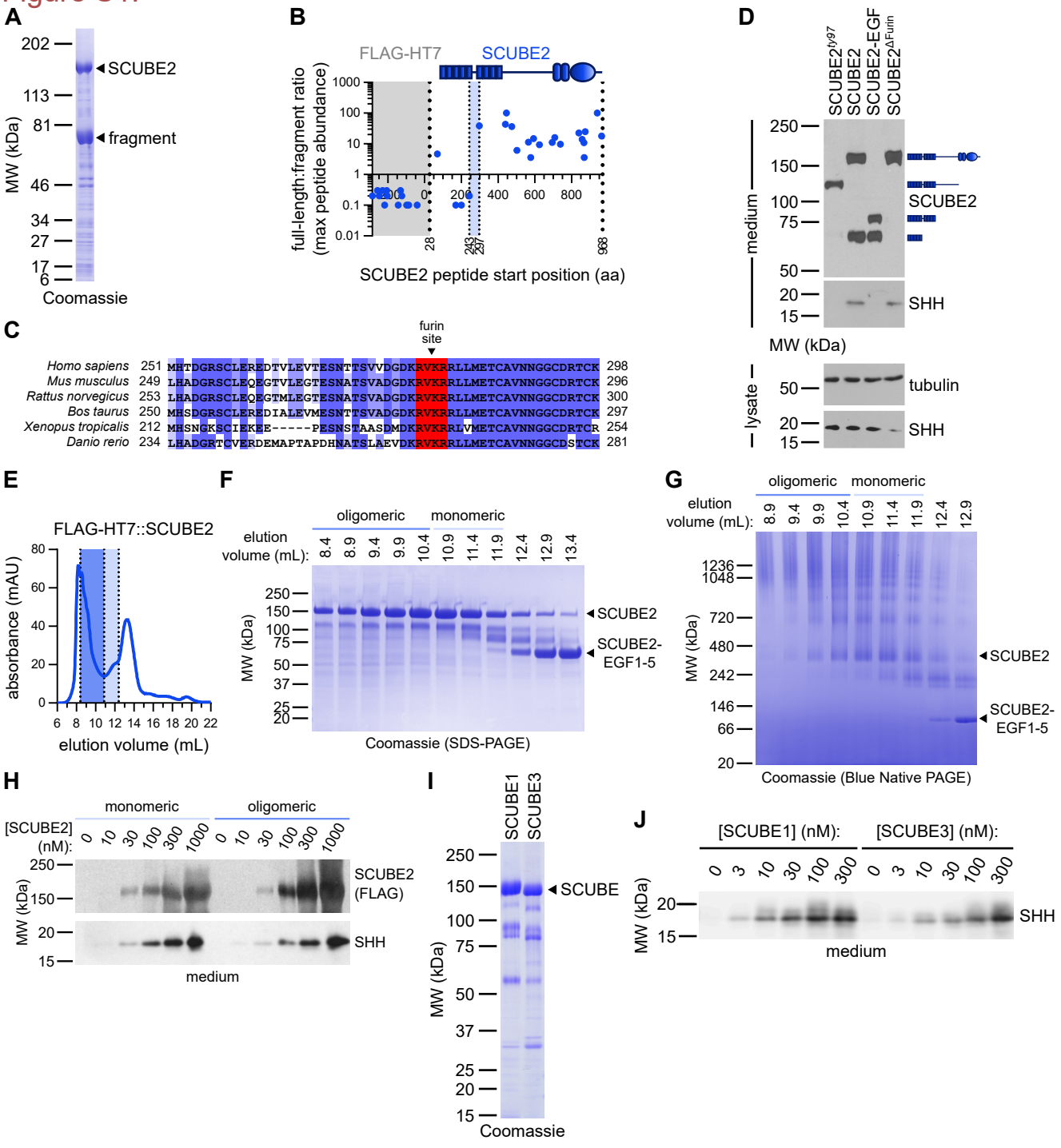
A
202
113
81
46
34
27
17
6
MW (kDa)
SCUBE2
fragment
Coomassie
B
FLAG-HT7
SCUBE2
full-length:fragment ratio (max peptide abundance)
1000
100
10
1
0.1
0.01
0
200
400
600
800
28
243
257
968
SCUBE2 peptide start position (aa)
C
furin site
Homo sapiens 251 MHTDGRSCLEREDTVLEVTESNTTSVVDGDKRVKRRLLMETCAVNNGGCDRTCK 298
Mus musculus 249 LHADGRSCLEQEGTVLEGTESNATSVADGDKRVKRRLLMETCAVNNGGCDRTCK 296
Rattus norvegicus 253 LHADGRSCLEQEGTMLEGTESNATSVADGDKRVKRRLLMETCAVNNGGCDRTCK 300
Bos taurus 250 MHSDGRSCLEREDIALEVMESNTTSVADGDKRVKRRLLMETCAVNNGGCDRTCK 297
Xenopus tropicalis 212 MHSNGKSCIEKEE-----PESNSTAASDMDKRVKRRLVMETCAVNNGGCDRTCR 254
Danio rerio 234 LHADGRTCVERDEMAPTAPDHNATSLAEVDKRVKRRLLMETCAVNNGGCDSTCK 281
D
SCUBE2^tv97
SCUBE2
SCUBE2-EGF
SCUBE2^ΔFurin
250
150
100
75
50
20
15
medium
SCUBE2
SHH
MW (kDa)
lysate
50
20
15
tubulin
SHH
E
FLAG-HT7::SCUBE2
absorbance (mAU)
80
60
40
20
0
6 8 10 12 14 16 18 20 22
elution volume (mL)
F
oligomeric
monomeric
elution volume (mL):
8.4 8.9 9.4 9.9 10.4 10.9 11.4 11.9 12.4 12.9 13.4
250
150
100
75
50
37
25
20
MW (kDa)
SCUBE2
SCUBE2-EGF1-5
Coomassie (SDS-PAGE)
G
oligomeric
monomeric
elution volume (mL):
8.9 9.4 9.9 10.4 10.9 11.4 11.9 12.4 12.9
1236
1048
720
480
242
146
66
20
MW (kDa)
SCUBE2
SCUBE2-EGF1-5
Coomassie (Blue Native PAGE)
H
monomeric
oligomeric
[SCUBE2] (nM):
0 10 30 100 300 1000 0 10 30 100 300 1000
250
150
20
15
MW (kDa)
SCUBE2 (FLAG)
SHH
medium
I
SCUBE1
SCUBE3
250
150
100
75
50
37
25
20
15
MW (kDa)
SCUBE
Coomassie
J
[SCUBE1] (nM):
[SCUBE3] (nM):
0 3 10 30 100 300 0 3 10 30 100 300
20
15
MW (kDa)
SHH
medium

Figure S1. Generation of furin-resistant SCUBE2 and characterization of SCUBE family proteins, Related to Figure 1

(A) Tagged wild-type SCUBE2 was affinity purified from conditioned media, and was analyzed by SDS-PAGE and Coomassie staining. Note presence of an abundant N-terminal cleavage product.

(B) Gel bands in (A) corresponding to full-length SCUBE2 and the N-terminal cleavage product were excised, and were subjected to mass spectrometric analysis. Full-length:cleaved abundance ratios were quantified and plotted for each tryptic peptide, revealing an inflection point between amino acid residues 243-296 (blue).

(C) Sequence analysis of the region identified in (B) revealed a consensus site for furin family proteases, which is conserved in SCUBE2 from zebrafish to humans.

(D) SHH-producing HEK293T cells were transfected with SCUBE2 constructs, and SCUBE2 proteolysis and SHH release were quantified by immunoblotting. Mutation of the furin site reduces SCUBE2 cleavage and preserves SHH release activity.

(E) Size-exclusion chromatogram (Superdex 200 10/300) of purified tagged SCUBE2. Oligomeric (dark blue) and monomeric (light blue) fractions were pooled and concentrated.

(F) Fractions from (E) were analyzed by SDS-PAGE and Coomassie staining.

(G) As in (F), but samples were analyzed by Blue Native PAGE.

(H) Purified monomeric and oligomeric species of SCUBE2 from (E) were added to SHH-producing HEK293T cells, and released SHH was quantified by immunoblotting. Both monomeric and oligomeric SCUBE2 are functional in SHH release.

(I) As in (A), but with tagged SCUBE1 and SCUBE3.

(J) As in (H), but using purified SCUBE1 or SCUBE3. SCUBE1 and SCUBE3 release SHH.

Figure S2.

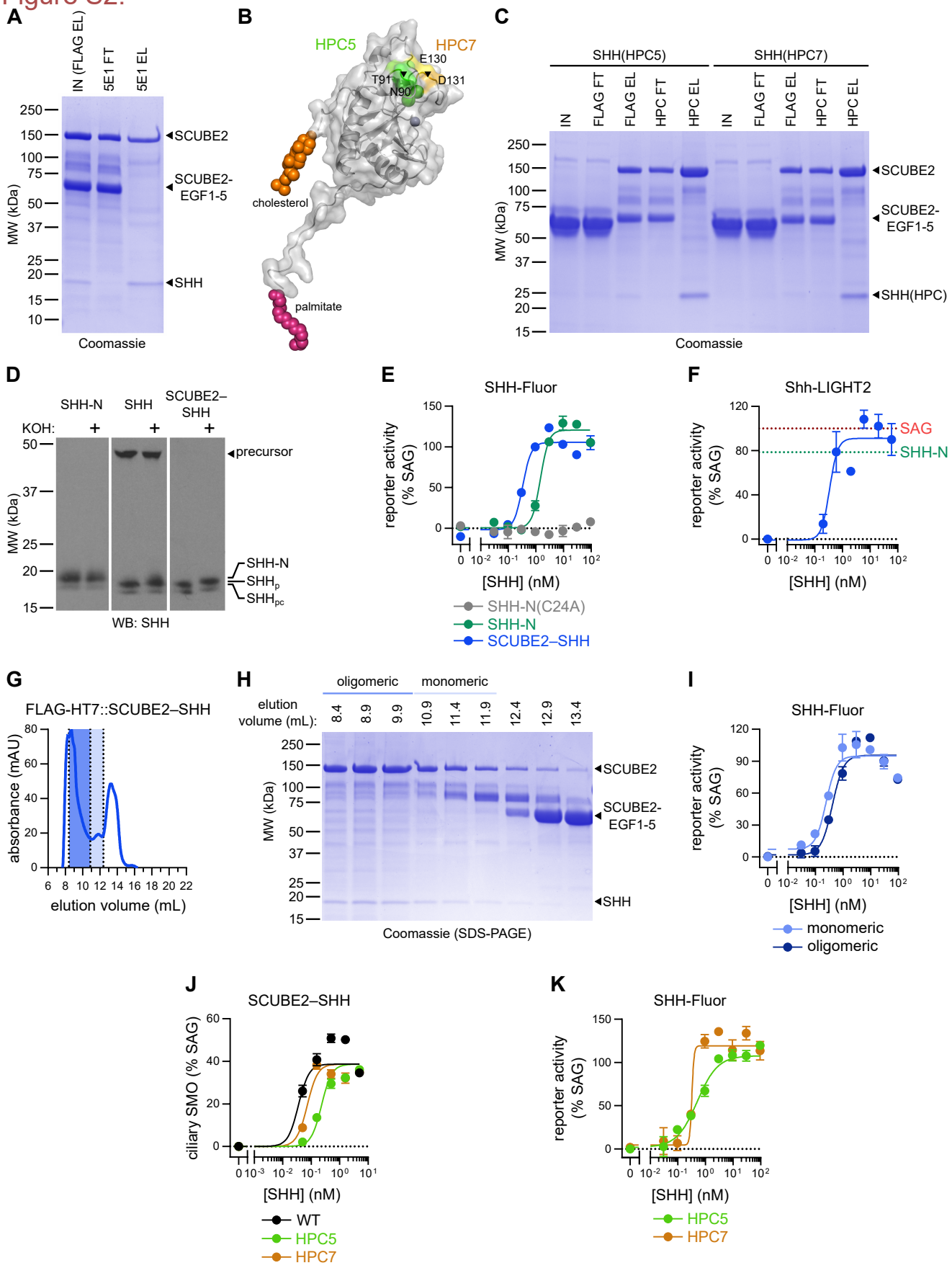
A
IN (FLAG EL)
5E1 FT
5E1 EL
MW (kDa)
SCUBE2
SCUBE2-EGF1-5
SHH
Coomassie
B
HPC5
HPC7
E130
T91
N90
D131
cholesterol
palmitate
C
SHH(HPC5)
SHH(HPC7)
IN
FLAG FT
FLAG EL
HPC FT
HPC EL
SCUBE2
SCUBE2-EGF1-5
SHH(HPC)
Coomassie
D
SHH-N
SHH
SCUBE2–SHH
KOH:
precursor
SHH-N
SHHp
SHHpc
WB: SHH
E
SHH-Fluor
reporter activity (% SAG)
[SHH] (nM)
SHH-N(C24A)
SHH-N
SCUBE2–SHH
F
Shh-LIGHT2
SAG
SHH-N
reporter activity (% SAG)
[SHH] (nM)
G
FLAG-HT7::SCUBE2–SHH
absorbance (mAU)
elution volume (mL)
H
oligomeric
monomeric
elution volume (mL):
8.4
8.9
9.9
10.9
11.4
11.9
12.4
12.9
13.4
MW (kDa)
SCUBE2
SCUBE2-EGF1-5
SHH
Coomassie (SDS-PAGE)
I
SHH-Fluor
reporter activity (% SAG)
[SHH] (nM)
monomeric
oligomeric
J
SCUBE2–SHH
ciliary SMO (% SAG)
[SHH] (nM)
WT
HPC5
HPC7
K
SHH-Fluor
reporter activity (% SAG)
[SHH] (nM)
HPC5
HPC7

Figure S2. Characterization of SCUBE2–SHH and SCUBE2–SHH(HPC) complexes, Related to Figure 1

(A) SCUBE2–SHH was subjected to affinity purification on anti-SHH (5E1) matrix. Fractions corresponding to input (IN), flowthrough (FT), and eluate (EL) were separated by SDS-PAGE, followed by Coomassie staining. Full-length SCUBE2, but not an N-terminal cleavage product, co-purifies with SHH.

(B) Schematic of two internal SHH sites (HPC5 and HPC7) used to introduce the HPC epitope, to generate tagged SHH [SHH(HPC)], without perturbing N- and C-terminal lipidation. (PDB: 6RVD:C)

(C) As in (A), but showing tandem affinity purification of SCUBE2–SHH(HPC) complexes, using anti-FLAG (SCUBE2) and anti-HPC (SHH) beads.

(D) Purified SCUBE2–SHH, or lysates containing palmitoylated SHH-N or dually lipidated SHH were treated with KOH, to hydrolyze the C-terminal cholesteryl ester (Porter et al., 1996b). The samples were then separated by SDS-PAGE, followed by immunoblotting with anti-SHH antibodies. Dually lipidated SHH migrates faster than SHH-N (Porter et al., 1996a), and KOH treatment reduces the mobility of cholesterol-modified SHH species. SHH in purified SCUBE2–SHH is doubly lipidated.

(E) Dose-response of purified SCUBE2–SHH, palmitoylated SHH-N, or unlipidated SHH-N on Hh transcriptional reporter cells (SHH-Fluor). Data are normalized between Hh pathway activation for untreated cells and cells treated with saturating SAG (100%). Points represent average activation for two replicates, and error bars represent SEM. At least 500 cells were measured per replicate. Data are fit with a four-parameter curve.

(F) Dose-response of purified SCUBE2–SHH on Shh-LIGHT2 luciferase reporter cells. Data are normalized as in (E). Points represent average activation for three replicates, and error bars represent SD. Data are fit with a four-parameter curve. Average activation by saturating doses of SHH-N and SAG is indicated with dotted lines.

(G) Size-exclusion chromatogram (Superdex 200 10/300) of purified tagged SCUBE2–SHH. Oligomeric (dark blue) and monomeric (light blue) fractions were pooled and concentrated.

(H) Fractions from (G) were separated by SDS-PAGE, followed by Coomassie staining.

(I) As in (E), but with monomeric and oligomeric SCUBE2–SHH from (G). At least 2000 cells were measured per replicate. Both species activate Hh signaling.

(J) Dose-responses for purified SCUBE2–SHH and SCUBE2–SHH(HPC) complexes on MEFs. Data are normalized as in (E). Points represent average ciliary SMO for three replicates, and error bars represent SEM. At least 700 cilia were measured per replicate. Data are fit with a four-parameter curve.

(K) As in (E), but using SCUBE2–SHH(HPC) complexes from (C). At least 3000 cells were measured per replicate.

Figure S3.

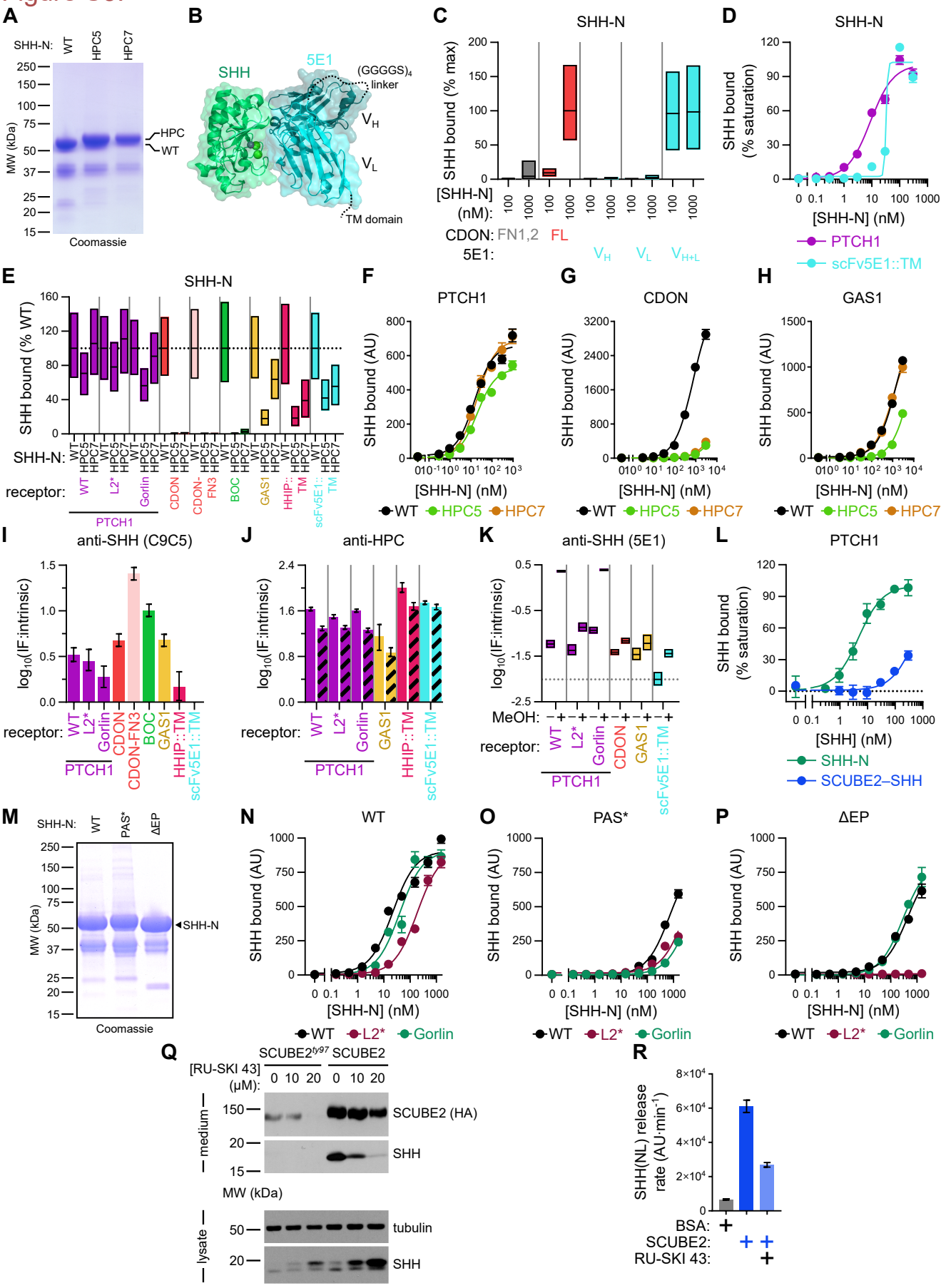
A
SHH-N: WT HPC5 HPC7
MW (kDa)
HPC
WT
Coomassie
B
SHH
5E1
(GGGGS)4 linker
VH
VL
TM domain
C
SHH-N
SHH bound (% max)
[SHH-N] (nM):
CDON: FN1,2 FL
5E1: VH VL VH+L
D
SHH-N
SHH bound (% saturation)
[SHH-N] (nM)
PTCH1
scFv5E1::TM
E
SHH-N
SHH bound (% WT)
SHH-N:
receptor:
PTCH1
F
PTCH1
G
CDON
H
GAS1
SHH bound (AU)
[SHH-N] (nM)
WT HPC5 HPC7
I
anti-SHH (C9C5)
log10(IF:intrinsic)
receptor:
PTCH1
J
anti-HPC
K
anti-SHH (5E1)
MeOH:
L
PTCH1
SHH bound (% saturation)
[SHH] (nM)
SHH-N
SCUBE2–SHH
M
SHH-N: WT PAS* ΔEP
MW (kDa)
SHH-N
Coomassie
N
WT
O
PAS*
P
ΔEP
WT L2* Gorlin
Q
SCUBE2ty97 SCUBE2
[RU-SKI 43] (μM): 0 10 20 0 10 20
medium
SCUBE2 (HA)
SHH
MW (kDa)
lysate
tubulin
SHH
R
SHH(NL) release rate (AU·min-1)
BSA:
SCUBE2:
RU-SKI 43:

Figure S3. Characterization of cell-based ligand–receptor binding assays, Related to Figure 2

(A) SHH-N, SHH-N(HPC5), and SHH-N(HPC7), tagged with HaloTag7-HPC (HT7-HPC) at the C terminus, were affinity purified on anti-HPC beads. Eluted protein was analyzed by SDS-PAGE and Coomassie staining.

(B) Schematic of the membrane-anchored, single-chain variable fragment anti-SHH 5E1 antibody (scFv5E1::TM) for cell-based binding experiments. (PDB: 3MXW)

(C) Tetramethylrhodamine (TMR)–labeled SHH-N was incubated with HEK293T cells expressing the following EGFP-tagged constructs: full-length SHH-binding coreceptor CDON (positive control); CDON-FN1,2, comprising the first two FN repeats of CDON (negative control); or membrane-anchored variable fragments of 5E1. SHH-N binding requires both the heavy and light chain of 5E1. Data are normalized between background signal (untreated cells) and binding to cells with the highest amount of bound ligand (100%). Box plots represent median, and first and third quartiles of ligand bound to cells. At least 400 cells were measured per condition.

(D) Purified SHH-N was added to HEK293T cells expressing EGFP-tagged PTCH1 or scFv5E1::TM, and bound ligand was measured. The scFv5E1::TM construct exhibits mid-nanomolar affinity for SHH-N. For each of the two SHH-binding proteins, data are normalized between the theoretical minimum and maximum of a four-parameter curve fit. Points represent average binding for four replicates, and error bars represent SEM. At least 100 cells were measured per replicate.

(E) As in (C), but comparing binding of SHH-N and SHH-N(HPC) variants to a panel of EGFP-tagged SHH interaction partners, including: the SHH receptor PTCH1; PTCH1^{L2*}, which is defective in SHH–PTCH1 protein–protein interaction; PTCH1^{Gorlin}, which is defective in SHH–PTCH1 palmitate–protein interaction; the SHH coreceptors CDON, BOC, and GAS1; the SHH-binding domain of CDON (CDON-FN3); a membrane-tethered version of the SHH antagonist HHIP; and scFv5E1::TM. SMO, the Hh pathway transducer, does not bind SHH and serves as a negative control. For each receptor, data are normalized between binding of wild-type SHH-N to SMO and to the receptor (100%). At least 500 cells were measured per condition.

(F) As in (D), but comparing binding of SHH-N or SHH-N(HPC) variants to PTCH1. Data is shown without normalization. SHH-N(HPC) variants show normal binding to PTCH1. At least 300 cells were measured per replicate.

(G) As in (F), but with binding to CDON. SHH-N(HPC) variants are impaired in binding CDON.

(H) As in (F), but with binding to GAS1. SHH-N(HPC7) binds GAS1 normally, while SHH-N(HPC5) exhibits a ~6-fold reduction in affinity.

(I) TMR-labeled SHH-N bound to cells in the experiment in (E) was subjected to anti-SHH (C9C5) immunofluorescence, to compare detection methods for SHH bound to different surface receptors. For each receptor, detection efficiency was defined as the background-subtracted log-transform of the ratio between the immunofluorescence and TMR (intrinsic) signals. SHH bound to different receptors is detected with varying efficiency by the anti-SHH (C9C5) antibody. This antibody cannot detect SHH bound to scFv5E1::TM. Bars represent median detection efficiency, and error bars represent first and third quartiles of the distribution.

(J) As in (I), but to validate use of the anti-HPC antibody for immunofluorescence detection of SHH-N(HPC5) (solid bar) and SHH-N(HPC7) (hatched bar). Anti-HPC efficiently detects SHH bound to all receptors.

(K) As in (E), but cells were treated with cold methanol after formaldehyde fixation, and anti-SHH (5E1) was used for detection. Methanol unmasks SHH bound to various receptors for recognition by anti-SHH (5E1), though to different degrees. Detection efficiency was calculated as in (I), except that no background subtraction was performed. Box plots represent median, and first and third quartiles for detection efficiency. At least 900 cells were measured per condition.

(L) Purified SCUBE2–SHH or SHH-N was added to HEK293T cells expressing EGFP-tagged PTCH1, and bound ligand was quantified by anti-SHH (C9C5) immunofluorescence (compare to Figure 2A, for which anti-SHH (5E1) was used for detection). The curve for SCUBE2–SHH is the same as in Figure 2D. SCUBE2 reduces SHH affinity for PTCH1. Data are normalized between background signal (untreated cells) and maximum SHH-N binding (100%), and are fit with a three-parameter curve. Points represent average binding for four replicates, and error bars represent SEM. At least 500 cells were measured per replicate.

(M) Purified HT7-HPC–tagged SHH-N, SHH-N^{PAS*}, and SHH-N$^{\Delta EP}$ were analyzed by SDS-PAGE and Coomassie staining.

(N) As in (F), but comparing binding of wild-type SHH-N to wild-type PTCH1 and to PTCH1 mutants defective in SHH binding modes. The curve for wild-type SHH-N is the same as in Figure 2C. SHH-N exhibits a defect in binding PTCH1^{L2*}. At least 100 cells were measured per replicate.

(O) As in (N), but with SHH-N^{PAS*}. The curve for wild-type PTCH1 is the same as in Figure 2C. SHH-N^{PAS*} exhibits a defect in binding PTCH1^{Gorlin}.

(P) As in (N), but with SHH-N$^{\Delta EP}$. The curve for wild-type PTCH1 is the same as in Figure 2C. Binding of SHH-N$^{\Delta EP}$ to PTCH1^{L2*} is completely abolished.

(Q) SHH-producing HEK293T cells were treated with the indicated doses of the HHAT inhibitor RU-SKI 43 (Petrova et al., 2013), to block SHH palmitoylation, and SHH release by co-expressed wild-type SCUBE2 or the SCUBE2^{ty97} truncation mutant (negative control) (Kawakami et al., 2005; Woods and Talbot, 2005; Hollway et al., 2006) was monitored. Blocking SHH palmitoylation inhibits SCUBE2-dependent release.
(R) Purified SCUBE2 (1μM) or BSA (negative control) was added to HEK293T cells stably expressing NanoLuc luciferase–tagged SHH [SHH(NL)], and SHH release rate was measured by luciferase assay. Inhibition of SHH palmitoylation by incubation with RU-SKI 43 (20μM) reduces the rate of SCUBE2-dependent SHH release. Bars represent average release rate across six time points, and error bars represent standard error of the linear fit to the release time course.

Figure S4.

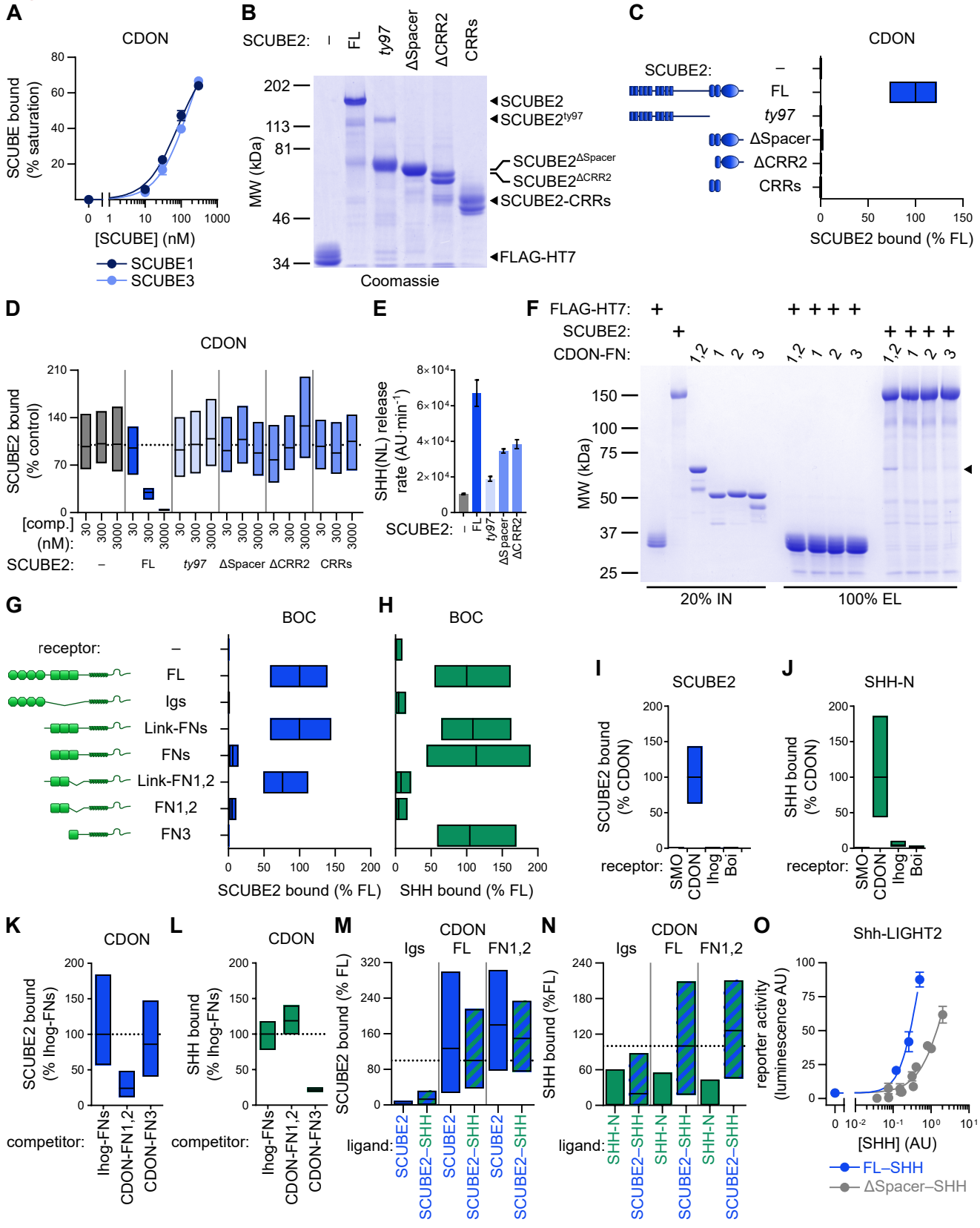
A
CDON
SCUBE bound (% saturation)
[SCUBE] (nM)
SCUBE1
SCUBE3
B
SCUBE2:
FL
ty97
ΔSpacer
ΔCRR2
CRRs
MW (kDa)
SCUBE2
SCUBE2ty97
SCUBE2ΔSpacer
SCUBE2ΔCRR2
SCUBE2-CRRs
FLAG-HT7
Coomassie
C
CDON
SCUBE2:
SCUBE2 bound (% FL)
D
CDON
SCUBE2 bound (% control)
[comp.] (nM):
E
SHH(NL) release rate (AU·min⁻¹)
F
FLAG-HT7:
SCUBE2:
CDON-FN:
20% IN
100% EL
G
BOC
receptor:
Igs
Link-FNs
FNs
Link-FN1,2
FN1,2
FN3
SCUBE2 bound (% FL)
H
BOC
SHH bound (% FL)
I
SCUBE2
SCUBE2 bound (% CDON)
J
SHH-N
SHH bound (% CDON)
K
CDON
SCUBE2 bound (% Ihog-FNs)
competitor:
Ihog-FNs
CDON-FN1,2
CDON-FN3
L
CDON
SHH bound (% Ihog-FNs)
M
CDON
Igs
FL
FN1,2
SCUBE2 bound (% FL)
ligand:
SCUBE2
SCUBE2–SHH
N
CDON
SHH bound (%FL)
SHH-N
SHH-N–SHH
O
Shh-LIGHT2
reporter activity (luminescence AU)
[SHH] (AU)
FL–SHH
ΔSpacer–SHH

Figure S4. Characterization of SCUBE2–CDON/BOC interaction, Related to Figure 4

(A) Binding of fluorescently labeled purified SCUBE1 and SCUBE3 to cells expressing EGFP-tagged CDON. Data are normalized between background signal (untreated cells) and maximum binding (100%), and are fit with a three-parameter curve. Points represent average binding for four replicates, and error bars represent SEM. At least 100 cells were measured per replicate.

(B) The indicated FLAG-HT7–tagged SCUBE2 constructs were affinity purified, and were analyzed by SDS-PAGE and Coomassie staining.

(C) Fluorescently labeled SCUBE2 constructs (100nM) were incubated with cells expressing EGFP-tagged CDON, and bound protein was quantified by fluorescence microscopy. Only full-length SCUBE2 binds CDON. Data are normalized between binding of negative control (FLAG-HT7) and binding of full-length SCUBE2 (100%). Box plots represent median, and first and third quartiles of binding. At least 400 cells were measured per condition.

(D) Fluorescently labeled SCUBE2 (30nM) was incubated with CDON-expressing cells, in the presence of unlabeled SCUBE2 truncation mutants, as competitors. None of the SCUBE2 truncation mutants compete binding of full-length SCUBE2 to CDON. Competition by negative control (FLAG-HT7) and by full-length SCUBE2 are the same as in Figure 4C, as these experiments were performed simultaneously. Data are normalized between background signal (untreated cells) and SCUBE2 binding to CDON in the presence of negative control competitor (100%). Box plots represent median, and first and third quartiles of binding. At least 400 cells were measured per condition.

(E) Purified SCUBE2 truncation mutants (1µM) were added to HEK293T cells stably expressing NanoLuc luciferase–tagged SHH [SHH(NL)], and SHH release rate was measured by luciferase assay. SCUBE2$^{\Delta Spacer}$ and SCUBE2$^{\Delta CRR2}$ release SHH less rapidly than full-length SCUBE2, but still faster than the inactive SCUBE2^{ty97}. BSA served as a negative control. Bars represent average release rate across six time points, and error bars represent standard error of the linear fit to the release time course.

(F) Purified FLAG-HT7–tagged SCUBE2 or FLAG-HT7 (negative control) was incubated with purified MBP-tagged CDON-FN domains, followed by anti-FLAG immunoprecipitation. Inputs (IN) and eluates (EL) were analyzed by SDS-PAGE and Coomassie staining. SCUBE2 binds CDON-FN1,2 but not CDON-FN3.

(G) Fluorescently labeled SCUBE2 (30nM) was incubated with cells expressing EGFP-tagged BOC truncation mutants, and bound ligand was quantified by fluorescence microscopy. SCUBE2 binds FN1,2 and an upstream linker of BOC. Notably, the SCUBE2-binding domains in CDON (Figure 4H) and BOC match precisely those shown to be required, together with the SHH-binding domain, for CDON/BOC function *in vivo* (Song et al., 2015). Data are normalized between binding to EGFP-tagged SMO (negative control) and to full-length BOC (100%). Box plots represent median, and first and third quartiles of binding. At least 400 cells were measured per condition.

(H) As in (G), but with binding of fluorescently labeled SHH-N (300nM). SHH-N binds FN3 of BOC.

(I) As in (G), but comparing binding of fluorescently labeled SCUBE2 (100nM) to CDON and the *Drosophila* CDON/BOC homologs, Ihog and Boi. SCUBE2 does not bind the invertebrate coreceptors.

(J) As in (I), but with fluorescently-labeled SHH-N (1µM). SHH does not bind the invertebrate coreceptors, as described (McLellan et al., 2008).

(K) As in (D), but with CDON-FN1,2, CDON-FN3, or Ihog-FNs (negative control) as competitors (3µM). Only CDON-FN1,2 competes SCUBE2 binding to CDON.

(L) As in (K), but measuring binding of fluorescently labeled SHH-N (1µM) in the presence of the indicated competitors (30µM). Only CDON-FN3 competes SHH binding to CDON.

(M) Fluorescently labeled SCUBE2 (600nM), alone or in complex with SHH(HPC7) (300nM), was incubated with cells expressing EGFP-tagged CDON constructs, and bound SCUBE2 was quantified by fluorescence microscopy. SCUBE2 binds to full-length CDON and CDON-FN1,2. Data are normalized between binding of SCUBE2–SHH(HPC) to CDON-Igs (negative control) and to full-length CDON (100%). Box plots represent median, and first and third quartiles of binding. At least 500 cells were measured per condition.

(N) As in (M), but using anti-HPC immunofluorescence to compare binding of SHH-N(HPC7) and SCUBE2–SHH(HPC7). SHH(HPC7), which is defective in CDON binding, is recruited to CDON by SCUBE2.

(O) Shh-LIGHT2 cells were treated with concentration-matched serial dilutions of SCUBE2–SHH and SCUBE2$^{\Delta Spacer}$–SHH conditioned media, and Hh pathway activation was measured by luciferase assay. SCUBE2$^{\Delta Spacer}$–SHH has reduced signaling activity. Points represent average activation for three replicates, and error bars represent SD.

Figure S5.

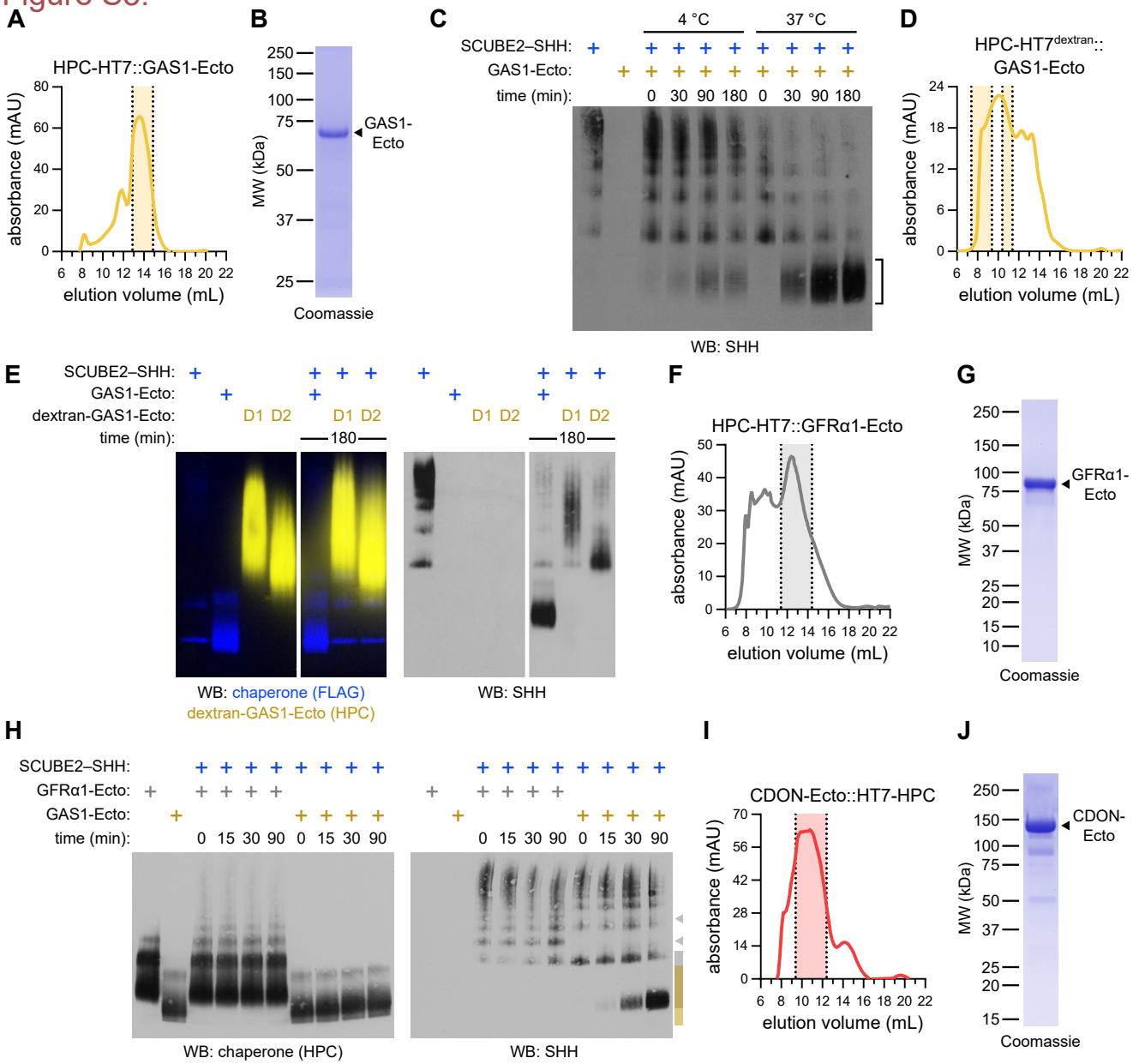
A
HPC-HT7::GAS1-Ecto
absorbance (mAU)
elution volume (mL)
B
MW (kDa)
GAS1-Ecto
Coomassie
C
4 °C
37 °C
SCUBE2–SHH:
GAS1-Ecto:
time (min):
0 30 90 180 0 30 90 180
WB: SHH
D
HPC-HT7dextran::GAS1-Ecto
absorbance (mAU)
elution volume (mL)
E
SCUBE2–SHH:
GAS1-Ecto:
dextran-GAS1-Ecto:
time (min):
D1 D2
180
WB: chaperone (FLAG)
dextran-GAS1-Ecto (HPC)
WB: SHH
F
HPC-HT7::GFRα1-Ecto
absorbance (mAU)
elution volume (mL)
G
MW (kDa)
GFRα1-Ecto
Coomassie
H
SCUBE2–SHH:
GFRα1-Ecto:
GAS1-Ecto:
time (min):
0 15 30 90 0 15 30 90
WB: chaperone (HPC)
WB: SHH
I
CDON-Ecto::HT7-HPC
absorbance (mAU)
elution volume (mL)
J
MW (kDa)
CDON-Ecto
Coomassie

Figure S5. Characterization of *in vitro* SHH transfer from SCUBE2 to GAS1, Related to Figure 5

(A) Size-exclusion chromatogram (Superdex 200 10/300) of purified GAS1-Ecto, tagged N-terminally with HPC-HT7 (HPC-HT7::GAS1-Ecto). The indicated monomeric fractions (shaded) were pooled and concentrated.

(B) The monomeric GAS1-Ecto fractions from (A) were analyzed by SDS-PAGE and Coomassie staining.

(C) Purified SCUBE2–SHH (400nM) was incubated with purified GAS1-Ecto (2μM), at 4°C or 37°C, followed by separation by Blue Native PAGE and immunoblotting. SHH transfer from SCUBE2 to GAS1-Ecto is temperature-dependent. Bracket indicates region occupied by GAS1-Ecto.

(D) As in (A), but for HPC-HT7::GAS1-Ecto conjugated to 70kDa dextran. Two pools of high–molecular weight GAS1-Ecto (D1 and D2) were isolated.

(E) As in (C), but comparing SHH transfer from SCUBE2–SHH to unmodified GAS1-Ecto (4μM), or to dextran-conjugated high–molecular weight GAS1-Ecto (4μM) from (D). Transferred SHH co-migrates with GAS1-Ecto.

(F) As in (A), but for purified HPC-HT7::GFRα1-Ecto.

(G) As in (B), but for monomeric fraction of GFRα1-Ecto from (F).

(H) As in (C), but comparing SHH transfer from SCUBE2–SHH to GAS1-Ecto or GFRα1-Ecto at 37°C. SHH is transferred to GAS1-Ecto but not to GFRα1-Ecto.

(I) As in (A), but for purified CDON-Ecto, C-terminally tagged with HT7-HPC (CDON-Ecto::HT7-HPC).

(J) As in (B), but for monomeric fraction of CDON-Ecto from (I).

Figure S6.

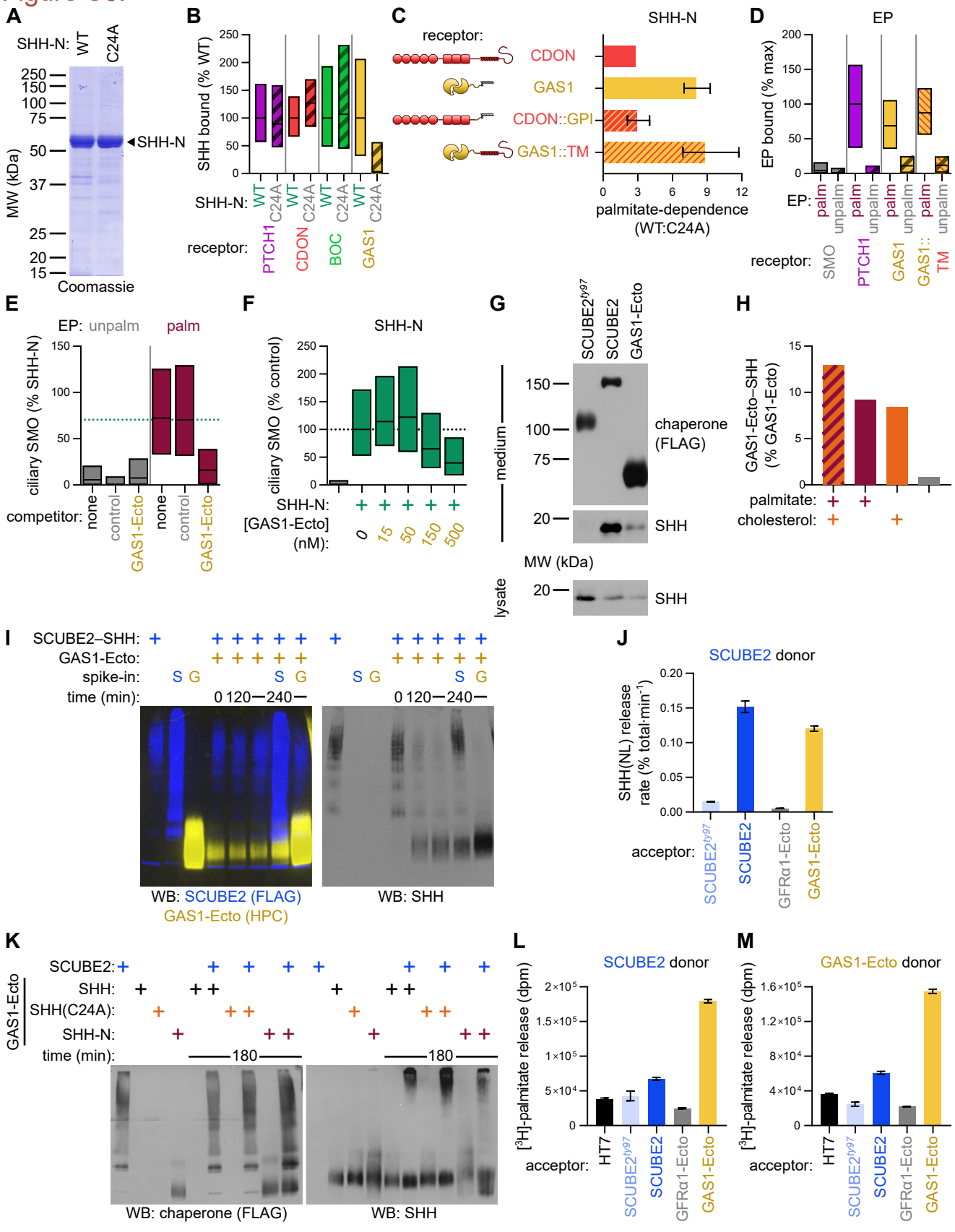
A
SHH-N: WT C24A
250
150
100
75
50
37
25
20
15
MW (kDa)
SHH-N
Coomassie
B
SHH bound (% WT)
SHH-N: WT C24A WT C24A WT C24A WT C24A
receptor: PTCH1 CDON BOC GAS1
C
receptor:
CDON
GAS1
CDON::GPI
GAS1::TM
SHH-N
palmitate-dependence (WT:C24A)
D
EP
EP bound (% max)
EP: palm unpalm palm unpalm palm unpalm palm unpalm
receptor: SMO PTCH1 GAS1 GAS1:: TM
E
EP: unpalm palm
ciliary SMO (% SHH-N)
competitor: none control GAS1-Ecto none control GAS1-Ecto
F
SHH-N
ciliary SMO (% control)
SHH-N: + + + + +
[GAS1-Ecto] (nM): 0 15 50 150 500
G
SCUBE2ty97 SCUBE2 GAS1-Ecto
medium
chaperone (FLAG)
SHH
MW (kDa)
lysate
SHH
H
GAS1-Ecto–SHH (% GAS1-Ecto)
palmitate: + +
cholesterol: + +
I
SCUBE2–SHH: + + + + + + + + + + + +
GAS1-Ecto: + + + + + + + + + + + +
spike-in: S G S G S G S G
time (min): 0 120 240 0 120 240
WB: SCUBE2 (FLAG)
GAS1-Ecto (HPC)
WB: SHH
J
SCUBE2 donor
SHH(NL) release rate (% total·min-1)
acceptor: SCUBE2ty97 SCUBE2 GFRα1-Ecto GAS1-Ecto
K
GAS1-Ecto
SCUBE2: + + + + + + + + + + + +
SHH: + + + + + +
SHH(C24A): + + + + + +
SHH-N: + + + + + +
time (min): 180 180
WB: chaperone (FLAG)
WB: SHH
L
SCUBE2 donor
[3H]-palmitate release (dpm)
acceptor: HT7 SCUBE2ty97 SCUBE2 GFRα1-Ecto GAS1-Ecto
M
GAS1-Ecto donor
[3H]-palmitate release (dpm)
acceptor: HT7 SCUBE2ty97 SCUBE2 GFRα1-Ecto GAS1-Ecto

Figure S6. Characterization of palmitate and cholesterol binding by GAS1, and of lipid transfer between SCUBE2 and GAS1, Related to Figure 5

(A) HT7-HPC–tagged palmitoylated SHH-N and unpalmitoylated SHH-N(C24A) were affinity purified, and were analyzed by SDS-PAGE and Coomassie staining.

(B) TMR-labeled palmitoylated SHH-N or unpalmitoylated SHH-N(C24A) was incubated (1μM) with cells expressing EGFP-tagged GAS1, CDON, BOC, PTCH1, or SMO (negative control). SHH binds GAS1 in a palmitate-dependent manner. This binding mode of GAS1 is unique among coreceptors. For each receptor, data are normalized between binding of SHH-N to cells expressing SMO or the receptor (100%). At least 400 cells were measured per condition.

(C) As in (B), but with the indicated CDON and GAS1 constructs. Palmitate-dependence was calculated as the ratio of bound SHH-N to bound SHH-N(C24A). The GPI anchor is dispensable for palmitate-dependent SHH binding to GAS1, as GAS1 fused to a transmembrane domain (TM) also binds SHH in palmitate-dependent manner. Error bars represent upper and lower bounds calculated based on SD of three replicates. At least 400 cells were measured per replicate.

(D) Fluorescent SHH N-terminal effector peptide (EP), with or without palmitate (see STAR Methods), was incubated (2.5μM) with cells expressing EGFP-tagged GAS1, GAS1::TM, PTCH1 (positive control), or SMO (negative control). Palmitoylated SHH EP binds GAS1. Data are normalized between EP binding to the negative control and the highest bound signal (100%). Box plots represent median, and first and third quartiles of binding. At least 400 cells were measured per condition.

(E) MEFs were treated with synthetic SHH EP (1μM), with or without palmitate, in the presence of purified GAS1-Ecto (2μM) or control competitor (FLAG-HT7) (2μM). Recruitment of endogenous SMO to cilia was measured by immunofluorescence. GAS1-Ecto inhibits Hh pathway activation by palmitoylated SHH EP. Data are normalized between ciliary SMO for untreated cells and cells treated with saturating levels of SHH-N (100%). Box plots represent median and first and third quartiles of SMO intensity. At least 200 cilia were measured per condition.

(F) As in (E), but with Hh pathway activation by SHH-N in the presence of the indicated doses of purified GAS1-Ecto. GAS1-Ecto antagonizes SHH-N in a dose-dependent manner. Data are normalized between ciliary SMO for untreated cells and cells treated with SHH-N and no GAS1-Ecto (100%).

(G) SHH-producing HEK293T cells were transfected with GAS1-Ecto, SCUBE2 (positive control), or SCUBE2^{ty97} (negative control), and SHH release was quantified by immunoblotting. GAS1-Ecto is sufficient to release dually lipidated SHH from cells.

(H) FLAG-HT7-tagged GAS1-Ecto was co-expressed with SHH(HPC7) (doubly lipidated), SHH-N(HPC7) (palmitoylated only), SHH(C24A; HPC7) (cholesterylated only), or SHH-N(C24A; HPC7) (unlipidated). Conditioned media were subjected to sequential FLAG and HPC affinity purifications, and the fraction of total GAS1-Ecto bound to SHH variants (ratio of GAS1 between the HPC and FLAG eluates) was calculated. One lipid is necessary and sufficient for GAS1–SHH interaction.

(I) Blot corresponding to the data quantified in Figure 5I.

(J) Purified SCUBE2–SHH(NL) was immobilized on beads, which were then incubated with purified GAS1-Ecto, GFRα1-Ecto, SCUBE2, or SCUBE2^{ty97} (2μM). SHH(NL) release was measured as a function of time, by luciferase assay. GAS1-Ecto and SCUBE2 release SHH, in contrast to the negative controls GFRα1-Ecto and SCUBE2^{ty97}. Bars represent average release rate across four time points, expressed as a percentage of total luminescence on beads. Error bars represent standard error of the linear fit to the release time course.

(K) GAS1-Ecto (400nM) in complex with SHH (doubly lipidated), SHH-N (palmitoylated only), or SHH(C24A) (cholesterylated only) was incubated with unliganded SCUBE2 (15μM), and the mixes were assayed by Blue Native PAGE and immunoblotting. Either lipid suffices for SHH back-transfer from GAS1-Ecto to SCUBE2.

(L) SCUBE2 was loaded with [^{3}H]-palmitate and was captured on beads. The beads were incubated with the indicated purified proteins (2μM), and released radioactivity was measured as a function of time. Palmitate is preferentially transferred from SCUBE2 to GAS1. Bars represent average release across the four time points, with error bars representing SEM.

(M) As in (L), but for release of [^{3}H]-palmitate from GAS1-Ecto on beads.

Figure S7.

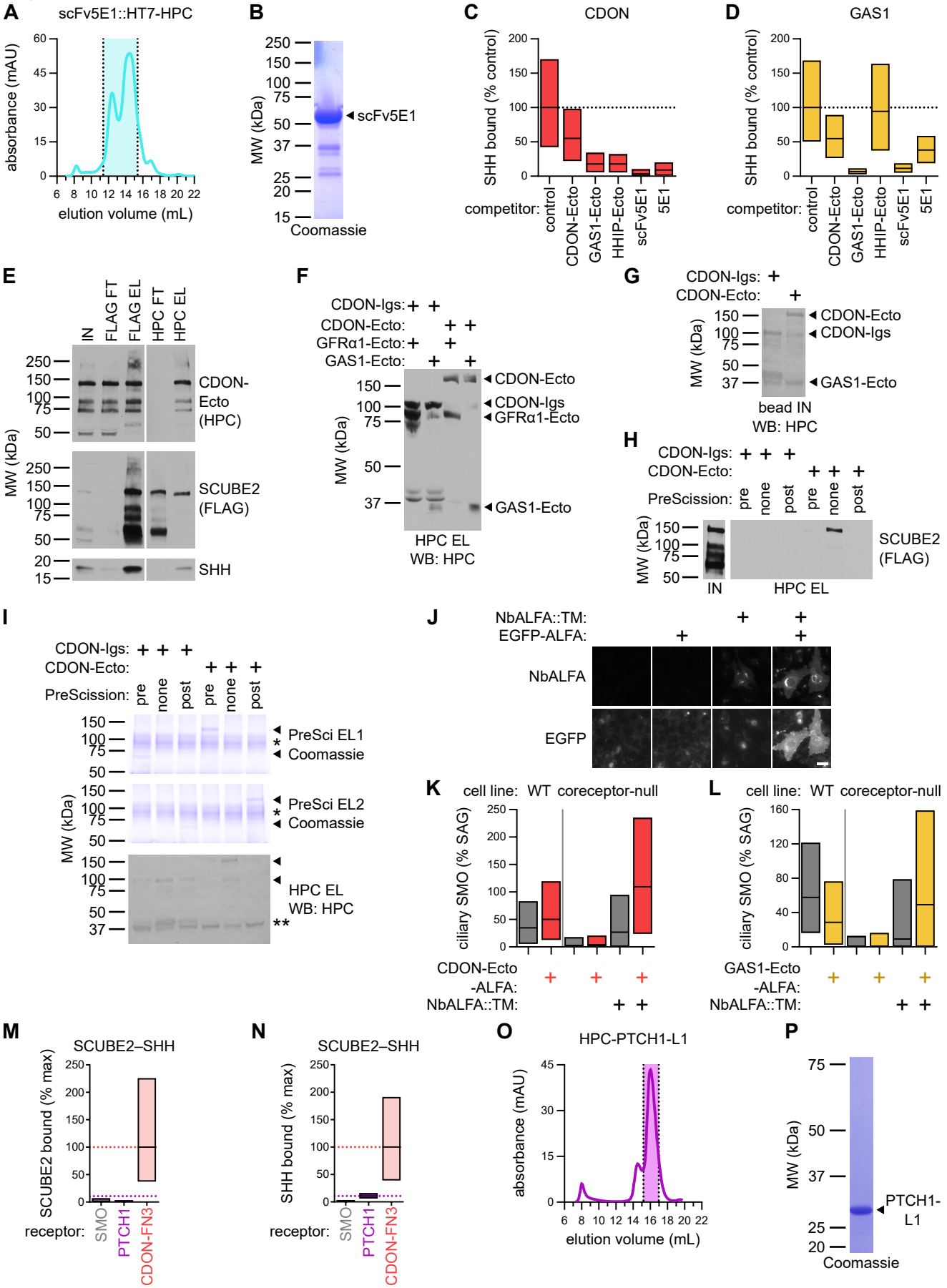
A
scFv5E1::HT7-HPC
absorbance (mAU)
elution volume (mL)
B
MW (kDa)
scFv5E1
Coomassie
C
CDON
SHH bound (% control)
competitor:
control
CDON-Ecto
GAS1-Ecto
HHIP-Ecto
scFv5E1
5E1
D
GAS1
E
IN
FLAG FT
FLAG EL
HPC FT
HPC EL
CDON-Ecto (HPC)
SCUBE2 (FLAG)
SHH
F
CDON-Igs:
CDON-Ecto:
GFRα1-Ecto:
GAS1-Ecto:
HPC EL
WB: HPC
G
bead IN
WB: HPC
H
PreScission:
pre
none
post
I
PreSci EL1
PreSci EL2
Coomassie
HPC EL
WB: HPC
J
NbALFA::TM:
EGFP-ALFA:
NbALFA
EGFP
K
cell line: WT coreceptor-null
ciliary SMO (% SAG)
CDON-Ecto -ALFA:
NbALFA::TM:
L
GAS1-Ecto -ALFA:
M
SCUBE2–SHH
SCUBE2 bound (% max)
receptor:
SMO
PTCH1
CDON-FN3
N
SHH bound (% max)
O
HPC-PTCH1-L1
P
PTCH1-L1

Figure S7. Characterization of purified proteins and recruitment/transfer assays, Related to Figure 6

(A) Size-exclusion chromatogram (Superdex 200 10/300) of affinity purified scFv5E1::HT7-HPC. The indicated fractions (shaded) were pooled and concentrated.

(B) The pooled fractions in (A) were analyzed by SDS-PAGE and Coomassie staining.

(C) Fluorescent SHH-N was incubated with CDON-expressing cells, in the presence of known SHH binders (2 μM), and bound SHH-N was measured. All constructs, including GAS1-Ecto, compete SHH-N binding to CDON. Data are normalized between background signal (untreated cells) and SHH-N binding to CDON in the presence of negative control competitor (FLAG-HT7) (100%). Box plots represent median, and first and third quartiles of binding. At least 400 cells were measured per condition.

(D) As in (C), but with binding to GAS1-expressing cells. CDON-Ecto competes SHH-N binding to GAS1.

(E) Immunoblots of fractions from sequential FLAG and HPC affinity purification of CDON-Ecto–SCUBE2–SHH complex secreted by cells co-expressing FLAG-HT7::SCUBE2, CDON-Ecto::HT7-HPC, and SHH. CDON-Ecto enriches for full-length SCUBE2 in the HPC eluate. SHH, but not SCUBE2, is depleted from the HPC flowthrough.

(F) Immunoblot of HPC elution fractions, without PreScission treatment, from beads used for the assay in Figure 6C.

(G) Immunoblot of protein mixtures used to generate beads for the assay in Figure 6D, indicating sizes of CDON-Igs and CDON-Ecto proteins.

(H) Immunoblot of SCUBE2–SHH(NL) input and HPC elution fractions from the assay in Figure 6D. SCUBE2 is recruited to, and retained on, only CDON-Ecto–bearing beads not treated with PreScission protease.

(I) Elution fractions for the assay in Figure 6D were separated by SDS-PAGE. Supernatant samples were taken following treatments with PreScission (PreSci EL1 and EL2), and bead-bound material was eluted with HPC peptide (HPC EL). Top: Coomassie staining. Arrowheads represent untagged CDON-Igs and CDON-Ecto eluted by protease treatment. Single asterisk indicates albumin used in blocking solution. Bottom: anti-HPC immunoblotting. Arrowheads represent tagged CDON-Igs and CDON-Ecto retained on beads. Double asterisk indicates free HT7-HPC tag, which runs at the same molecular weight as GAS1-Ecto.

(J) Coreceptor-null MEFs rescued or not by stable expression of HPC-tagged membrane-anchored ALFA nanobody (Götzke et al., 2019) (NbALFA::TM), were incubated with purified ALFA-tagged EGFP (1μM) for 2 h. Representative images of fixed cells are shown. EGFP-ALFA is recruited to the surface of cells expressing NbALFA::TM. Scale bar = 20μm.

(K) Wild-type MEFs, or coreceptor-null MEFs expressing or not NbALFA::TM, were treated with SCUBE2–SHH (1nM) together with ALFA-tagged CDON-Ecto (1μM) or EGFP-ALFA (1μM). Hh pathway activation was measured by endogenous SMO recruitment to cilia. Recruited CDON-Ecto-ALFA rescues responsiveness to SCUBE2–SHH. For each cell line, data are normalized between untreated and cells treated with saturating SAG (100%). Box plots represent median, and first and third quartiles of SMO intensity. At least 600 cilia were measured per condition.

(L) As in (K), but cells were treated with SCUBE2–SHH (0.3nM) together with ALFA-tagged GAS1-Ecto (1μM) or EGFP-ALFA (1μM). Recruited GAS1-Ecto rescues responsiveness to SCUBE2–SHH.

(M) Fluorescently-labeled SCUBE2–SHH (500nM) was incubated with cells expressing PTCH1, CDON-FN3 (positive control), or SMO (negative control), and bound SCUBE2 was measured by fluorescence microscopy. SCUBE2 is stably recruited to CDON-FN3 by SHH; however, SCUBE2 does not accumulate on cells expressing PTCH1. Data are normalized between binding of SCUBE2 to the negative and positive controls.

(N) As in (M), but using anti-SHH (C9C5) immunofluorescence to detect bound SHH. Binding to SMO and PTCH1 are the same data as in Figure 6G, as these experiments were performed together. At least 300 cells were measured per condition.

(O) As in (A), but for purified HPC-PTCH1-L1.

(P) The pooled monomeric fractions in (O) were analyzed by SDS-PAGE and Coomassie staining.